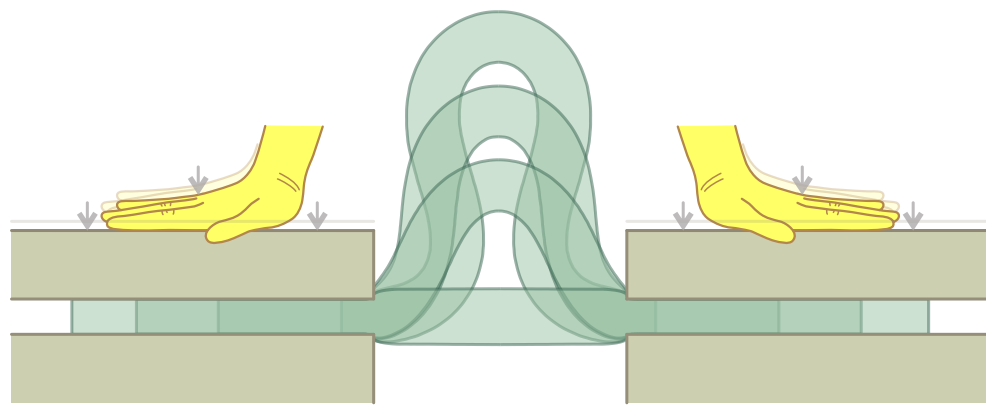


Curriculum 3. Modelling and Simulation

Marco Amato

## Elastic solids under frictionless rigid contact and configurational force





UNIVERSITY OF TRENTO - Italy

Department of Civil, Environmental  
and Mechanical Engineering



Doctoral School in Civil, Environmental and Mechanical Engineering  
Topic 3. Modelling and Simulation - 36 cycle 2020/2024

Doctoral Thesis - May 2024

Marco Amato

## **Elastic solids under frictionless rigid contact and configurational force**

### **Supervisors**

Prof. Francesco Dal Corso, University of Trento

Prof. Davide Bigoni, University of Trento

Prof. Andrea Piccolroaz, University of Trento



Contents on this book are licensed under a Creative Common Attribution  
Non Commercial - No Derivatives  
4.0 International License, except for the parts already published by other publishers.

University of Trento  
Doctoral School in Civil, Environmental and Mechanical Engineering  
<http://web.unitn.it/en/dricam>  
Via Mesiano 77, I-38123 Trento  
Tel. +39 0461 282670 / 2611 - [dicamphd@unitn.it](mailto:dicamphd@unitn.it)

*To my family*



## Acknowledgements

The author acknowledges financial support from the European Research Council (ERC) under the European Union's Horizon 2020 research and innovation programme, Grant agreement No. ERC-ADG-2021-101052956-BEYOND.





## Abstract

A homogeneous elastic solid, bounded by a flat surface in its unstressed configuration, undergoes a finite strain when in frictionless contact against a rigid and rectilinear constraint, ending with a rounded or sharp corner, in a two-dimensional formulation. With a strong analogy to fracture mechanics, it is shown that (i.) a path-independent  $J$ -integral can be defined for frictionless contact problems, (ii.) which is equal to the energy release rate  $G$  associated with an infinitesimal growth in the size of the frictionless constraint, and thus gives the value of the configurational force component along the sliding direction. Furthermore, it is found that (iii.) such a configurational sliding force is the Newtonian force component exerted by the elastic solid on the constraint at the frictionless contact. Assuming the kinematics of an Euler-Bernoulli rod for an elastic body of rectangular shape, the results (i.)–(iii.) lead to a new interpretation from a nonlinear solid mechanics perspective of the configurational forces recently disclosed for one-dimensional structures of variable length. Finally, approximate but closed-form solutions (validated with finite element simulations) are exploited to provide further insight into the effect of configurational forces. In particular, two applications are presented which show that a transverse compression can lead to Eulerian buckling or to longitudinal dynamic motion, both realizing novel examples of soft actuation mechanisms. As an application to biology, our results may provide a mechanical explanation for the observed phenomenon of negative durotaxis, where cells migrate from stiffer to softer environments.



## Contents

<b>1</b>	<b>Introduction</b>	<b>3</b>
<b>2</b>	<b>Finite Elasticity</b>	<b>7</b>
2.1	Kinematics . . . . .	7
2.2	Statics . . . . .	13
2.3	Balance Principles . . . . .	15
2.4	Hyperelasticity . . . . .	19
<b>3</b>	<b>Prologue: non-accidental coincidences in contact mechanics at small strain</b>	<b>21</b>
3.1	$J$ -integral and energy release rate $G$ for the indentation of a linear elastic material . . . . .	22
3.2	Horizontal contact reaction force at the indenter with rounded corner . . . . .	26
<b>4</b>	<b>Frictionless contact reaction component through energy-momentum tensor(s) and J-integral</b>	<b>29</b>
4.1	Frictionless contact problem: target and contactor .	30
4.2	Two energy-momentum tensors . . . . .	33
4.3	Different energy-momentum tensors in the solution of rectangular elastic domains under pressure loading	35
4.3.1	Reaction forces $R_1^a + R_1^b$ and $R_1(\partial\mathcal{P}_0^{\text{tou}})$ from the energy momentum tensor $\mathbf{P}$ . . . . .	35
4.3.2	Reaction force $R_1^a + R_1^b$ from the energy momentum tensor $\mathbf{C}$ . . . . .	37

---

<b>5 Energy release rate <math>G</math> and the configurational nature of the frictionless contact force component <math>R_1</math></b>	<b>41</b>
5.1 Variation in the length of a flat, frictionless, and rigid constraint ending with a sharp corner . . . . .	42
5.2 Variation in the length of the constraint with a rounded corner . . . . .	47
<b>6 Connection with the configurational structural mechanics</b>	<b>49</b>
6.1 Rod's kinematics . . . . .	49
6.2 Sliding sleeve constraint and the evaluation of the configurational force component $F_1^c$ . . . . .	51
6.3 Configurational force via a variational approach . . . . .	54
6.4 Application to rods characterized by a quadratic energy density . . . . .	56
<b>7 Reaction force <math>R_1</math> and applications in instability and dynamics</b>	<b>59</b>
7.1 The horizontal reaction force $R_1$ at the corner of a frictionless flat punch . . . . .	62
7.2 Eulerian buckling induced by transverse compression . . . . .	67
7.3 Dynamic longitudinal ejection of incompressible solids through transverse compression . . . . .	72
<b>Conclusions</b>	<b>77</b>
<b>Appendices</b>	<b>79</b>
A Another example of use of the energy-momentum tensor $\mathbf{C}$ for rectangular domains under dead loading conditions . . . . .	79
B Reaction force at a frictionless contact from the principle of virtual works . . . . .	80
<b>Bibliography</b>	<b>83</b>

# 1

## Introduction

Initiated by Eshelby [15–17], configurational mechanics provides a groundbreaking insight into problems where a defect can change its position or increase in size and release energy, which is associated to a force, called ‘configurational’, acting on the defect and causing its movement. In the specific case of a rectilinear crack in a linear elastic material, the energy release rate  $G$  associated with a crack advancement was found by Cherepanov [11] and Rice [40, 41] to be given by a path-independent integral, the so-called  $J$ -integral. The latter author involved the energy-momentum tensor  $\mathbf{P}$  introduced by Eshelby, so that a crack driving force can be related to fracture growth.

Historically, configurational forces were assumed to be different in nature from Newtonian forces, which enter the equations of motion of a solid [22, 27]. However, a number of elastic structures with variable length has been recently investigated to show that a special class of configurational forces are Newtonian forces and, as such, can even be determined experimentally. These structures include a rod with one end sliding inside a frictionless sleeve (in both quasi-static [5, 30] and dynamic [1, 29, 45] settings), a rod subjected to torsion [6] and a rod moving inside a frictionless, rigid and curved channel [14]. Remarkably, a common feature of these structures is the possibility of a free movement in a certain direction, to which the configurational force becomes energetically conjugate.

Inspired by these results in structural mechanics, Ballarini and Royer-Carfagni proposed an interpretation of configurational forces as resultants of Newtonian contact forces acting on defects, through the solution of simplified models, representative of a solid containing

an edge dislocation or a crack [2].

Along the same research line, the frictionless contact is addressed in the present work of a homogeneous elastic solid, bounded with a planar surface and undergoing large deformations against a flat and rigid indenter, ending with a rounded or sharp corner. In this situation, it is shown that a path-independent  $J$ -integral can be defined (so far restricted to small strain states [31, 32, 47]) and corresponds to the energy release rate  $G$ , also known as configurational force, associated with the constraint growth (expressions for  $J$  and  $G$  are deferred to Chapters 4 and 5). In turn, the configurational force is shown to coincide with the negative of the reaction force  $R_1$  (parallel to the undeformed flat boundary of the solid) which the corner of the constraint transmits to the elastic solid, in summary,

$$G = J = -R_1. \quad (1.1)$$

Two paradigmatic examples of generation of a horizontal configurational force are systematically referred, Fig. 1.1 (the rollers visualize bilateral smooth contact, while the brown element symbolize unilateral contact), where an elastic solid of rectangular shape of undeformed height  $h_0$  is subjected to a nominal transverse stretch  $\bar{\lambda}_2 < 1$ . It will be shown that in both cases the horizontal reaction force  $R_1$  at the corner is provided with an excellent approximation by

$$R_1 \approx \frac{\Phi^l h_0}{\lambda_1^l}, \quad (1.2)$$

where  $\Phi^l$  is the strain energy density and  $\lambda_1^l$  the stretch, both evaluated at the left edge  $\partial\mathcal{B}_0^l$  of the elastic rectangle where these are assumed constant. The simple approximate expression (1.2) is obtained within a large deformation framework for hyperelastic materials and is valid for both rounded and sharp corners, as well as for both types of boundary conditions (unilateral or bilateral frictionless contact) applied at the lower side of the rectangular domain. With the purpose of connecting the present solid mechanics framework with the recent results obtained in configurational structural mechanics [5, 6, 14, 30, 37], a rectangular elastic solid is analyzed, subject to the kinematics of an Euler-Bernoulli rod. In this way, a novel derivation from a nonlinear solid mechanics perspective is obtained for the outward tangential reaction, generated at the end of a sliding sleeve constraining an elastic rod, previously disclosed only through one-dimensional models.

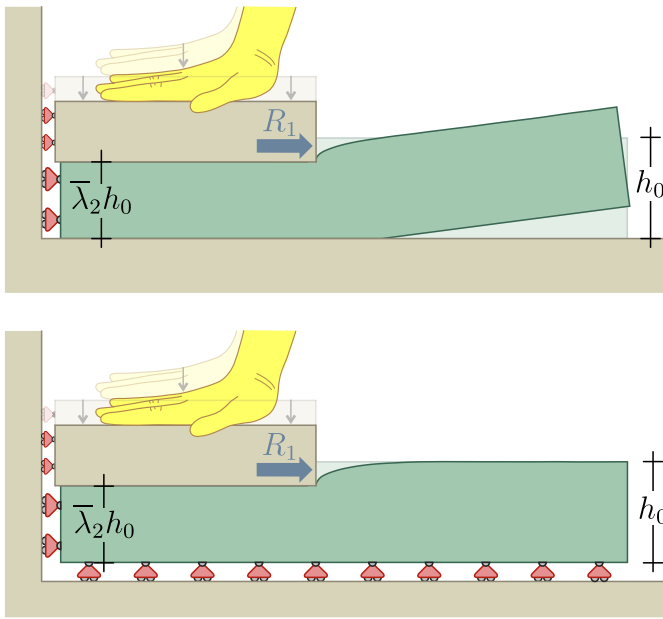


**Figure 1.1:** A rectangular elastic solid (green) of initial height  $h_0$  is deformed through a transverse compression (of nominal stretch  $\bar{\lambda}_2 < 1$ ) against a flat, rigid, and frictionless punch (brown) ending with a sharp corner. Rollers denote bilateral, while brown elements unilateral, frictionless contact. The transverse compression generates a concentrated reaction force  $R_1$ , shown in this work to be coincident with the negative of the  $J$ -integral, which in turn defines a configurational force, eqn (1.1), and that can be evaluated with an excellent approximation through eqn (1.2).

The relevance of our results to the design of new soft actuation mechanisms is demonstrated by two applications whose approximate solution is obtained analytically and validated by finite element simulations. In particular, it is shown that the configurational forces induced by a transverse compression may lead in one case to Eulerian buckling and in the other to the longitudinal motion of an elastic layer. The latter result may introduce a mechanical explanation to the so-called *negative durotaxis*, a biological process in which cells migrate from a stiffer towards a softer environment [25].



# 2

## Finite Elasticity

The purpose of this chapter is to introduce the basic principles of finite deformation solid mechanics, an important branch of mechanics. Mechanics is a crucial discipline for understanding the behaviour of materials and structures under various conditions. The study of elasticity is central to explain the mechanical response of materials when subjected to external forces and deformations.

In the present chapter the kinematics is initially introduced, including material and spatial representations, and strain tensors. Statics follows through the presentation of the Cauchy theorem and the stress tensors. The conservation of mass, balance of linear and angular momentum, and the equations of motion are recalled. The various measures of stress and deformation are shown to be conjugate in the sense of work by the theorem of Power Expended. A final section focuses on hyperelasticity, a fundamental concept that governs the behaviour of many materials, such as biological tissues and elastomers. Here, the strain energy density function is introduced together with the incompressibility constraint.

Interested readers are invited to consult [4, 21, 24, 38] for further details.

### 2.1 Kinematics

One can imagine a body, denoted as  $\mathcal{C}$ , as a collection of particles, represented as  $P \in \mathcal{C}$ . When  $\mathcal{C}$  moves in three-dimensional Euclidean space, it occupies different spatial regions during transitions from one moment to another. These distinct spatial arrangements are known as *configurations* and are symbolically denoted as  $\mathcal{B}$ . Among

these configurations, it is possible to identify one, the preferred one, against which all others must be referenced, called the *reference configuration*  $\mathcal{B}_0$

In the reference configuration  $\mathcal{B}_0$ , any point  $x_0$  can be identified by its position vector  $\mathbf{x}_0 = x_i^0 \mathbf{e}_i^0$ , where the set  $\mathbf{e}_i^0$  define three unit vectors representing the orthonormal basis of three-dimensional space. In the current configuration, any point  $x$  is represented as  $\mathbf{x} = x_i \mathbf{e}_i$ . Assuming that the basis remains constant throughout the process, only  $\mathbf{e}_i$  will be used.

The motion of a particle can be described using the transformation function  $\mathbf{g}$ :

$$\mathbf{x} = \mathbf{g}(\mathbf{x}_0, t). \quad (2.1)$$

To prevent penetration and material laceration, it is essential that the function  $\mathbf{g}(\mathbf{x}_0, t)$  is biejective. This criteria include the need for continuous derivatives in both space and time and the need to be invertible. The capability to invert this function is pivotal, as it allows one to determine the original position from the current one:

$$\mathbf{x}_0 = \mathbf{g}^{-1}(\mathbf{x}, t). \quad (2.2)$$

From these descriptions of motion, it becomes clear that there are two fundamental approaches to characterizing kinematics. The first is the material description (also known as referential or Lagrangian description), which defines motion with respect to the reference configuration. The second is the spatial (current or Eulerian description), which characterizes motion with respect to the current configuration.

Since the definitions of the description are provided, let us go through the material and spatial time derivatives. These derivatives are essential for capturing the dynamic aspects of motion.

Let us proceed by considering a material field represented as  $\phi = \phi(\mathbf{x}_0, t)$  and explore the concept of material time derivatives:

$$\dot{\phi}(\mathbf{x}_0, t) = \frac{\partial \phi(\mathbf{x}_0, t)}{\partial t}, \quad (2.3)$$

conversely, for a spatial field  $\phi = \phi(\mathbf{x}, t)$ , its spatial time derivative is simply denoted by  $\partial \phi(\mathbf{x}, t) / \partial t$ . Its material time derivative is

$$\dot{\phi}(\mathbf{x}, t) = \frac{\partial \phi(\mathbf{x}, t)}{\partial t} + \text{grad}\phi(\mathbf{x}, t) \cdot \mathbf{v}(\mathbf{x}, t). \quad (2.4)$$

The displacement field is a vectorial field which relate the actual position to the referential. It represent at any time the distance

between the two points. In the material description:

$$\mathbf{u}_0(\mathbf{x}_0, t) = \mathbf{x}(\mathbf{x}_0, t) - \mathbf{x}_0, \quad (2.5)$$

in the spacial:

$$\mathbf{u}(\mathbf{x}, t) = \mathbf{x} - \mathbf{x}_0(\mathbf{x}, t). \quad (2.6)$$

it is important to note that  $\mathbf{u}_0 = \mathbf{u}$ .

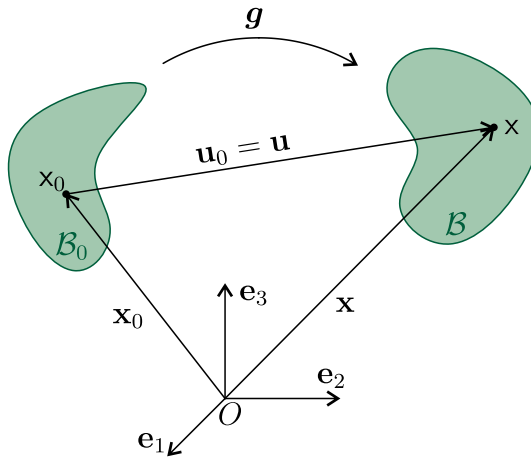


**Figure 2.1:** The particles of a body can be uniquely identified in a three-dimensional Euclidean space by defining an orthonormal basis  $\mathbf{e}_i$  by their position vector  $\mathbf{x}_i$ . The mapping of its points in the different configurations  $\mathcal{B}$  is defined by the deformation function  $\mathbf{g}$  when a reference configuration  $\mathcal{B}_0$  is selected.

The velocity field is the derivative of the motion with respect to time:

$$\mathbf{v}_0(\mathbf{x}_0, t) = \frac{\partial \mathbf{g}(\mathbf{x}_0, t)}{\partial t}; \quad \mathbf{v}(\mathbf{x}, t) = \frac{\partial \mathbf{g}^{-1}(\mathbf{x}, t)}{\partial t}. \quad (2.7)$$

it is important to note that  $\mathbf{v}_0 = \mathbf{v}$ .

The acceleration field is the second derivative of the motion with respect to time:

$$\mathbf{a}_0(\mathbf{x}_0, t) = \frac{\partial^2 \mathbf{g}(\mathbf{x}_0, t)}{\partial t^2}; \quad \mathbf{a}(\mathbf{x}, t) = \frac{\partial^2 \mathbf{g}^{-1}(\mathbf{x}, t)}{\partial t^2}. \quad (2.8)$$

it is important to note that  $\mathbf{a}_0 = \mathbf{a}$ .

Considering now two points identified by the position vectors  $\mathbf{x}_0$  and  $\mathbf{y}_0$ , where the latter is in the neighbourhood the previous, in the referential configuration  $\mathcal{B}_0$ . These points are transformed in the current configuration  $\mathcal{B}$  as:

$$\mathbf{x} = \mathbf{g}(\mathbf{x}_0); \quad \mathbf{y} = \mathbf{g}(\mathbf{y}_0), \quad (2.9)$$

If one does the Taylor series expansions of  $\mathbf{g}(\mathbf{y}_0)$  around  $\mathbf{x}_0$  obtains:

$$\mathbf{g}(\mathbf{y}_0) \approx \mathbf{g}(\mathbf{x}_0) + \frac{\partial \mathbf{g}(\mathbf{x}_0)}{\partial \mathbf{x}_0} (\mathbf{y}_0 - \mathbf{x}_0) \quad (2.10)$$

so that the vector who join the points in the deformed configuration is:

$$\mathbf{y} - \mathbf{x} = \mathbf{g}(\mathbf{y}_0) - \mathbf{g}(\mathbf{x}_0) \approx \mathbf{F}(\mathbf{x}_0)(\mathbf{y}_0 - \mathbf{x}_0) \quad (2.11)$$

where  $\mathbf{F}$  is the deformation gradient, by definition it is:

$$\mathbf{F}(\mathbf{x}_0) = \frac{\partial \mathbf{g}(\mathbf{x}_0)}{\partial \mathbf{x}_0}; \quad \mathbf{F}^{-1}(\mathbf{x}) = \frac{\partial \mathbf{g}^{-1}(\mathbf{x})}{\partial \mathbf{x}}. \quad (2.12)$$

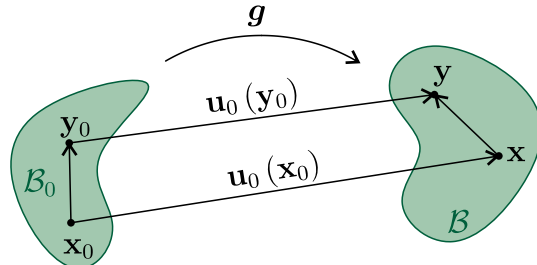


**Figure 2.2:** Two point  $\mathbf{x}_0$  and  $\mathbf{y}_0$  in the same neighborhood of a continuum body in the reference configuration  $\mathcal{B}_0$  after a deformation  $\mathbf{g}$  are mapped in  $\mathbf{x}$  and  $\mathbf{y}$ . The distance of the two point in the current configuration is ruled by the deformation gradient as  $(\mathbf{y} - \mathbf{x}) = \mathbf{F}(\mathbf{y}_0 - \mathbf{x}_0)$

While, the displacement gradient is:

$$\begin{aligned} \nabla \mathbf{u}_0 &= \frac{\partial \mathbf{u}_0}{\partial \mathbf{x}_0} = \frac{\partial \mathbf{x}}{\partial \mathbf{x}_0} - \frac{\partial \mathbf{x}_0}{\partial \mathbf{x}_0} = \mathbf{F} - \mathbf{I} \\ \nabla \mathbf{u} &= \frac{\partial \mathbf{u}}{\partial \mathbf{x}} = \frac{\partial \mathbf{x}}{\partial \mathbf{x}} - \frac{\partial \mathbf{x}_0}{\partial \mathbf{x}} = \mathbf{I} - \mathbf{F}^{-1}. \end{aligned} \quad (2.13)$$

The infinitesimal reference volume can be evaluated as:

$$dv_0 = |(\mathbf{d}\mathbf{x}_0 \times \mathbf{d}\mathbf{y}_0) \cdot \mathbf{d}\mathbf{z}_0|, \quad (2.14)$$

while the infinitesimal current volume:

$$dv = |(\mathbf{dx} \times \mathbf{dy}) \cdot \mathbf{dz}|, \quad (2.15)$$

but recalling the deformation gradient one obtains:

$$dv = |(\mathbf{F}d\mathbf{x}_0 \times \mathbf{F}d\mathbf{y}_0) \cdot \mathbf{F}d\mathbf{z}_0| = \mathcal{J}dv_0. \quad (2.16)$$

where  $\mathcal{J} = \det \mathbf{F}$  is known as the volume ratio or Jacobian determinant. Since  $\mathbf{F}$  is invertible is not possible to have  $\mathcal{J} = 0$  and because of the impenetrability of matter one expect only positive volume so the Jacobian must be positive  $\mathcal{J} > 0$ . A special case must be highlighted: when  $\mathcal{J} = 1$  the deformation is called isochoric or volume-preserving and the body keeps the volume constant during all the processes.

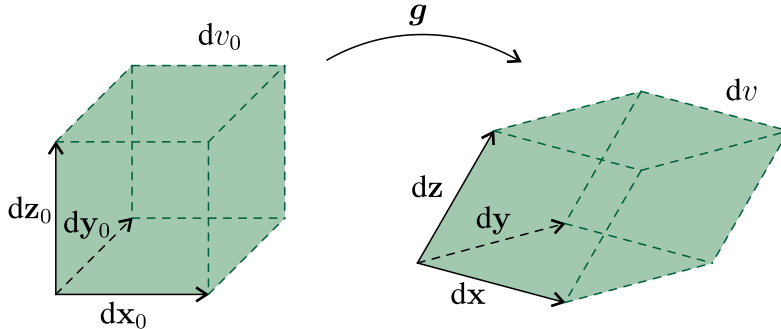


**Figure 2.3:** A reference infinitesimal cubic volume  $dv_0$  having edges  $dx_0$ ,  $dy_0$  and  $dz_0$  after a deformation  $\mathbf{g}$  is transformed in the current configuration in a prism with edges  $dx$ ,  $dy$ ,  $dz$  and volume  $dv$

If one consider now an infinitesimal deformed volume as the scalar product of an oriented area and a vector obtains:

$$dv = d\mathbf{s} \cdot d\mathbf{x} = \mathcal{J}d\mathbf{s}_0 \cdot d\mathbf{x}_0 \quad (2.17)$$

where  $d\mathbf{s} = d\mathbf{s}\mathbf{n}$  and  $d\mathbf{s}_0 = d\mathbf{s}_0\mathbf{n}_0$  denoting the oriented area in the actual and referential system. Then introducing the deformation gradient:

$$(\mathbf{F}^T d\mathbf{s} - \mathcal{J}d\mathbf{s}_0) \cdot d\mathbf{x}_0 = 0 \quad (2.18)$$

since it must be valid for every infinitesimal vector  $d\mathbf{x}_0$  one obtains the Nanson's rule:

$$d\mathbf{s} = \mathcal{J}\mathbf{F}^{-T}d\mathbf{s}_0. \quad (2.19)$$

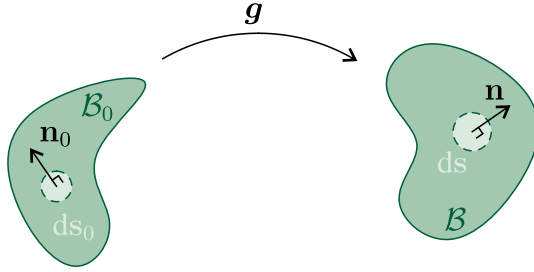


**Figure 2.4:** An infinitesimal reference oriented area  $ds_0 = ds_0 \mathbf{n}_0$  after the deformation  $\mathbf{g}$  is transformed in the current configuration via the Nanson's rule as  $ds = d\mathbf{s}\mathbf{n} = \mathcal{J}\mathbf{F}^{-T}ds_0$ .

From a material point of view, the stretch vector  $\lambda_{\mathbf{w}_0}$  in the direction of the unit vector  $\mathbf{w}_0$  at  $\mathbf{x}_0 \in \mathcal{B}_0$  can be defined as:

$$\lambda_{\mathbf{w}_0}(\mathbf{x}_0, t) = \mathbf{F}(\mathbf{x}_0, t) \mathbf{w}_0 \quad (2.20)$$

its length is the stretch ratio  $\lambda = |\lambda_{\mathbf{w}_0}|$ . According to this definition of stretch ratio a material line element can extend ( $\lambda > 1$ ), compress ( $\lambda < 1$ ) or preserve its length ( $\lambda = 1$ ). The square of the stretch ratio can be computed as:

$$\lambda^2 = \lambda_{\mathbf{w}_0} \cdot \lambda_{\mathbf{w}_0} = \mathbf{F}\mathbf{w}_0 \cdot \mathbf{F}\mathbf{w}_0 = \mathbf{w}_0 \cdot \mathbf{F}^T \mathbf{F}\mathbf{w}_0 = \mathbf{w}_0 \cdot \mathbf{C}\mathbf{w}_0 \quad (2.21)$$

where  $\mathbf{C} = \mathbf{F}^T \mathbf{F}$  is defined as the right Cauchy-Green tensor, it is symmetric and positive definite.

Analogously, in a spacial point of view the stretch vector  $\lambda_{\mathbf{w}}$  in the direction of the unit vector  $\mathbf{w}$  at  $\mathbf{x} \in \mathcal{B}$  can be defined as:

$$\lambda_{\mathbf{w}}^{-1}(\mathbf{x}, t) = \mathbf{F}^{-1}(\mathbf{x}, t) \mathbf{w} \quad (2.22)$$

its length is the inverse stretch ratio  $\lambda^{-1} = |\lambda_{\mathbf{w}}^{-1}|$ . The square of the inverse stretch ratio can be computed as:

$$\lambda^{-2} = \lambda_{\mathbf{w}} \cdot \lambda_{\mathbf{w}} = \mathbf{F}^{-1}\mathbf{w} \cdot \mathbf{F}^{-1}\mathbf{w} = \mathbf{w} \cdot \mathbf{F}^{-T}\mathbf{F}^{-1}\mathbf{w} = \mathbf{w} \cdot \mathbf{b}^{-1}\mathbf{w} \quad (2.23)$$

where  $\mathbf{b} = \mathbf{F}\mathbf{F}^T$  is defined as the left Cauchy-Green tensor, it is symmetric and positive definite.

It is always possible to decompose a tensor  $\mathbf{F}$  into a pure stretch tensor and a pure rotation tensor thanks to the polar decomposition theorem:

$$\mathbf{F} = \mathbf{R}\mathbf{U}; \quad \mathbf{F} = \mathbf{V}\mathbf{R} \quad (2.24)$$

where  $\mathbf{U} = \mathbf{C}^{1/2}$  and  $\mathbf{V} = \mathbf{B}^{1/2}$  define unique, positive definite and symmetric tensors called the right stretch tensor and left stretch tensor, while  $\mathbf{R}$  is a orthogonal tensor with  $\det \mathbf{R} = 1$  called rotation tensor.

With all these ingredients one can now write the more general strain tensor measure:

$$\mathbf{E}^{(m)} = \begin{cases} \frac{\mathbf{U}^m - \mathbf{I}}{m} & m \neq 0 \\ \log \mathbf{U} & m = 0 \end{cases}; \quad \mathbf{G}^{(m)} = \begin{cases} \frac{\mathbf{V}^m - \mathbf{I}}{m} & m \neq 0 \\ \log \mathbf{V} & m = 0 \end{cases}. \quad (2.25)$$

## 2.2 Statics

Imagine a body  $\mathcal{C}$  in the current configuration  $\mathcal{B}$  subjected to forces which act on the surface of the body  $\boldsymbol{\sigma}$  and forces which act on the interior volume of the solid  $\mathbf{b}$ . Imposing now the equilibrium of the body:

$$\begin{aligned} \int_{\mathcal{C}} \mathbf{b} + \int_{\partial\mathcal{C}} \boldsymbol{\sigma} &= \mathbf{0} \\ \int_{\mathcal{C}} (\mathbf{x} - \mathbf{o}) \times \mathbf{b} + \int_{\partial\mathcal{C}} (\mathbf{x} - \mathbf{o}) \times \boldsymbol{\sigma} &= \mathbf{0} \end{aligned} \quad (2.26)$$

where  $\mathbf{o}$  is any origin. Let the body be cut by a plane which passes any given point  $\tilde{\mathbf{x}}$  and separate the body into two portions. Postulating that another force field exists inside the body: the stress vector or traction  $\mathbf{s}$  defined per unit area. Under Cauchy hypothesis, this traction vector depends only on the unit normal  $\mathbf{n}$  and the point  $\tilde{\mathbf{x}}$  as  $\mathbf{s} = \mathbf{s}(\tilde{\mathbf{x}}, \mathbf{n})$ .

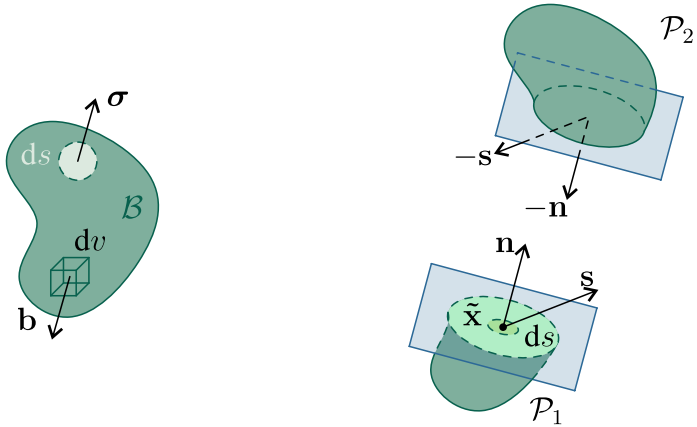


**Figure 2.5:** A body in equilibrium under surface and body forces (left). The body is cut by a plane defined by its normal  $\mathbf{n}$  to show the traction vector  $\mathbf{s}$  (right).

Since balance holds, any portion  $\mathcal{P}$  must be in equilibrium so:

$$\begin{aligned} \int_{\mathcal{P}} \mathbf{b} + \int_{\partial\mathcal{P}} \boldsymbol{\sigma} &= \mathbf{0} \\ \int_{\mathcal{P}} (\mathbf{x} - \mathbf{o}) \times \mathbf{b} + \int_{\partial\mathcal{P}} (\mathbf{x} - \mathbf{o}) \times \boldsymbol{\sigma} &= \mathbf{0} \end{aligned} \quad (2.27)$$

The Cauchy theorem state that if  $\boldsymbol{\sigma}$  and  $\mathbf{b}$  are system of forces for  $\mathcal{C}$ , a necessary and sufficient condition for (2.27) to hold for any part  $\mathcal{P} \in \mathcal{C}$  is the existence of a spatial field  $\mathbf{T}(\tilde{\mathbf{x}}, \mathbf{n})$ , the so-called Cauchy stress tensor, such that:

- the traction vector is a linear function of the unit normal  $\mathbf{n}$  through the Cauchy stress tensor

$$\mathbf{s}(\tilde{\mathbf{x}}, \mathbf{n}) = \mathbf{T}(\tilde{\mathbf{x}}, \mathbf{n}) \mathbf{n} \quad (2.28)$$

transforming the spatial unit normal to the spatial vector  $\mathbf{s}$

- the Cauchy stress tensor is symmetric

$$\mathbf{T} = \mathbf{T}^T \quad (2.29)$$

- the Cauchy stress tensor  $\mathbf{T}$  satisfies the local equilibrium equation

$$\operatorname{div} \mathbf{T} + \mathbf{b} = \mathbf{0} \quad (2.30)$$

Stress is the internal counterpart to forces applied by the environment to the body in its actual configuration: it intrinsically represents, therefore, a spatial quantity. However, the following identity may be derived easily from Nanson's formula:

$$\mathbf{T} \mathbf{n} ds = \mathbf{S} \mathbf{n}_0 ds_0 \quad (2.31)$$

where

$$\mathbf{S} = \mathcal{J} \mathbf{T} \mathbf{F}^{-T} \quad (2.32)$$

is the first Piola-Kirchhoff stress tensor and  $\mathbf{s}_0 = \mathbf{S} \mathbf{n}_0$  is the nominal traction which satisfies:

$$\int_{\partial \mathcal{P}_0} \mathbf{S} \mathbf{n}_0 = \int_{\partial \mathcal{P}} \mathbf{T} \mathbf{n} \quad (2.33)$$

Tensor  $\mathbf{S}$  is in general un-symmetric but thanks to the symmetry of  $\mathbf{T}$  the following identity holds:

$$\mathbf{S} \mathbf{F}^T = \mathbf{F} \mathbf{S}^T \quad (2.34)$$

Last consideration about the local equilibrium equation in both reference and current configuration in absence of body forces state:

$$\text{Div} \mathbf{S} = \mathbf{0}; \quad \text{div} \mathbf{T} = \mathbf{0} \quad (2.35)$$

thanks to divergence theorem:

$$\int_{\mathcal{P}_0} \mathbf{S} \mathbf{n}_0 = \mathbf{0}; \quad \int_{\mathcal{P}} \mathbf{T} \mathbf{n} = \mathbf{0} \quad (2.36)$$

showing that both first Piola-Kirchhoff and Cauchy stress tensors are solenoidal.

## 2.3 Balance Principles

Every body  $\mathcal{C}$  possesses a mass  $m$ . It is possible to define the mass as the amount of matter which define the body  $\mathcal{C}$ . The mass is a fundamental physical quantity. It is a positive scalar invariant during the motion.

In general is it possible to identify three different kinds of system: the closed, the isolated and the open system. The closed system is characterized by a fixed amount of mass. In a closed system no mass can cross the border of the system, only energy in the form of

work or heat can do that. A system in which not even energy can cross the edge is said to be isolated. Conversely, an open system is the one in which the volume is fixed and both mass and energy can cross the edge.

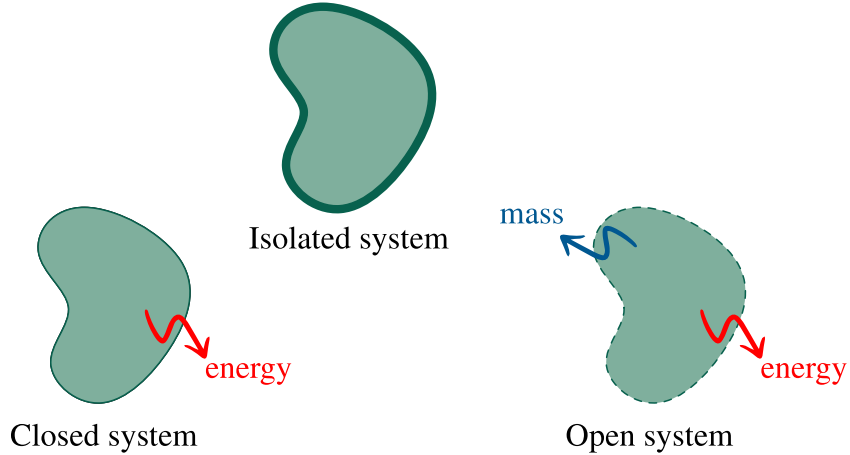


**Figure 2.6:** The closed system (left), in which no mass can cross the boundary, only energy can. The isolated system (centre), where neither mass nor energy can pass through. The open system (right) is the one in which both mass and energy can cross the boundary.

In the following treatment attention is devoted to the closed system. Starting with the consideration that mass cannot be produced or destroyed, one can writes:

$$m(\mathcal{B}_0) = m(\mathcal{B}) > 0. \quad (2.37)$$

The mass of  $\mathcal{B}_0$  and  $\mathcal{B}$  is characterized by a continuous scalar field: the mass density. The mass density is defined as:

$$\rho_0(\mathbf{x}_0) = \lim_{\Delta v_0(\mathcal{B}_0) \rightarrow 0} \frac{\Delta m(\mathcal{B}_0)}{\Delta v_0(\mathcal{B}_0)}, \quad \rho(\mathbf{x}, t) = \lim_{\Delta v(\mathcal{B}) \rightarrow 0} \frac{\Delta m(\mathcal{B})}{\Delta v(\mathcal{B})} \quad (2.38)$$

so the infinitesimal mass element is:

$$dm = \rho_0(\mathbf{x}_0) dv_0 = \rho(\mathbf{x}, t) dv > 0 \quad (2.39)$$

as a consequence the total mass:

$$m = \int_{\mathcal{B}_0} \rho_0(\mathbf{x}_0) dv_0 = \int_{\mathcal{B}} \rho(\mathbf{x}, t) dv = \text{const} > 0 \quad (2.40)$$

which implies:

$$\dot{m} = 0. \quad (2.41)$$

A relation between referential and actual mass density could be found starting from (2.40):

$$\int_{\mathcal{B}_0} [\rho_0(\mathbf{x}_0) - \rho(\mathbf{g}(\mathbf{x}_0, t), t) \mathcal{J}(\mathbf{x}_0, t)] dv_0 = 0 \quad (2.42)$$

which leads to:

$$\rho_0(\mathbf{x}_0) = \rho(\mathbf{g}(\mathbf{x}_0, t), t) \mathcal{J}(\mathbf{x}_0, t) \quad (2.43)$$

from which one can obtain:

$$\dot{\rho}_0(\mathbf{x}_0) = 0; \quad \dot{\rho}(\mathbf{x}, t) + \rho(\mathbf{x}, t) \operatorname{div} \mathbf{v}(\mathbf{x}, t) = 0. \quad (2.44)$$

The Reynolds' transport theorem, provides the material time derivative of a volume integral of a generic (either scalar or vectorial) spatial field  $\phi = \phi(\mathbf{x}, t)$ :

$$\frac{d}{dt} \int_{\mathcal{B}} \phi dv = \int_{\mathcal{B}} (\dot{\phi} + \phi \operatorname{div} \mathbf{v}) dv \quad (2.45)$$

or

$$\frac{d}{dt} \int_{\mathcal{B}} \phi dv = \int_{\mathcal{B}} \frac{\partial \phi}{\partial t} dv + \int_{\partial \mathcal{B}} \phi (\mathbf{v} \cdot \mathbf{n}) dv \quad (2.46)$$

A particular case of (2.45) is:

$$\frac{d}{dt} \int_{\mathcal{B}} \rho \phi dv = \int_{\mathcal{B}} \rho \dot{\phi} dv. \quad (2.47)$$

Considering now a body  $\mathcal{C}$  with mass density  $\rho = \rho(\mathbf{x}, t)$ , given motion  $\mathbf{x} = \mathbf{g}(\mathbf{x}_0, t)$  and spatial velocity field  $\mathbf{v} = \mathbf{v}(\mathbf{x}, t)$ , one can define linear momentum  $\mathbf{L}$  the following amount:

$$\mathbf{L}(t) = \int_{\mathcal{B}} \rho(\mathbf{x}, t) \mathbf{v}(\mathbf{x}, t) dv = \int_{\mathcal{B}_0} \rho_0(\mathbf{x}_0) \mathbf{v}_0(\mathbf{x}_0, t) dv_0 \quad (2.48)$$

and the angular momentum  $\mathbf{J}$  with respect to a fixed point  $\tilde{\mathbf{x}}$ :

$$\mathbf{J}(t) = \int_{\mathcal{B}} \mathbf{r} \times \rho(\mathbf{x}, t) \mathbf{v}(\mathbf{x}, t) dv = \int_{\mathcal{B}_0} \mathbf{r} \times \rho_0(\mathbf{x}_0) \mathbf{v}_0(\mathbf{x}_0, t) dv_0 \quad (2.49)$$

where:

$$\mathbf{r} = \mathbf{x} - \tilde{\mathbf{x}}. \quad (2.50)$$

One can now postulate that the first time derivative of the linear momentum leads to the resultant force and the first time derivative of the angular momentum to the resultant moment:

$$\begin{aligned}\dot{\mathbf{L}}(t) &= \int_{\mathcal{B}} \rho \dot{\mathbf{v}} dv = \int_{\mathcal{B}_0} \rho_0 \dot{\mathbf{v}}_0 dv_0 = \mathbf{F}(t) \\ \dot{\mathbf{J}}(t) &= \int_{\mathcal{B}} \mathbf{r} \times \rho \dot{\mathbf{v}} dv = \int_{\mathcal{B}_0} \mathbf{r} \times \rho_0 \dot{\mathbf{v}}_0 dv_0 = \mathbf{M}(t)\end{aligned}\quad (2.51)$$

where the terms  $\rho \dot{\mathbf{v}}$  and  $\rho_0 \dot{\mathbf{v}}_0$  denote the inertia forces per unit of current and reference volume respectively.

Hence, the resultant force and the resultant moment on the body have the additive forms:

$$\mathbf{F}(t) = \int_{\partial\mathcal{B}} \boldsymbol{\sigma} ds + \int_{\mathcal{B}} \mathbf{b} dv; \quad \mathbf{M}(t) = \int_{\partial\mathcal{B}} \mathbf{r} \times \boldsymbol{\sigma} ds + \int_{\mathcal{B}} \mathbf{r} \times \mathbf{b} dv \quad (2.52)$$

as a consequence the balance of linear and angular momentum in the spatial description reads:

$$\begin{aligned}\frac{d}{dt} \int_{\mathcal{B}} \rho \mathbf{v} dv &= \int_{\partial\mathcal{B}} \boldsymbol{\sigma} ds + \int_{\mathcal{B}} \mathbf{b} dv \\ \frac{d}{dt} \int_{\mathcal{B}} \mathbf{r} \times \rho \mathbf{v} dv &= \int_{\partial\mathcal{B}} \mathbf{r} \times \boldsymbol{\sigma} ds + \int_{\mathcal{B}} \mathbf{r} \times \mathbf{b} dv\end{aligned}\quad (2.53)$$

while in material description:

$$\begin{aligned}\frac{d}{dt} \int_{\mathcal{B}_0} \rho_0 \mathbf{v}_0 dv_0 &= \int_{\partial\mathcal{B}_0} \boldsymbol{\sigma}_0 dS + \int_{\mathcal{B}_0} \mathbf{b}_0 dv_0 \\ \frac{d}{dt} \int_{\mathcal{B}_0} \mathbf{r} \times \rho_0 \mathbf{v}_0 dv_0 &= \int_{\partial\mathcal{B}_0} \mathbf{r} \times \boldsymbol{\sigma}_0 dS + \int_{\mathcal{B}_0} \mathbf{r} \times \mathbf{b}_0 dv_0.\end{aligned}\quad (2.54)$$

Now, starting from (2.53)<sub>1</sub> and (2.54)<sub>1</sub> and using the divergence theorem one obtains the equation of motion respectively in spatial and material description:

$$\text{div} \mathbf{T} + \mathbf{b} = \rho \dot{\mathbf{v}}; \quad \text{Div} \mathbf{S} + \mathbf{b}_0 = \rho_0 \dot{\mathbf{v}}_0. \quad (2.55)$$

Let us now define the external power as:

$$\mathcal{P}_{\text{ext}}(t) = \int_{\partial\mathcal{B}} \boldsymbol{\sigma} \cdot \mathbf{v} ds + \int_{\mathcal{B}} \mathbf{b} \cdot \mathbf{v} dv = \int_{\partial\mathcal{B}_0} \boldsymbol{\sigma}_0 \cdot \mathbf{v}_0 dS + \int_{\mathcal{B}_0} \mathbf{b}_0 \cdot \mathbf{v}_0 dv_0 \quad (2.56)$$

the internal power as:

$$\mathcal{P}_{\text{int}}(t) = \int_{\mathcal{B}} \mathbf{T} \cdot \text{grad} \mathbf{v} dv = \int_{\mathcal{B}_0} \mathbf{S} \cdot \text{Grad} \mathbf{v}_0 dv_0 \quad (2.57)$$

the kinetic energy as:

$$\mathcal{K}(t) = \int_{\mathcal{B}} \frac{1}{2} \rho \mathbf{v}^2 dv = \int_{\mathcal{B}_0} \frac{1}{2} \rho_0 \mathbf{v}_0^2 dv_0 \quad (2.58)$$

Finally, the theorem of power expended state:

$$\frac{d}{dt} \mathcal{K}(t) + \mathcal{P}_{\text{int}}(t) = \mathcal{P}_{\text{ext}}(t) \quad (2.59)$$

in spatial description:

$$\frac{d}{dt} \int_{\mathcal{B}} \frac{1}{2} \rho \mathbf{v}^2 dv + \int_{\mathcal{B}} \mathbf{T} \cdot \text{grad} \mathbf{v} dv = \int_{\partial \mathcal{B}} \boldsymbol{\sigma} \cdot \mathbf{v} ds + \int_{\mathcal{B}} \mathbf{b} \cdot \mathbf{v} dv \quad (2.60)$$

in material description:

$$\frac{d}{dt} \int_{\mathcal{B}_0} \frac{1}{2} \rho_0 \mathbf{v}_0^2 dv_0 + \int_{\mathcal{B}_0} \mathbf{S} \cdot \text{Grad} \mathbf{v}_0 dv_0 = \int_{\partial \mathcal{B}_0} \boldsymbol{\sigma}_0 \cdot \mathbf{v}_0 dS + \int_{\mathcal{B}_0} \mathbf{b}_0 \cdot \mathbf{v}_0 dv_0 \quad (2.61)$$

which define the mechanical energy balance in deformable continuum.

## 2.4 Hyperelasticity

A material is said to be *hyperelastic* or a *Green's* material when posses a strain energy density function defined per unit of reference volume  $\Phi = \Phi(\mathbf{F})$  which depends solely on the deformation gradient  $\mathbf{F}$ . The strain energy density function is required to be polyconvex. An empirical constitutive model for hyperelastic material is:

$$\mathbf{S} = \frac{\partial \Phi(\mathbf{F})}{\partial \mathbf{F}}; \quad \mathbf{T} = \mathcal{J}^{-1} \frac{\partial \Phi(\mathbf{F})}{\partial \mathbf{F}} \mathbf{F}^T \quad (2.62)$$

For convenience, one can require that the strain energy function vanishes in the reference configuration  $\mathbf{F} = \mathbf{I}$ :

$$\Phi(\mathbf{I}) = 0 \quad (2.63)$$

From physical observation is known that the strain energy function increases with the deformation, therefore:

$$\Phi(\mathbf{F}) \geq 0 \quad (2.64)$$

Particular attention is paid to a specific class of materials: incompressible materials. A material which keeps the volume constant during the motion is characterized by the incompressible constraint  $\mathcal{J} = 1$ . A general form of constitutive equation of this class of material is:

$$\Phi = \Phi(\mathbf{F}) - p(\mathcal{J} - 1) \quad (2.65)$$

where the scalar  $p$  is introduced as a lagrangian multiplier which can be identified as a hydrostatic pressure. It can only be determined from equilibrium equations and boundary conditions. Knowing that the constitutive models are:

$$\mathbf{S} = -p\mathbf{F}^{-T} + \frac{\partial\Phi(\mathbf{F})}{\partial\mathbf{F}}; \quad \mathbf{T} = -p\mathbf{I} + \frac{\partial\Phi(\mathbf{F})}{\partial\mathbf{F}}\mathbf{F}^T \quad (2.66)$$

# 3

## Prologue: non-accidental coincidences in contact mechanics at small strain

Linear elastic solutions available in the literature for contact problems [3, 12, 13, 26, 32] are used to show that a non-null horizontal reaction force  $R_1$  is present at each (smooth, or even sharp) corner of a frictionless, rigid, flat punch indenting an elastic solid due to an external vertical load  $P$ . The presence of this nonlinear horizontal force is particularly surprising due to the fact that it is generated within the context of infinitesimal elasticity and even when the corner is sharp.

More specifically, with reference to the indentation of an elastic half space, it is shown that the horizontal reaction force  $R_1$  acting at each corner of the punch is quadratic in the external vertical load  $P$  and coincides with the negative of the path-independent  $J$ -integral evaluation at the corresponding corner, which in turn is equal to the energy release rate  $G$  associated with an infinitesimal growth of an edge of the punch, namely,

$$R_1 = \frac{(1 - \nu^2)P^2}{2\pi a E} = -J = -G, \quad (3.1)$$

where  $a$  is the punch half-width, while  $E$  and  $\nu$  are the Young's modulus and the Poisson's ratio of the indented half-space, respectively. The coincidence of the horizontal reaction  $R_1$  with the negative of the  $J$ -integral finds an explanation in the use of the energy-momentum tensor for frictionless contact problem, as shown in Ch. 4. Moreover, the interpretation of  $J$  as the energy release rate  $G$  in a configurational mechanics framework is shown in Ch. 5.

### 3.1 *J*-integral and energy release rate $G$ for the indentation of a linear elastic material with a frictionless, rigid, flat punch with sharp corners

The two-dimensional (plane strain) problem is considered in the  $x_1$ – $x_2$  plane for a frictionless, rigid, and flat punch indenting a linear elastic isotropic solid on its surface, straight in the undeformed configuration and defined by  $x_2 = 0$ .

Restricting the attention to the right corner of the indenter (located at coordinate  $x_1 = a, x_2 = 0$ ), the leading-order term in the asymptotic expansion at this point for the components of the Cauchy stress tensor  $\mathbf{T}$  in polar coordinates [ $\rho > 0, \theta \in (0, \pi)$ , so that  $x_1 = a - \rho \cos \theta, x_2 = \rho \sin \theta$ , Fig. 3.1, (a)] is given by [3, 19, 46]

$$\left\{ \begin{array}{l} T_{\rho\rho}(\rho, \theta) \\ T_{\theta\theta}(\rho, \theta) \\ T_{\rho\theta}(\rho, \theta) \end{array} \right\} = \frac{K_I}{\sqrt{2\pi\rho}} \left\{ \begin{array}{l} \cos \frac{\theta}{2} \left( 1 + \sin^2 \frac{\theta}{2} \right) \\ \cos^3 \frac{\theta}{2} \\ \sin \frac{\theta}{2} \cos^2 \frac{\theta}{2} \end{array} \right\}, \quad (3.2)$$

where  $K_I$  is the Stress Intensity Factor (SIF) representing the magnitude of the singular fields ‘condensing’ the boundary conditions as

$$K_I = \lim_{\rho \rightarrow 0} \sqrt{2\pi\rho} T_{\theta\theta}(\rho, \theta = 0). \quad (3.3)$$

It is noted that the square root singular stress asymptotics (3.2) present at the sharp corner of a frictionless rigid punch coincides with the analogue holding for a crack tip under Mode I loading conditions, when a proper linear transformation of the angular coordinate is applied. Moreover, the free surface ahead of the punch tip ( $\theta = \pi$ ) displays the following first-order term for the normal displacement  $u_\theta$  [3]

$$u_\theta(\rho, \theta = \pi) = -\frac{4(1 - \nu^2)}{E} K_I \sqrt{\frac{\rho}{2\pi}}, \quad (3.4)$$

where  $E > 0$  and  $\nu \in (-1, 1/2]$  are the Young’s modulus and Poisson’s ratio, respectively.

Introducing the elastic strain energy density  $\Phi$  and the displacement field  $u_i$ , the path-independent  $J$ -integral used in fracture

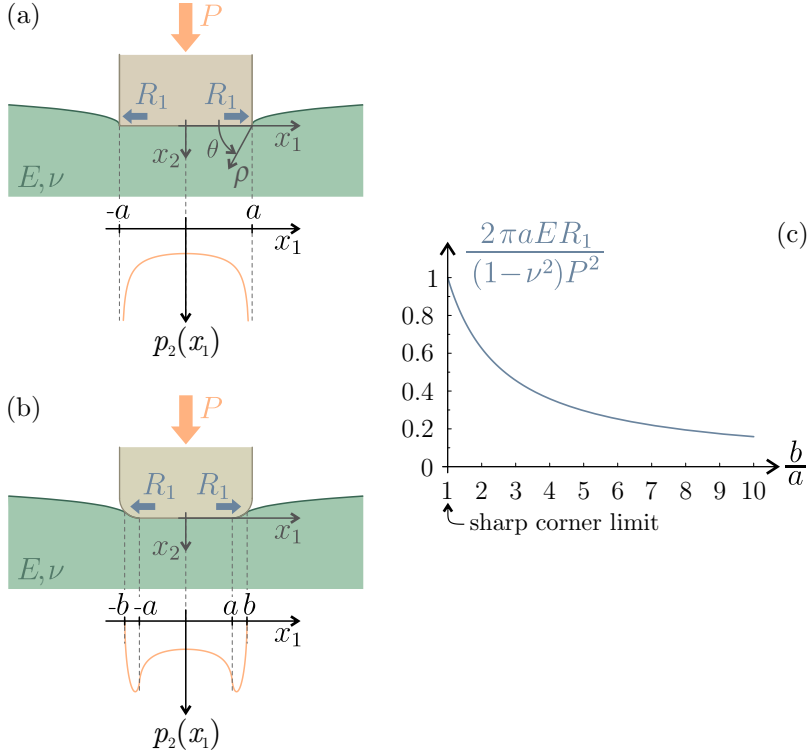


**Figure 3.1:** The planar contact of a flat punch with (a) sharp and (b) rounded corners. In both cases the contact with a linear elastic isotropic half space is frictionless and provided by a vertical force  $P$ . The vertical component  $p_2$  of the pressure along the contact surface (marked by the horizontal coordinate  $x_1$ ) is reported below the sketches (pressure is considered positive when compressive). In (c): Horizontal component  $R_1$  of the contact force reaction present at each rounded corner (made dimensionless through division by  $(1 - \nu^2)P^2/(2\pi a E)$ ) and obtained from Ciavarella et al. [12]), as a function of the parameter  $b/a \geq 1$ , describing the ratio between the width of the contact region,  $2b$ , and the width of its flat portion,  $2a$ .

mechanics at small strains is defined as [40]

$$J = \int_{\Gamma_0} \left( \Phi n_i - T_{ij} n_j \frac{\partial u_i}{\partial x_1} \right) d\gamma_0, \quad i, j = 1, 2, \quad (3.5)$$

where  $\Gamma_0$  is a continuous counter-clockwise path with outward unit normal  $n_i$ . In the context of linear elasticity, the path-independence of the  $J$ -integral, eqn (3.5), has been extended to flat punch problems by assuming the path  $\Gamma_0$  starting from beneath the indenter and ending at the free surface [32, 47] (Fig. 3.2). Reducing  $\Gamma_0$

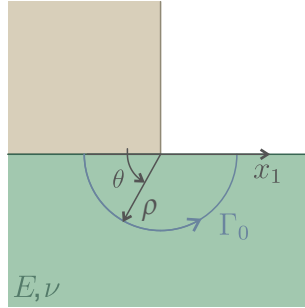


**Figure 3.2:** In the context of a rigid flat punch indenting a linear elastic isotropic half space the  $J$ -integral is performed along the semi-circular counter-clockwise path  $\Gamma_0$  starting from beneath the indenter and ending at the free surface and it is centered at the right corner.

to a semi-circular path of infinitesimal radius  $r$  and centered at the right corner, the  $J$ -integral can be rewritten in terms of polar components as

$$J = \lim_{r \rightarrow 0} \int_0^\pi [\Phi(r, \theta) \cos \theta + \\ -T_{i\rho}(r, \theta) \left( \frac{\sin \theta}{r} \frac{\partial u_i(r, \theta)}{\partial \theta} - \cos \theta \frac{\partial u_i(r, \theta)}{\partial r} \right)] r d\theta, \\ i = \rho, \theta. \quad (3.6)$$

Considering the asymptotic expressions (3.2) and the linear constitutive relations, the  $J$ -integral (3.6) for the flat rigid indentation problem results

$$J = -\frac{1-\nu^2}{2E} K_I^2 < 0, \quad (3.7)$$

which differs by a factor  $-2$  from the  $J$ -integral found for Mode I fracture. Similarly to rigid line inclusion problems [7, 20], the  $J$ -integral associated to the flat punch with sharp corners is always non-positive.

Following Rice [41], the energy release rate  $G$ , associated with a growth  $\Delta\xi$  of the punch corner and defined as the negative of the derivative of the potential energy  $\mathcal{V}$  with respect to the configurational parameter  $\xi$ , can be evaluated as

$$G = -\frac{d\mathcal{V}(\xi)}{d\xi} = \lim_{\Delta\xi \rightarrow 0} \frac{1}{2\Delta\xi} \int_0^{\Delta\xi} T_{\theta\theta}(\Delta\xi - r, 0) u_\theta(r, \pi) dr, \quad (3.8)$$

which, considering the asymptotic expansions (3.2) and (3.4), equals the  $J$ -integral

$$G = J < 0. \quad (3.9)$$

Equation (3.9) shows that a growth in the punch size leads to an increase of the total potential energy of the system, implying that the process is not favourable, as in the stiffener problem, but opposite to crack growth where the energy release is always positive for an advance of the tip.

It is noted that, although the path-independent  $J$ -integral, eqn (3.5), was already known in flat punch problems of linear elasticity it has never been related to the energy release rate  $G$  associated with a flat punch growth. Indeed, the  $J$ -integral has been so far used only in the investigation of failure mechanisms connected with crack initiation [32] or dislocation nucleation [31] at the sharp corners of flat punches. Moreover, in [47] the  $J$ -integral was found to be null for a rigid-body sliding of the whole punch, a result which is correct, but trivial because the two opposite forces  $R_1$  cancel each other (Fig. 3.1).

**Indenting an elastic half space.** The above results can be used to analyze a linear elastic isotropic half space ( $x_1 \in (-\infty, \infty)$ ,  $x_2 > 0$ ) indented by a (frictionless, rigid, and flat) punch, with horizontal base of width  $2a$  (and centered at  $x_1 = x_2 = 0$ ). When the punch is subjected to a given compressive normal force  $P$  (Fig. 3.1, (a)), the pressure distribution  $p(x_1)$  (positive when compressive) at the contact has only a vertical component ( $p_1(x_1) = 0$ ,  $p_2(x_1) > 0$ ) given by [26]

$$p(x_1) = p_2(x_1) = \frac{P}{\pi \sqrt{a^2 - x_1^2}}, \quad (3.10)$$

which approaches an infinite value at the two sharp corners ( $x_1 = \pm a$ ) and leads to the following stress  $T_{ij}$  ( $i, j = 1, 2$ ) distribution [42]

$$\left\{ \begin{array}{l} T_{11}(x_1, x_2) \\ T_{22}(x_1, x_2) \\ T_{12}(x_1, x_2) \end{array} \right\} = -\frac{2P}{\pi^2} \left\{ \begin{array}{l} x_2 \int_{-a}^a \frac{(x_1 - s)^2}{\sqrt{a^2 - s^2} [(x_1 - s)^2 + x_2^2]^2} ds \\ x_2^3 \int_{-a}^a \frac{1}{\sqrt{a^2 - s^2} [(x_1 - s)^2 + x_2^2]^2} ds \\ x_2^2 \int_{-a}^a \frac{x_1 - s}{\sqrt{a^2 - s^2} [(x_1 - s)^2 + x_2^2]^2} ds \end{array} \right\}. \quad (3.11)$$

Considering the full-field representation (3.11) for the stress  $\mathbf{T}$ , the Stress Intensity Factor (SIF)  $K_I$  (3.3) for a flat punch of width  $2a$  subject to a vertical load  $P$  indenting an elastic half space results to be [19, 46]

$$K_I = -\frac{P}{\sqrt{\pi a}}, \quad (3.12)$$

and the  $J$ -integral (3.7) reduces to

$$J = -\frac{1-\nu^2}{2\pi a E} P^2 < 0. \quad (3.13)$$

Exploiting the path-independence of the  $J$ -integral and the null value of its integrand at the punch contact and at the free surface (namely,  $x_2 = 0$  and excluding the corner point) and at infinite (namely,  $\sqrt{x_1^2 + x_2^2} \rightarrow \infty$ ), the  $J$ -integral (3.13) can be evaluated as

$$J = - \int_0^\infty \left[ \Phi(x_1, x_2) - T_{11}(x_1, x_2) \frac{\partial u_1(x_1, x_2)}{\partial x_1} \right] \Big|_{x_1=0} dx_2. \quad (3.14)$$

Within the context of configurational mechanics for an hyperelastic solid undergoing large deformations, the  $J$ -integral, eqn (3.5), is proven in Ch. 5 to equal the energy release associated with an increase in the size of the frictionless straight constraint with a corner and therefore to correspond to the horizontal force exerted by the elastic solid on the rigid constraint. This result is anticipated below for the rigid flat punch, by showing that the negative of the  $J$ -integral (3.7) matches the horizontal reaction force at its corner. To this purpose, an indenter with rounded corners is considered in the Sect. 3.2, including the limit of vanishing curvature radius.

### 3.2 Horizontal contact reaction force $R_1$ at the indenter with rounded corner in linear elasticity

A rigid punch with rounded corners is considered (Fig. 3.1, (b)), with a central flat portion of width  $2a$ , rounded at both ends with a parabola of radius of curvature  $R$ , described by  $x_2 = h(x_1)$ . The latter function has the following derivative

$$h'(x_1) = \begin{cases} 0, & \text{if } x_1 \in [-a, a], \\ -\frac{x_1 \mp a}{R}, & \text{if } x_1 \in [\pm a, \pm b], \end{cases} \quad (3.15)$$

where  $2b \geq 2a$  defines the unknown contact width, measured as the projection of the contact zone onto  $x_1$ . On introduction of a mapping for the horizontal coordinate  $x_1 \in [-b, b]$  in terms of the angle  $\phi \in [-\pi/2, \pi/2]$  as

$$x_1(\phi) = \frac{\sin \phi}{\sin \phi_0} a, \quad \text{with} \quad b = \frac{a}{\sin \phi_0}, \quad (3.16)$$

the component  $p_2(x_1)$  of the pressure distribution  $p$  at the contact is evaluated for an applied vertical force  $P$  as [12, 13, 28]

$$\begin{aligned} p_2(\phi) = & \frac{2P}{\pi(\pi - 2\phi_0 - \sin 2\phi_0)b} \left\{ (\pi - 2\phi_0) \cos \phi \right. \\ & \left. + \ln \left[ \left| \frac{\sin(\phi + \phi_0)}{\sin(\phi - \phi_0)} \right|^{\sin \phi} \left| \tan \frac{\phi + \phi_0}{2} \tan \frac{\phi - \phi_0}{2} \right|^{\sin \phi_0} \right] \right\}. \end{aligned} \quad (3.17)$$

The unknown angle  $\phi_0 \in (0, \pi/2]$  (and therefore the corresponding detachment semi-distance  $b \geq a$ ) can be evaluated as the solution of the following nonlinear equation

$$\frac{(1 - \nu^2)PR}{a^2 E} = \frac{\pi - 2\phi_0}{4 \sin^2 \phi_0} - \frac{\cot \phi_0}{2}. \quad (3.18)$$

Note that the pressure distribution  $p_2(x_1)$ , eqn (3.17), has never been exploited to evaluate the horizontal resultant force  $R_1$  of the contact pressure at each rounded corner, where the two forces have opposite directions and thus satisfy equilibrium. Such horizontal resultant  $R_1$  can be calculated as the following positive quantity

$$\begin{aligned} R_1 &= - \int_a^b p_2(x_1) h'(x_1) dx_1 \\ &= \frac{a^2}{R \sin \phi_0} \int_{\phi_0}^{\frac{\pi}{2}} p_2(\phi) \left( \frac{\sin \phi}{\sin \phi_0} - 1 \right) \cos \phi d\phi > 0, \end{aligned} \quad (3.19)$$

confirming that the horizontal reaction  $R_1$  has an outward direction at each rounded corner. Exploiting eqns (3.17) and (3.18), the horizontal force  $R_1$  (3.19) can be rewritten as

$$\begin{aligned} R_1 &= \frac{8(1 - \nu^2)P^2 \sin \phi_0}{\pi a E (\pi - 2\phi_0 - \sin 2\phi_0)^2} \int_{\phi_0}^{\frac{\pi}{2}} (\sin \phi - \sin \phi_0) \{ (\pi - 2\phi_0) \cos \phi \\ &+ \ln \left[ \left| \frac{\sin(\phi + \phi_0)}{\sin(\phi - \phi_0)} \right|^{\sin \phi} \left| \tan \frac{\phi + \phi_0}{2} \tan \frac{\phi - \phi_0}{2} \right|^{\sin \phi_0} \right] \} d\phi. \end{aligned} \quad (3.20)$$

The horizontal reaction force  $R_1$ , present at each rounded corner, can be evaluated through a numerical integration of equation (3.20). The result is reported in Fig. 3.1 (c), where the force is represented as a function of the ratio  $b/a \geq 1$ .

The expression for the horizontal force  $R_1$ , eqn (3.20), can be expanded by assuming a vanishing small contact region at the rounded corner ( $\phi_0 \rightarrow \pi^-/2$ ,  $b \rightarrow a^+$ ) as follows

$$R_1(b/a) = \frac{(1 - \nu^2)P^2}{2\pi a E} \left[ 1 - \frac{3}{5} \left( \frac{b}{a} - 1 \right) \right] + o(b/a - 1), \quad (3.21)$$

which shows that the horizontal reaction attains a non-null finite value in the case of non-rounded, and therefore sharp, corner ( $b \rightarrow a^+$ ),

$$\lim_{b \rightarrow a^+} R_1(b/a) = \frac{(1 - \nu^2)P^2}{2\pi a E}. \quad (3.22)$$

The above equation confirms the presence of a non-null horizontal reaction force  $R_1$  at each sharp corner of a frictionless rigid indenter, which is quadratic in  $P$ , similarly to the configurational force acting on an inextensible rod constrained with a sliding sleeve [1, 5, 14, 37]. Interestingly, the limit value of the horizontal reaction  $R_1$ , eqn (3.22), equals the negative of the  $J$ -integral and the energy release rate  $G$ , evaluated for the flat punch problem, eqs (3.7) and (3.9), namely

$$\lim_{b \rightarrow a^+} R_1(b/a) = -J = -G. \quad (3.23)$$

The coincidence of the reaction force component  $R_1$  with the negative of the  $J$ -integral is proven in the next Chapter within a finite elasticity framework, where both cases of contact with a sharp corner or a rounded surface are addressed. Moreover, through the evaluation of energy variation for an increase of the frictionless rigid surface of a flat indenter, the  $J$ -integral is found in Ch. 5 to coincide with the energy release rate  $G$  and therefore representative of a configurational force component (called  $F_1^c$ ).

# 4

## Frictionless contact reaction component $R_1$ through energy-momentum tensor(s) and $J$ -integral

It is shown that the reaction component force  $R_1$  acting at the contact between a frictionless constraint and an elastic solid coincide with the negative of the  $J$ -integral, even when large deformations occur and the end of the constraint is both a smooth or sharp corner. To this purpose, the definition (3.5) for the  $J$ -integral is extended as follows

$$J = \int_{\Gamma_0} \left( \Phi n_1^0 - S_{ij} n_j^0 \frac{\partial u_i}{\partial x_1^0} \right) d\gamma_0, \quad i, j = 1, 2, \quad (4.1)$$

where  $\mathbf{S}$  is the first Piola-Kirchhoff stress tensor,  $\Gamma_0$  is a counter-clockwise path with initial and final points selected on the boundary in contact, and the superscript 0 stands for quantities evaluated in the undeformed configuration.

After recalling concepts of finite elasticity, frictionless contact, and energy momentum tensors, the  $J$ -integral is shown to provide the reaction force component  $R_1$  acting on a generic portion of a smooth contact region  $\partial\mathcal{P}_0^{\text{tou}}$  of an elastic solid defined as the undeformed domain  $\mathcal{B}_0$ , namely,

$$R_1(\partial\mathcal{P}_0^{\text{tou}}) = -J(\Gamma_0 \equiv \partial\mathcal{P}_0 \setminus \partial\mathcal{P}_0^{\text{tou}}), \quad \forall \mathcal{P}_0 \in \mathcal{B}_0, \quad (4.2)$$

and therefore the path independence of  $J$  holds only for every path  $\Gamma_0$  emanating from a selected point ( $A_0$  in Fig. 4.1) and ending to another fixed point ( $B_0$  in Fig. 4.1). Points  $A_0$  and  $B_0$  enclose a given portion of the boundary  $\partial\mathcal{P}_0^{\text{tou}}$ .

Assuming proper regularity conditions, equation (4.2) holds true even for a flat indenter with a sharp corner, where point  $A_0$  is located in the contact region, while point  $B_0$  on the right of the corner, on a free boundary. Therefore, the reaction force  $R_1$  at the sharp corner can be evaluated as the negative of the  $J$ -integral,

$$R_1 = -J(\Gamma_0), \quad \forall \Gamma_0, \quad (4.3)$$

where  $\Gamma_0$  is any contour enclosing the corner, so that  $J$  is path-independent with regards to every pair of points  $A_0$  and  $B_0$ . An-

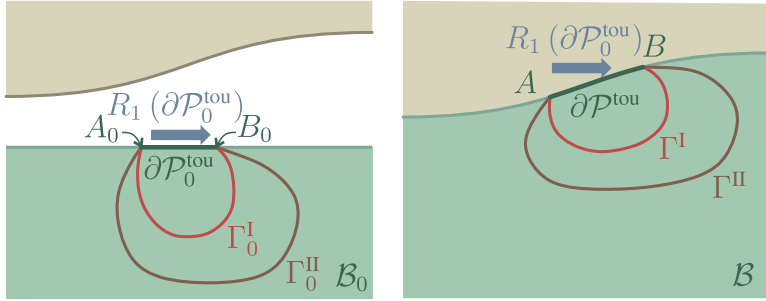


**Figure 4.1:** Undeformed (left) and deformed (right) configurations for an elastic solid (green) having its initially flat boundary in frictionless contact with a rigid constraint (brown) with smooth boundary. The contact reaction force  $R_1$  associated with the contact region  $\partial\mathcal{P}_0^{\text{tou}}$  can be evaluated through the  $J$ -integral, whose path-independence is restricted to all paths  $\Gamma_0$  ( $\Gamma_0^I$  and  $\Gamma_0^{II}$  in the reference configuration,  $\Gamma^I$  and  $\Gamma^{II}$  in the current one) emanating from the same initial point ( $A_0$  in the reference configuration and  $A$  in the current) and terminating at the same final ( $B_0$  and  $B$ ) point.

ticipating results obtained at the end of this Chapter, it can be pointed out that the application of eqn (4.2) to rectangular elastic solids with edges subject to uniform loading conditions, as sketched in both parts of Fig. 1.1, provides the estimation of the reaction force component  $R_1$  at both sharp and rounded corner as given by eqn (1.2).

## 4.1 Frictionless contact problem: target and contactor

The boundary of a rigid and frictionless constraint, called ‘target’, is described by the implicit surface (assumed here smooth for simplicity, Fig. 4.2)

$$\Sigma(\mathbf{x}) = 0, \quad (4.4)$$

so that the points  $\mathbf{x}$  in the current configuration can be divided in three disjoint sets as:

$$\Sigma(\mathbf{x}) : \begin{cases} < 0, & \text{points } \mathbf{x} \text{ inside the constraint,} \\ = 0, & \text{points } \mathbf{x} \text{ on the constraint boundary,} \\ > 0, & \text{points } \mathbf{x} \text{ outside the constraint.} \end{cases} \quad (4.5)$$

The ‘contactor’ body, in its reference configuration  $\mathcal{B}_0$ , assumed undeformed, is transformed through a sufficiently regular function  $\mathbf{g}(\mathbf{x}_0)$ , to become in frictionless contact with the target, thus reaching an *equilibrium* configuration  $\mathcal{B}$  under the action of prescribed dead tractions on  $\partial\mathcal{B}^\sigma$  and displacements on  $\partial\mathcal{B}_0^u$ . Therefore, points of boundary  $\mathbf{x} = \mathbf{g}(\mathbf{x}_0) \in \partial\mathcal{B}$ , transformed of the corresponding points in the reference configuration  $\mathbf{x}_0 \in \partial\mathcal{B}_0$ , can be classified as:

- Points  $\mathbf{x}$  (equivalently,  $\mathbf{x}_0$ ) belonging to  $\partial\mathcal{B}^{\text{sep}}$  ( $\partial\mathcal{B}_0^{\text{sep}}$ ) separated from the constraint, when  $\mathbf{x} = \mathbf{g}(\mathbf{x}_0)$  are outside the constraint, set (4.5)<sub>3</sub>;
- Points  $\mathbf{x}$  (equivalently,  $\mathbf{x}_0$ ) belonging to  $\partial\mathcal{B}^{\text{tou}}$  ( $\partial\mathcal{B}_0^{\text{tou}}$ ) touching the constraint, when  $\mathbf{x} = \mathbf{g}(\mathbf{x}_0)$  is on the boundary of the constraint, set (4.5)<sub>2</sub>.

The subset of separated points  $\partial\mathcal{B}_0^{\text{sep}}$  can be partitioned as subject to prescribed loading (assumed dead for simplicity) or displacement

$$\partial\mathcal{B}_0^{\text{sep}} \equiv \partial\mathcal{B}_0^u \cup \partial\mathcal{B}_0^\sigma, \quad \text{and equivalently } \partial\mathcal{B}^{\text{sep}} \equiv \partial\mathcal{B}^u \cup \partial\mathcal{B}^\sigma. \quad (4.6)$$

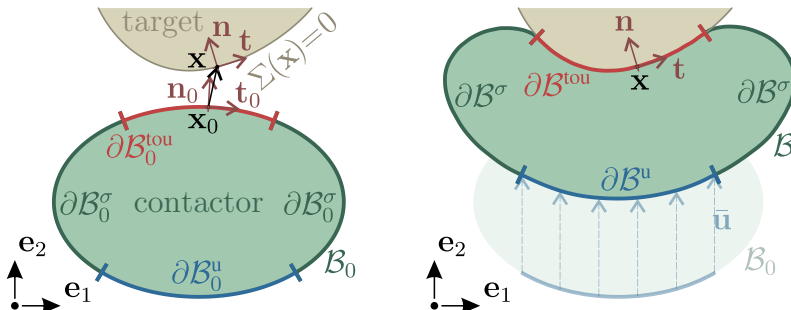


**Figure 4.2:** The contact problem between a ‘contactor’ elastic body (green) and a rigid and frictionless ‘target’ (brown). Left: The point  $\mathbf{x}_0$  on the boundary of the body in the reference configuration has unit outward normal  $\mathbf{n}_0$  and unit tangent  $\mathbf{t}_0$ . Right: The deformation transforms these quantities to  $\mathbf{x}$  on the contact surface and to  $\mathbf{n}$  and  $\mathbf{t}$ , which become the inward unit normal and the tangent to the target, respectively. The contact is sketched as the result of an imposed displacement  $\bar{\mathbf{u}}$  on  $\partial\mathcal{B}_0$ .

It is assumed that a portion of the boundary outside  $\partial\mathcal{B}^{\text{tou}}$  and bordering with it at its two edges exists, where tractions are null, so that the ends of the constraint can be moved on a free portion of the boundary of the elastic body.

The subset of touching points  $\partial\mathcal{B}_0^{\text{tou}}$  can be subdivided into a subtle partition, with reference to the Cauchy stress  $\mathbf{T}$  and its spatial counterpart of the first Piola-Kirchhoff stress  $\mathbf{S}$ , eqn (2.62), as

$$\begin{aligned} \text{Grazing} \quad & \partial\mathcal{B}^G := \{ \mathbf{x} \in \partial\mathcal{B}^{\text{tou}} \mid \mathbf{T}\mathbf{n} = \mathbf{0} \}, \\ \text{and equivalently} \quad & \partial\mathcal{B}_0^G := \{ \mathbf{x}_0 \in \partial\mathcal{B}_0^{\text{tou}} \mid \mathbf{S}\mathbf{n}_0 = \mathbf{0} \}, \\ \text{Full contact} \quad & \partial\mathcal{B}^C := \{ \mathbf{x} \in \partial\mathcal{B}^{\text{tou}} \mid \mathbf{n} \cdot \mathbf{T}\mathbf{n} < 0 \}, \\ \text{and equivalently} \quad & \partial\mathcal{B}_0^C := \{ \mathbf{x}_0 \in \partial\mathcal{B}_0^{\text{tou}} \mid \mathbf{n}_0 \cdot \mathbf{F}^{-1}\mathbf{S}\mathbf{n}_0 < 0 \}, \end{aligned} \quad (4.7)$$

where grazing (full contact) defines the condition for surfaces of target and contactor occupying the same region without (with) force interaction, so that

$$\partial\mathcal{B}_0^{\text{tou}} \equiv \partial\mathcal{B}_0^G \cup \partial\mathcal{B}_0^C, \quad \text{and equivalently } \partial\mathcal{B}^{\text{tou}} \equiv \partial\mathcal{B}^G \cup \partial\mathcal{B}^C. \quad (4.8)$$

In both the above cases along the touching boundary, the frictionless contact condition holds

$$\begin{aligned} (\mathbf{I} - \mathbf{n} \otimes \mathbf{n})\mathbf{T}\mathbf{n} &= \mathbf{0} \quad \text{on } \partial\mathcal{B}^{\text{tou}}, \\ \text{and equivalently} \quad & (\mathbf{I} - \mathbf{F}^{-T}\mathbf{n}_0 \otimes \mathbf{F}^{-T}\mathbf{n}_0)\mathbf{S}\mathbf{n}_0 = \mathbf{0} \quad \text{on } \partial\mathcal{B}_0^{\text{tou}}, \end{aligned} \quad (4.9)$$

which can also be rewritten with reference to every tangent vectors  $\mathbf{t}_0$  and  $\mathbf{t}$  ( $\mathbf{t} \cdot \mathbf{n} = \mathbf{t}_0 \cdot \mathbf{n}_0 = 0$ ) as

$$\mathbf{t} \cdot \mathbf{T}\mathbf{n} = 0 \quad \text{on } \partial\mathcal{B}^{\text{tou}}, \quad \text{and equivalently} \quad \mathbf{t}_0 \cdot \mathbf{F}^T \mathbf{S} \mathbf{n}_0 = 0 \quad \text{on } \partial\mathcal{B}_0^{\text{tou}}. \quad (4.10)$$

Interestingly, eqn (2.13) shows that the eqn (4.10)<sub>2</sub> implies the validity of the following identity at every point of the frictionless contact surface in the undeformed configuration

$$\mathbf{t}_0 \cdot \mathbf{S}\mathbf{n}_0 = -\mathbf{t}_0 \cdot (\nabla \mathbf{u})^T \mathbf{S} \mathbf{n}_0, \quad \text{on } \partial\mathcal{B}_0^{\text{tou}}. \quad (4.11)$$

An application of the virtual work principle to the mechanics of sliding contact is provided for completeness in Appendix B.

## 4.2 Two energy-momentum tensors

Two different definitions of the energy-momentum tensor for solids subject to large deformation can be found in the literature. In particular, Eshelby [17] introduced the energy-momentum tensor  $\mathbf{P}$  as

$$\mathbf{P} = \Phi \mathbf{I} - (\nabla \mathbf{u})^T \mathbf{S}, \quad (4.12)$$

while Gurtin [22] defined a different energy-momentum tensor  $\mathbf{C}$  as<sup>1</sup>

$$\mathbf{C} = \Phi \mathbf{I} - \mathbf{F}^T \mathbf{S}, \quad (4.13)$$

where the two tensors can easily be related using the definition (2.13)<sub>2</sub> of the deformation gradient  $\mathbf{F}$  as

$$\mathbf{C} = \mathbf{P} - \mathbf{S}. \quad (4.14)$$

It is noted that the  $J$ -integral (4.1) involves the energy-momentum tensor  $\mathbf{P}$ , because it can be rewritten as

$$J = \mathbf{e}_1 \cdot \int_{\Gamma_0} \mathbf{P} \mathbf{n}_0 d\gamma_0. \quad (4.15)$$

The divergence of the energy-momentum tensor  $\mathbf{C}$  (4.13) can be evaluated as

$$\frac{\partial C_{ij}}{\partial x_j^0} = \frac{\partial \Phi}{\partial x_i^0} - \frac{\partial F_{ki}}{\partial x_j^0} S_{kj} - F_{ki} \frac{\partial S_{kj}}{\partial x_j^0}, \quad (4.16)$$

which, recalling the constitutive relation (2.62), simplifies to

$$\frac{\partial C_{ij}}{\partial x_j^0} = S_{hk} \frac{\partial F_{hk}}{\partial x_i^0} - \frac{\partial F_{ki}}{\partial x_j^0} S_{kj} - F_{ki} \frac{\partial S_{kj}}{\partial x_j^0}. \quad (4.17)$$

Considering again the definition (2.13)<sub>2</sub> of the deformation gradient  $\mathbf{F}$ , the application of the Schwarz theorem implies

$$S_{hk} \frac{\partial F_{hk}}{\partial x_i^0} - \frac{\partial F_{ki}}{\partial x_j^0} S_{kj} = S_{hk} \frac{\partial^2 x_h}{\partial x_k^0 \partial x_i^0} - \frac{\partial^2 x_k}{\partial x_i^0 \partial x_j^0} S_{kj} = 0, \quad (4.18)$$

so that eqn (4.17) further simplifies as

$$\frac{\partial C_{ij}}{\partial x_j^0} = -F_{ki} \frac{\partial S_{kj}}{\partial x_j^0}. \quad (4.19)$$

<sup>1</sup> The divergence operator here used is, in Cartesian rectangular coordinates,  $(\text{Div } \mathbf{C})_i = \partial C_{ij}/\partial x_j^0$ . If the definition of divergence is changed, so that the first index is repeated, the transpose of  $\mathbf{C}$  is accordingly used, as in [10]. A further definition of energy-momentum tensor has been introduced by Maugin [34].

Due to equilibrium equation (2.35), eqn (4.19) implies the null divergence of both the energy momentum tensors  $\mathbf{C}$  and  $\mathbf{P}$ ,

$$\text{Div } \mathbf{C} = \mathbf{0}, \quad \text{Div } \mathbf{P} = \mathbf{0}. \quad (4.20)$$

Assuming continuity of the fields and therefore *excluding material discontinuities and stress singularities within the generic volume  $\mathcal{P}_0 \subseteq \mathcal{B}_0$  described by its boundary  $\partial\mathcal{P}_0$* , the divergence theorem yields

$$\int_{\partial\mathcal{P}_0} \mathbf{C}\mathbf{n}_0 = \mathbf{0}, \quad \int_{\partial\mathcal{P}_0} \mathbf{P}\mathbf{n}_0 = \mathbf{0}, \quad (4.21)$$

showing that both the energy momentum tensors  $\mathbf{C}$  and  $\mathbf{P}$  are solenoidal, as the first Piola-Kirchhoff stress tensor  $\mathbf{S}$ , eqn (2.36), is.

The solenoidal property is now used to solve the equilibrium condition of a solid loaded through a generic pressure loading  $p(\mathbf{x})$  on its boundary  $\partial\mathcal{B}$ , so that the static boundary condition is

$$\mathbf{T}\mathbf{n} = -p\mathbf{n}, \quad \text{on } \partial\mathcal{B}, \quad (4.22)$$

which, by considering the traction equivalence (2.31), implies

$$\mathbf{S}\mathbf{n}_0 = -p\mathcal{J}\mathbf{F}^{-T}\mathbf{n}_0 = -p\frac{da}{da_0}\mathbf{n}, \quad \text{on } \partial\mathcal{B}_0 \text{ and } \partial\mathcal{B}, \quad (4.23)$$

and therefore

$$\mathbf{F}^T\mathbf{S}\mathbf{n}_0 = -p\mathcal{J}\mathbf{n}_0, \quad \text{on } \partial\mathcal{B}_0. \quad (4.24)$$

It follows that under the pressure loading of (4.22), the solenoidal property (4.21) for the energy-momentum tensor  $\mathbf{C}$  can be expressed for  $\partial\mathcal{P}_0 \equiv \partial\mathcal{B}_0$  as

$$\int_{\partial\mathcal{B}_0} (\Phi + p\mathcal{J})\mathbf{n}_0 = \mathbf{0}. \quad (4.25)$$

Equation (4.25) applies to any (non-singular) solid boundary  $\partial\mathcal{B}_0$  and any non-uniform distribution of the pressure  $p$ . Equation (4.25) relates the elastic energy to the pressure (multiplied by  $\mathcal{J}$ ) on the boundary and is trivially satisfied when  $\Phi$  and  $p\mathcal{J}$  are uniform. It is noted that the pressure loading  $p(\mathbf{x})$  on the boundary can be realized through the contact with both a unilateral or a bilateral frictionless constraint. While  $p \geq 0$  for unilateral contact,  $p$  may have any sign when the contact becomes bilateral. The latter contact condition will be visualized in the following as obtained with rollers.

If the boundary  $\partial\mathcal{B}_0$  is subjected to a pressure  $p$  only on its portion  $\partial\mathcal{B}_0^p \subset \partial\mathcal{B}_0$ , equation (4.25) changes into

$$\int_{\partial\mathcal{B}_0^p} (\Phi + p\mathcal{J}) \mathbf{n}_0 + \int_{\partial\mathcal{B}_0 \setminus \partial\mathcal{B}_0^p} \mathbf{C}\mathbf{n}_0 = \mathbf{0}, \quad (4.26)$$

where the appropriate boundary conditions have to be imposed on  $\partial\mathcal{B}_0 \setminus \partial\mathcal{B}_0^p$ . In terms of tensor  $\mathbf{P}$ , an equivalent of equation (4.26) is obtained as

$$\int_{\partial\mathcal{B}_0^p} [\Phi\mathbf{I} + p\mathcal{J}(\mathbf{I} - \mathbf{F}^{-T})] \mathbf{n}_0 + \int_{\partial\mathcal{B}_0 \setminus \partial\mathcal{B}_0^p} \mathbf{P}\mathbf{n}_0 = \mathbf{0}. \quad (4.27)$$

### 4.3 Different energy-momentum tensors in the solution of rectangular elastic domains under pressure loading

Attention is now restricted to plane problems of solids with an undeformed rectangular domain  $\mathcal{B}_0$ , having sides parallel and orthogonal to the two unit vectors  $\mathbf{e}_1$  and  $\mathbf{e}_2$  defining the Cartesian reference system. Thus the domain is described as

$$\mathcal{B}_0 := \{x_1^0 \in [0, \ell_0], x_2^0 \in [h_0/2, -h_0/2]\}, \quad (4.28)$$

where  $\ell_0$  and  $h_0$  are respectively the length of the sides parallel to  $\mathbf{e}_1$  and  $\mathbf{e}_2$ . The boundary  $\partial\mathcal{B}_0$  is given by the union of the four rectangle sides  $\partial\mathcal{B}_0 \equiv \partial\mathcal{B}_0^l \cup \partial\mathcal{B}_0^a \cup \partial\mathcal{B}_0^r \cup \partial\mathcal{B}_0^b$ , with corresponding outward unit normal  $\mathbf{n}_0$  respectively equal to  $-\mathbf{e}_1$ ,  $\mathbf{e}_2$ ,  $\mathbf{e}_1$ , and  $-\mathbf{e}_2$ , Fig. 4.3. A pressure loading condition  $p$  is considered on the boundary portions  $\partial\mathcal{B}_0^a$  and  $\partial\mathcal{B}_0^b$ , constraining the traction vector to

$$\mathbf{T}\mathbf{n} = -p\mathbf{n}, \quad \text{on } \partial\mathcal{B}_0^a \cup \partial\mathcal{B}_0^b. \quad (4.29)$$

#### 4.3.1 Reaction forces $R_1^a + R_1^b$ and $R_1(\partial\mathcal{P}_0^{\text{tou}})$ from the energy momentum tensor $\mathbf{P}$

The projection along  $\mathbf{e}_1$  of the soleinodal property of  $\mathbf{P}$ , eqn (4.21)<sub>2</sub>, implies that

$$\mathbf{e}_1 \cdot \int_{\partial\mathcal{B}_0^a \cup \partial\mathcal{B}_0^b} \mathbf{P}\mathbf{n}_0 = -\mathbf{e}_1 \cdot \int_{\partial\mathcal{B}_0^l \cup \partial\mathcal{B}_0^r} \mathbf{P}\mathbf{n}_0, \quad (4.30)$$

where the left hand side, because of the applied pressure loading (4.29), the related property (4.11) and the special choice of  $\mathbf{n}_0 = \mathbf{e}_2$ ,

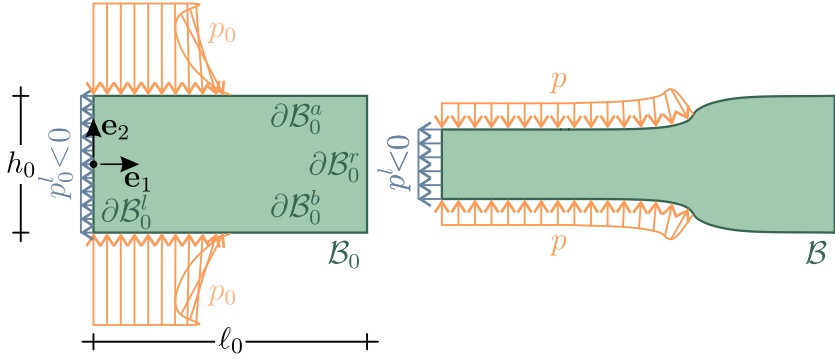


**Figure 4.3:** Left: An elastic solid of undeformed rectangular shape  $\partial\mathcal{B}_0$  with the image of a pressure loading distribution  $p$ , symmetric with respect to  $\mathbf{e}_1$ , on the boundary portions  $\partial\mathcal{B}_0^l$ ,  $\partial\mathcal{B}_0^a$ , and  $\partial\mathcal{B}_0^r$ . Right: Deformed configuration. Exploiting the concept of energy-momentum tensor  $\mathbf{C}$ , the resultant of the unknown loading pressure  $p^l$ , enforcing equilibrium, can be evaluated with an excellent approximation through eqn (1.2).

can be rewritten as

$$\mathbf{e}_1 \cdot \int_{\partial\mathcal{B}_0^a \cup \partial\mathcal{B}_0^b} \mathbf{P}\mathbf{n}_0 = \mathbf{e}_1 \cdot \int_{\partial\mathcal{B}_0^a \cup \partial\mathcal{B}_0^b} \mathbf{S}\mathbf{n}_0. \quad (4.31)$$

Introducing the contact force components  $R_1^a$  and  $R_1^b$  along  $\mathbf{e}_1$  on the two respective boundary portions  $\partial\mathcal{B}_0^a$  and  $\partial\mathcal{B}_0^b$  as

$$R_1^a = \mathbf{e}_1 \cdot \int_{\partial\mathcal{B}_0^a} \mathbf{S}\mathbf{n}_0, \quad R_1^b = \mathbf{e}_1 \cdot \int_{\partial\mathcal{B}_0^b} \mathbf{S}\mathbf{n}_0, \quad (4.32)$$

and considering the equilibrium equation (2.36) and eqn (4.31), leads to

$$R_1^a + R_1^b = -\mathbf{e}_1 \cdot \int_{\partial\mathcal{B}_0^l \cup \partial\mathcal{B}_0^r} \mathbf{P}\mathbf{n}_0. \quad (4.33)$$

A generalization of eqn (4.33) can be obtained for any arbitrary surface  $\partial\mathcal{P}_0$  having a non-null portion in contact  $\partial\mathcal{P}_0^{\text{tou}} \in \partial\mathcal{P}_0$  with outward normal  $\mathbf{n}_0 = \pm\mathbf{e}_2$  (Fig. 4.4). The component  $R_1(\partial\mathcal{P}_0^{\text{tou}})$  of the resultant force of the pressure distribution acting on  $\partial\mathcal{P}_0^{\text{tou}}$  can be computed using any line integral with initial and ending point coincident with the limit points of the contact region for which the reaction force is evaluated

$$R_1(\partial\mathcal{P}_0^{\text{tou}}) = \mathbf{e}_1 \cdot \int_{\partial\mathcal{P}_0^{\text{tou}}} \mathbf{S}\mathbf{n}_0 = \mathbf{e}_1 \cdot \int_{\partial\mathcal{P}_0^{\text{tou}}} \mathbf{P}\mathbf{n}_0 = -\mathbf{e}_1 \cdot \int_{\partial\mathcal{P}_0 \setminus \partial\mathcal{P}_0^{\text{tou}}} \mathbf{P}\mathbf{n}_0. \quad (4.34)$$

From eqn (4.34) it can be concluded that, even in the case of smooth constraints, the contact reaction force component  $R_1$  transmitted to the body from the contact region  $\partial\mathcal{P}_0^{\text{tou}}$  coincides with the negative of the  $J$ -integral (4.1), evaluated for a path  $\Gamma_0 \equiv \partial\mathcal{P}_0 \setminus \partial\mathcal{P}_0^{\text{tou}}$  as expressed by eqn (4.34). It follows that the  $J$ -integral path-independence is preserved only for all paths with the same initial and final points, because the reaction force  $R_1$  depends on the extension of the specific contact region, Fig. 4.1. In the case of a flat constraint ending with a sharp corner, the initial and final points of  $\Gamma_0$  can be chosen on the left and on the right of the discontinuity in curvature, respectively, in the contact and in the traction-free surface. Thus, assuming a sufficiently regular behaviour, the equation (4.34) becomes equation (4.2) and a path-independence of the  $J$ -integral is found.

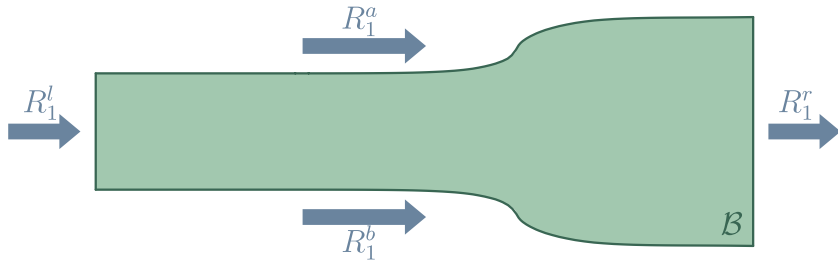


**Figure 4.4:** Reaction force acting on an elastic body from any pressure distribution.

### 4.3.2 Reaction force $R_1^a + R_1^b$ from the energy momentum tensor $\mathbf{C}$

It is now interesting to readdress the equilibrium of an elastic rectangular undeformed domain subject to either a pressure loading  $p$  on  $\partial\mathcal{B}_0^a$  and  $\partial\mathcal{B}_0^b$ , by exploiting the solenoidal property of  $\mathbf{C}$ . Considering the normal direction  $\mathbf{n}_0 = \pm\mathbf{e}_2$  and the property (4.10)<sub>2</sub>, it follows that

$$\mathbf{e}_1 \cdot \mathbf{C} \mathbf{n}_0 = 0, \quad \text{on } \partial\mathcal{B}_0^a \cup \partial\mathcal{B}_0^b, \quad (4.35)$$

and therefore taking the scalar product with  $\mathbf{e}_1$ , the solenoidal property of  $\mathbf{C}$  reduces to

$$\int_{\partial\mathcal{B}_0^l} (\Phi - \mathbf{F} \mathbf{e}_1 \cdot \mathbf{S} \mathbf{e}_1) - \int_{\partial\mathcal{B}_0^r} (\Phi - \mathbf{F} \mathbf{e}_1 \cdot \mathbf{S} \mathbf{e}_1) = 0. \quad (4.36)$$

If either a pressure  $p$  or a dead loading  $\mathbf{Sn}_0$  is applied on the boundary portions  $\partial\mathcal{B}_0^l$  and  $\partial\mathcal{B}_0^r$ , eqn (4.36) simplifies as

$$\int_{\partial\mathcal{B}_0^l} \left( \Phi - \left\{ \begin{array}{c} -p\mathcal{J} \\ S_{11}F_{11} + S_{21}F_{21} \end{array} \right\} \right) - \int_{\partial\mathcal{B}_0^r} \left( \Phi - \left\{ \begin{array}{c} -p\mathcal{J} \\ S_{11}F_{11} + S_{21}F_{21} \end{array} \right\} \right) = 0, \quad (4.37)$$

where the left curly brackets are introduced to synthetically display the two equations corresponding to pressure  $p$  (first line) or a dead loading  $\mathbf{Sn}_0$  (second line). Introducing the further assumption of homogeneous deformation gradient  $\mathbf{F}$  in the neighborhood of the two boundaries  $\partial\mathcal{B}_0^l$  and  $\partial\mathcal{B}_0^r$ , as sketched in Fig. 4.3, the integrals in equation (4.37) can be trivially solved to yield

$$\Phi^l - \left\{ \begin{array}{c} -p^l\mathcal{J}^l \\ S_{11}^lF_{11}^l + S_{21}^lF_{21}^l \end{array} \right\} - \Phi^r + \left\{ \begin{array}{c} -p^r\mathcal{J}^r \\ S_{11}^rF_{11}^r + S_{21}^rF_{21}^r \end{array} \right\} = 0, \quad (4.38)$$

where the superscripts  $l$  and  $r$  respectively identify the relevant (constant) quantity evaluated on the boundaries  $\partial\mathcal{B}_0^l$  and  $\partial\mathcal{B}_0^r$ . Interestingly, the expression obtained by restricting eqn (4.38) to only the terms in  $p$ ,

$$\Phi^l + p^l\mathcal{J}^l = \Phi^r + p^r\mathcal{J}^r, \quad (4.39)$$

shares some similarities with Bernoulli's equation for stationary flow in fluid mechanics.

It should be noted that  $\Phi^j$ ,  $\mathcal{J}^j$ ,  $F_{11}^j$ , and  $F_{21}^j$  ( $j = l, r$ ) in eqns (4.38) are all functions of: (i.) the contact (pressure) distribution  $p$  on the boundaries  $\partial\mathcal{B}_0^a$  and  $\partial\mathcal{B}_0^b$ , not explicitly appearing in eqns (4.36)–(4.38) and (ii.) the pressure distribution  $p$  or the dead loading  $\mathbf{Sn}_0$  on the boundaries  $\partial\mathcal{B}_0^l$  and  $\partial\mathcal{B}_0^r$ , as in Figs. 1.1 and 4.3. Except for trivial cases, the pressure or dead load (ii.) cannot easily be related to the pressure distribution (i.), because equilibrium has to be satisfied, therefore eqns (4.38) contain more than one unknown. However, assuming  $S_{21}^l = S_{21}^r = 0$  and that the lateral load (ii.) is applied only on the boundary  $\partial\mathcal{B}_0^j$  ( $j = l$  or  $r$ ) while the boundary  $\partial\mathcal{B}_0^i$  ( $i = l$  or  $r$ , with  $i \neq j$ ) remains unloaded, equations (4.38) can be used to define the unknown loading, either  $p^j$  or  $S_{11}^j$ . In particular, eqns (4.38) lead to

$$\left. \begin{array}{c} p^j\mathcal{J}^j \\ -S_{11}^jF_{11}^j \end{array} \right\} = \Phi^i - \Phi^j, \quad i, j = l, r, \quad \text{with } i \neq j, \quad (4.40)$$

so that, when the load (i.) (the pressure distribution  $p$  on the boundaries  $\partial\mathcal{B}_0^a$  and  $\partial\mathcal{B}_0^b$ ) is prescribed, the relevant equation becomes a nonlinear implicit equation in the variable representing

the load (ii.), applied on the boundary  $\partial\mathcal{B}_0^j$ , either  $p^j$  or  $S_{11}^j$  ( $j = l, r$ ). The sum of the two components  $R_1^a + R_1^b$  of the resultant force along  $\mathbf{e}_1$  of the pressure  $p$  applied on the boundaries  $\partial\mathcal{B}_0^a$  and  $\partial\mathcal{B}_0^b$  can be obtained from equilibrium for the two loading cases as

$$R_1^a + R_1^b = \begin{cases} -p^l h^l, \\ S_{11}^l h_0, \end{cases}, \quad \text{and} \quad R_1^a + R_1^b = \begin{cases} p^r h^r, \\ -S_{11}^r h_0. \end{cases} \quad (4.41)$$

Assuming now  $F_{21}^j = 0$ , so that  $\lambda_1^j = F_{11}^j$ ,  $\lambda_2^j = F_{22}^j$ , and  $h^j = \lambda_2^j h_0$  on the loaded boundary  $\partial\mathcal{B}_0^j$  ( $j = l$  or  $r$ ), equation (4.40) implies

$$R_1^a + R_1^b = \frac{\Phi^l - \Phi^r}{\lambda_1^j} h_0, \quad \text{with } j = l \text{ or } r, \quad (4.42)$$

an expression that can alternatively be derived from eqn (4.33) by recalling from eqn (2.13) that  $\lambda_1 = 1 + u_{1,1}$ . Equation (4.42) shows that only a non-null difference in the strain energy  $\Phi$  at the two boundaries  $\partial\mathcal{B}_0^l$  and  $\partial\mathcal{B}_0^r$  induces a force  $R_1 = R_1^a + R_1^b$  and reduces to eqn (1.2) when the right edge is unloaded,  $\Phi^r = 0$ , as is the case of the loading conditions sketched in Fig. 1.1.



# 5

## Energy release rate $G$ and the configurational nature of the frictionless contact force component $R_1$

A rigid, frictionless, and flat constraint ending with a rounded or sharp corner is in contact against the boundary of a hyperelastic body with a flat surface in its reference configuration. The frictionless constraint is assumed to be capable of altering its extension of contact by increasing the size of its flat surface through an horizontal growth of the position of its, say right, corner. Analogously to the concept of configurational force on defects or inhomogeneities introduced by Eshelby [16], the idea of a configurational force acting on the corner of frictionless and rigid constraints can be introduced.

For a growth  $\delta\xi_0$  in the size of the frictionless constraint along  $\mathbf{e}_1$ , defined with respect to the undeformed configuration of a hyperelastic solid, the configurational force component  $F_1^c$  parallel to the growth direction can be defined as an energy release rate  $G$

$$F_1^c = G = -\frac{\partial \mathcal{V}}{\partial \xi_0}, \quad (5.1)$$

where  $\mathcal{V}$  is the total potential energy of the mechanical system at equilibrium. For both cases of sharp or rounded corner, it is shown that the configurational force component  $F_1^c$  equals the  $J$ -integral,

$$F_1^c = J. \quad (5.2)$$

The treatment is restricted for simplicity to two-dimensions, where surfaces are curves and planes straight lines. Final applications are referred to a rectangular undeformed shape  $\mathcal{B}_0$  of the contactor, as

described by eqn 4.28). As a generalization of the results presented in Ch. 3, it is shown that a frictionless punch ending with a sharp corner can generate a horizontal configurational force even when in contact with a planar surface of an elastic solid.

## 5.1 Variation in the length of a flat, frictionless, and rigid constraint ending with a sharp corner

The contactor has an initially flat boundary  $\partial\mathcal{B}_0^a$  having unit normal  $\mathbf{e}_2$ , while the target has a rectilinear surface (with outward unit normal  $-\mathbf{e}_2$ ) ending with a corner, located at point  $\mathbf{y}$ , Fig. 5.1. The frictionless constraint is in contact with the elastic body on the portion of the boundary  $\partial\mathcal{B}_0^{a,C}$ . The contact is assumed to be ‘full’, so that grazing does not occur and all the points on the touching surface  $\mathbf{x} \in \partial\mathcal{B}_0^{a,tou}$  belong to  $\partial\mathcal{B}_0^{a,C} = \partial\mathcal{B}_0^{a,tou}$ , including the corner point  $\mathbf{y}$ . On the solid, the latter point is back-transformed in the reference configuration into  $\mathbf{y}_0$ . The latter point is perturbed by postulating a small growth, parallel to the rectilinear contact surface of the constraint, to a neighbouring point  $\mathbf{y}_0 + \delta\xi_0\mathbf{e}_1$ . It is therefore possible to strictly follow Eshelby [16], thus defining a surface  $\partial\mathcal{S}_0$  enclosing a region  $\mathcal{S}_0$  which contains the corner  $\mathbf{y}_0$  in the reference configuration  $\mathcal{B}_0$ , called ‘original surface’ and introducing a ‘replica’ region equal to  $\mathcal{S}_0$ , but translated to the region  $\mathcal{S}'_0$  with surface  $\partial\mathcal{S}'_0$ , obtained by applying a rigid displacement vector  $-\delta\xi_0\mathbf{e}_1$  to  $\mathcal{S}_0$ . Note that the surfaces  $\partial\mathcal{S}_0$  and  $\partial\mathcal{S}'_0$  are punctured at the singular point  $\mathbf{y}_0$ . The steps below are followed.

- (i.) In the reference configuration  $\mathcal{B}_0$ , the material in the region  $\mathcal{S}_0$  is cut out and kept aside. Both the latter and the rest of the body are considered to still be subject to the nominal tractions that were exchanged across the surface cut out of the body, in addition, the cut out piece is also assumed to be subjected to the surface forces transmitted by the constraint.
- (ii.) Consider the material in the replica region, inside of  $\mathcal{S}'_0$ , and apply on its surface  $\partial\mathcal{S}'_0$  the nominal tractions transmitted by the rest of the deformable body and by the constraint. Comparing the energies inside  $\mathcal{S}'_0$  and  $\mathcal{S}_0$  and taking the limit of vanishing  $\delta\xi_0$ , the Leibniz integral rule for a closed curve  $\partial\mathcal{S}_0$  in a two-dimensional domain, rigidly shifted inside  $\mathcal{B}_0$ , is

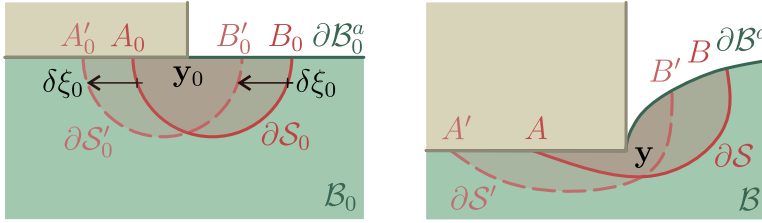


**Figure 5.1:** An elastic solid (green) with a planar surface is pressed against a flat, rigid, and frictionless constraint (brown). Left (Right): The constraint has a corner touching the elastic body at point  $y_0$  (at point  $y$ ) in the reference (the current) configuration  $\mathcal{B}_0$  ( $\mathcal{B}$ ). In a setting which follows Eshelby, the corner of the frictionless constraint is assumed to grow of an amount  $\delta\xi_0 \mathbf{e}_1$  in the reference configuration. Two identical regions  $S_0$  and  $S'_0$  are assumed in the reference configuration differing in a rigid horizontal shift  $-\delta\xi_0 \mathbf{e}_1$ , both enclosing  $y_0$ . The two regions are transformed by the deformation into the regions  $S$  and  $S'$ , both enclosing the corner of the constraint at point  $y$ .

obtained [18]

$$\frac{d}{d\xi_0} \int_{S_0(\xi_0)} \Phi = - \int_{\partial S_0} \Phi \mathbf{n}_0 \cdot \mathbf{e}_1, \quad (5.3)$$

where  $\mathbf{n}_0$  is outward unit normal to  $\partial S_0$ , so that the surface on the horizontal edge of  $\partial S_0$  does not contribute. Equation (5.3) may be understood in a generalized sense, depending on the kind of possible singularity present at the end of the target, and provides the differentiation of the elastic energy corresponding to an infinitesimal translation of  $S_0$ , equivalent to an infinitesimal increase in the length of the target.

- (iii.) Due to the deformation, the deformed replica  $S'$  (transformed of  $S'_0$ ) does not fit into the hole left by the ‘excision’ of  $S$  (transformed of  $S_0$ ). In particular, any point  $\mathbf{r}_0$  inside the region of the replica equals a corresponding point  $\mathbf{x}_0$  inside  $S_0$ , plus the shift  $-\delta\xi_0 \mathbf{e}_1$ . Therefore the displacement of  $\mathbf{r}_0$  is  $\mathbf{u}(\mathbf{r}_0) = \mathbf{u}(\mathbf{x}_0 - \delta\xi_0 \mathbf{e}_1)$ , so that at first-order

$$\mathbf{u}(\mathbf{r}_0) = \mathbf{u}(\mathbf{x}_0) - \delta\xi_0 \nabla \mathbf{u}(\mathbf{x}_0) \mathbf{e}_1. \quad (5.4)$$

It follows from eqn (5.4) that, in addition to a rigid-body translation  $\delta\xi_0 \mathbf{e}_1$  (which does not produce any work), to fit the deformed  $S'$  into the deformed hole left by  $S$ , an additional displacement has to be added to the displacement  $\mathbf{u}(\mathbf{x}_0)$  on the surface  $\partial S_0$  of the hole left in  $\mathcal{B}_0$ . In differential terms,

the latter displacement satisfies

$$\frac{\partial \mathbf{u}}{\partial \xi_0} = -(\nabla \mathbf{u}) \mathbf{e}_1, \quad (5.5)$$

so that the amount of work done by the tractions on the surface of the hole  $\partial\mathcal{S}_0$  is equal to

$$\frac{\partial W}{\partial \xi_0} = \int_{\partial\mathcal{S}_0} \mathbf{e}_1 \cdot \nabla \mathbf{u}^T \mathbf{S} \mathbf{n}_0, \quad (5.6)$$

where again  $\mathbf{n}_0$  is the outward unit normal to  $\partial\mathcal{S}_0$ .

- (iv.) The change in the total potential energy  $\mathcal{V}$  is the sum of equations (5.3) and (5.6),

$$\frac{\partial \mathcal{V}}{\partial \xi_0} = \frac{\partial W}{\partial \xi_0} + \frac{d}{d \xi_0} \int_{\mathcal{S}_0(\xi_0)} \Phi, \quad (5.7)$$

which, using equations (5.3) and (5.6), yields to the energy release rate  $G$  as

$$G = -\frac{\partial \mathcal{V}}{\partial \xi_0} = \int_{\partial\mathcal{S}_0} \mathbf{e}_1 \cdot (\Phi \mathbf{I} - \nabla \mathbf{u}^T \mathbf{S}) \mathbf{n}_0. \quad (5.8)$$

Note that the surface  $\partial\mathcal{S}_0$  comprises only the part inside the solid, while contributions on the flat boundary vanish. This statement is trivial for the term  $\Phi$  because  $\mathbf{n}_0$  is orthogonal to  $\mathbf{e}_1$  on the flat contact edge of the elastic solid. Regarding the term  $\nabla \mathbf{u}^T \mathbf{S} \mathbf{n}_0$ , it may be observed that  $\mathbf{S} \mathbf{n}_0 = \mathbf{0}$  on the flat boundary outside the constraint, while inside the constraint equation (2.13) together with the frictionless condition (4.9) and the fact that  $\mathbf{F} \mathbf{e}_1$  is parallel to  $\mathbf{e}_1$  along the contact allow to conclude.

- (v.) Now  $\mathcal{S}'$  fits the hole left by  $\mathcal{S}$  in the original body and can be welded in it. The nominal tractions on both sides of the surface  $\partial\mathcal{S}_0$  differ on a force distribution which gives higher-order effects and can be neglected. *We are now left with the system as it was to begin with, except that the end of the constraint is shifted of an amount  $\delta\xi_0 \mathbf{e}_1$  with respect to its initial position defined in the reference configuration.*

The operations (i.)–(iii.) involved in the Eshelby proof are summarized in Fig. 5.2. Equation (5.8) can be viewed as the work done by the *configurational force*  $\mathbf{F}^c$  for a unit displacement in the

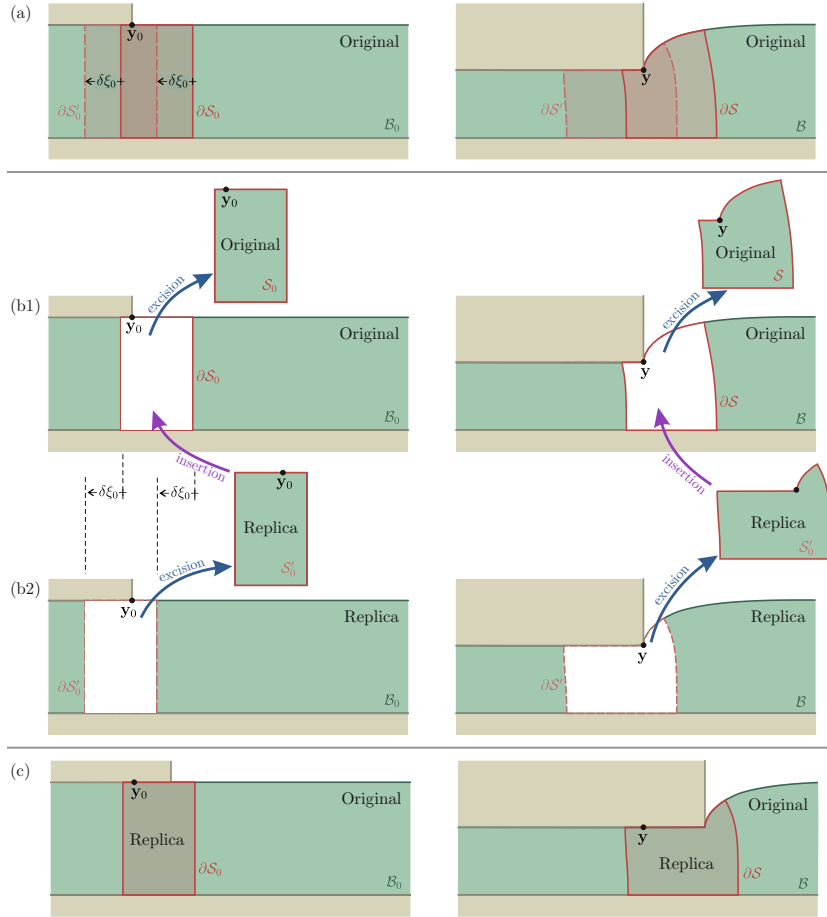


**Figure 5.2:** Sequence of operations in the Eshelby scheme for the deformation of an elastic body against a rigid and frictionless constraint, which increases its length of an amount  $\delta\xi_0$  in the reference configuration. Reference (current) configurations are shown on the left (on the right). (a) The referential regions  $S_0$  and  $S'_0$  (the latter is the image of the former obtained through a shift of amount  $-\delta\xi_0$ ) enclose the end of the constraint and are transformed by the deformation into  $S$  and  $S'$  in the current configuration. (b1) The region  $S_0$  and its transformed counterpart  $S$  are ideally ‘excised’ from the original body. (b2) The region  $S'_0$  and its transformed counterpart  $S'$  are ideally ‘excised’ from a ‘replica’ version of the original body. The elastic energies contained within  $S_0$  and  $S'_0$  differ only in the crescent-shaped regions obtained by superposition of  $S_0$  and  $S'_0$ , so that the derivative of the elastic energy with respect to the configurational parameter is given by eqn (5.3). The deformed ‘replica’ region  $S'$  does not fit the hole left in the original region by the excision of  $S$ , so that displacements have to be applied on the boundary of the hole, producing the increment of work expressed by eqn (5.6). (c) The replica finally fits the hole in the original body and the corner of the rigid constraint is advanced of an amount  $\delta\xi_0$  with respect to the original reference configuration. The remaining mismatch in the traction vector at the boundary of the region is higher-order and can be neglected.

direction  $\mathbf{e}_1$ , and therefore by the configurational force component  $F_1^c = \mathbf{F}^c \cdot \mathbf{e}_1$

$$F_1^c = G = \mathbf{e}_1 \cdot \int_{\partial\mathcal{S}_0} (\Phi \mathbf{I} - \nabla \mathbf{u}^T \mathbf{S}) \mathbf{n}_0. \quad (5.9)$$

Note that the configurational force  $\mathbf{F}^c$  remains determined only in its component  $F_1^c$  along  $\mathbf{e}_1$ , because the translation of  $\mathcal{S}_0$  is not arbitrary, differently from the original treatment by Eshelby, but prescribed parallel to the direction  $\mathbf{e}_1$ .

Finally, recalling the energy-momentum tensor  $\mathbf{P}$ , eqn (4.12), equation (5.9) becomes

$$F_1^c = \mathbf{e}_1 \cdot \int_{\partial\mathcal{S}_0} \mathbf{P} \mathbf{n}_0, \quad (5.10)$$

where the integrand is null on the upper flat portion of the boundary, except possibly at the point  $\mathbf{y}_0$  where the corner of the constraint is present. The surface  $\partial\mathcal{S}_0$  can be shrunk up to the limit of that point, without changing the value of the integral. This leads to the path-independent  $J$ -integral, when the target is flat and ends with a corner,

$$J = F_1^c, \quad (5.11)$$

so that the configurational force in the direction  $\mathbf{e}_1$  is equal to the horizontal resultant of the force acting on the solid with reversed sign

$$F_1^c = -R_1. \quad (5.12)$$

**Application to rectangular elastic domains.** It is interesting to note that, when a rectangular undeformed elastic solid is considered, the region  $\mathcal{S}_0$  can be assumed as illustrated in Fig. 5.2(a), namely, rectangular with boundary  $\partial\mathcal{S}_0^l \cup \partial\mathcal{S}_0^b \cup \partial\mathcal{S}_0^r$ , so that, assuming the frictionless condition on  $\partial\mathcal{S}_0^b \subseteq \partial\mathcal{B}_0^b$ , the configurational force component  $F_1^c$  reduces to

$$F_1^c = \int_{\partial\mathcal{S}_0^r} [\Phi - u_{1,1} S_{11} - u_{2,1} S_{21}] - \int_{\partial\mathcal{S}_0^l} [\Phi - u_{1,1} S_{11} - u_{2,1} S_{21}], \quad (5.13)$$

which is equivalent to eqns (4.33) and (4.36) (respectively obtained through the solenoidal property of the energy-momentum tensors  $\mathbf{P}$  and  $\mathbf{C}$  in the absence of singularities) because equilibrium implies

$$R_1 = \int_{\partial\mathcal{S}_0^r} S_{11} - \int_{\partial\mathcal{S}_0^l} S_{11}. \quad (5.14)$$

## 5.2 Variation in the length of the constraint with a rounded corner

The presence of a smooth-end is now addressed. Analogously to the treatment of the growth of a flat surface notch in a two-dimensional deformation field given by Rice [41], the right end of the frictionless and straight constraint is considered to have a smooth ‘cap’, along which the contact with the elastic body is lost.

The end of the constraint is assumed to be able to rigidly translate in the direction  $\mathbf{e}_1$ , parallel to the constraint before the initiation of the smooth cap. The treatment developed in the previous Section still holds under the caution that  $\partial\mathcal{S}_0$  has to contain all the zone contacting with the smooth ‘movable’ cap. A repetition of the calculations developed in the previous Section leads now again to equation (5.10), where now  $\partial\mathcal{S}_0$  is any surface enclosing all the zone in contact with the smooth ‘movable’ cap. Consequently, equation (5.11) is again obtained, in agreement with the evaluation of  $R_1$  provided by eqn (4.34), following from the solenoidal property of the energy-momentum tensor  $\mathbf{P}$ .



# 6

## Connection with the configurational structural mechanics

The introduced theoretical framework, disclosing the development of configurational sliding forces at the (sharp or rounded) corner of a frictionless, rigid, and flat surface acting on an elastic body, is now used to throw light on the akin problem of elastic rods partially constrained with a sliding sleeve. The presence of configurational forces at the end of a sliding sleeve was disclosed by analyzing one-dimensional flexible structures through a variational approach [1, 5, 29] or by imposing jump conditions in the material momentum balance law [23, 35, 36]. This result is confirmed here through the application of the framework developed in the previous Sections to an elastic solid of rectangular shape in its undeformed configuration  $\mathcal{B}_0$ , as defined by eqn (4.28), in contact with two frictionless rigid surfaces realizing a sliding sleeve constraint.

### 6.1 Rod's kinematics

According to the kinematic assumptions usually made in rod mechanics [33], the deformation for an elastic solid of rectangular shape is prescribed to provide null transverse strain and to be described by the following expressions, linearized in the variable  $x_2^0$  (Fig. 6.1,

top),

$$\begin{cases} x_1(x_1^0, x_2^0) = x_1^0 + u(x_1^0) - x_2^0 \sin \theta(x_1^0), \\ x_2(x_1^0, x_2^0) = v(x_1^0) + x_2^0 \cos \theta(x_1^0), \end{cases} \quad \text{in } \mathcal{B}_0 := \left\{ x_1^0 \in [0, \ell_0], x_2^0 \in \left[ \frac{h_0}{2}, -\frac{h_0}{2} \right] \right\}, \quad (6.1)$$

where  $u(x_1^0)$ ,  $v(x_1^0)$ , and  $\theta(x_1^0)$  are the three kinematic fields describing the deformed configuration of the solid, respectively, the displacement components along  $\mathbf{e}_1$  and  $\mathbf{e}_2$ , and the inclination angle of the rod's axis with respect to the direction  $\mathbf{e}_1$ , corresponding to the undeformed tangent. Only two among the three kinematic descriptors  $u$ ,  $v$ , and  $\theta$  are independent, since the Euler–Bernoulli assumption implies

$$\tan \theta(x_1^0) = \frac{v'(x_1^0)}{1 + u'(x_1^0)}, \quad (6.2)$$

where a prime denotes differentiation with respect to the axial coordinate  $x_1^0$ , while impenetrability imposes the constraint  $u'(x_1^0) > -1$  on the displacement. The two primary kinematic fields measuring the deformed state of the extensible elastica are the generalized curvature  $\theta'(x_1^0)$  and the rod's axis axial deformation  $\eta(x_1^0)$  (which satisfies  $\eta(x_1^0) > -1$  because of the impenetrability constraint)

$$\eta(x_1^0) = \sqrt{[1 + u'(x_1^0)]^2 + [v'(x_1^0)]^2} - 1, \quad (6.3)$$

through which the following geometrical relations can be derived

$$\sin \theta(x_1^0) = \frac{v'(x_1^0)}{1 + \eta(x_1^0)}, \quad \cos \theta(x_1^0) = \frac{1 + u'(x_1^0)}{1 + \eta(x_1^0)}. \quad (6.4)$$

The resultant force components  $N_1$  and  $N_2$ , respectively aligned parallel to  $\mathbf{e}_1$  and  $\mathbf{e}_2$ , and the moment  $M$  are given from the equilibrium equivalence, imposed for the cross section at the generic coordinate  $x_1^0$ , as

$$\begin{aligned} N_1(x_1^0) &= \int_{-\frac{h_0}{2}}^{\frac{h_0}{2}} S_{11} dx_2^0, \\ N_2(x_1^0) &= \int_{-\frac{h_0}{2}}^{\frac{h_0}{2}} S_{21} dx_2^0, \\ M(x_1^0) &= - \int_{-\frac{h_0}{2}}^{\frac{h_0}{2}} [S_{11} \cos \theta + S_{21} \sin \theta] x_2^0 dx_2^0, \end{aligned} \quad (6.5)$$

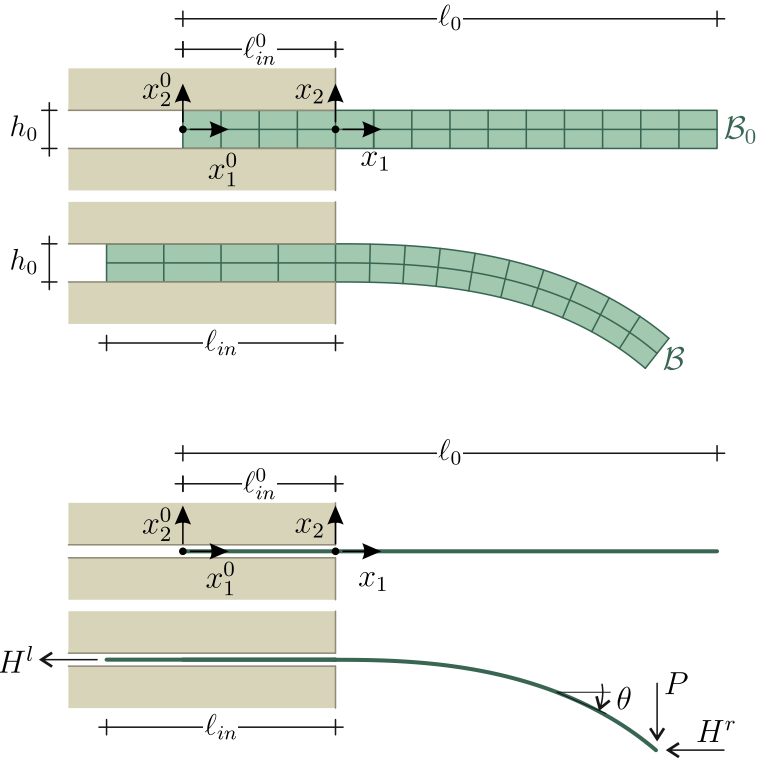


**Figure 6.1:** Top: The kinematic assumptions, usually introduced for a rod, eqn (6.1), are imposed to an elastic solid of rectangular shape in its undeformed configuration, constrained between two rigid and frictionless constraints. Bottom: the rod's model, representing an extensible version of the variable-length elastica subject to end loads.

where the first two components can be composed to evaluate the axial and shear forces  $N$  and  $T$

$$\begin{aligned} N(x_1^0) &= N_1(x_1^0) \cos \theta(x_1^0) + N_2(x_1^0) \sin \theta(x_1^0), \\ T(x_1^0) &= -N_1(x_1^0) \sin \theta(x_1^0) + N_2(x_1^0) \cos \theta(x_1^0). \end{aligned} \quad (6.6)$$

## 6.2 Sliding sleeve constraint and the evaluation of the configurational force component $F_1^c$

The elastic rectangular solid under consideration is assumed in partial contact with two symmetric straight, frictionless, and rigid constraints, realizing a sliding sleeve with sliding direction parallel to  $\mathbf{e}_1$ , in a setting similar to that reported in Fig. 6.1 (top). The sliding

sleeve is assumed to have its exit point located at the cross section marked by the coordinate  $x_1^0 = \ell_{in}^0$  (with  $\ell_{in}^0 \in [0, \ell_0]$ ), referred to the undeformed rod. Thus, the following constraints apply

$$\theta(x_1^0) = v(x_1^0) = 0, \quad \text{for } x_1^0 \in [0, \ell_{in}^0], \quad (6.7)$$

which, considering the origin of the reference system  $x_1-x_2$  coincident with the sliding sleeve exit,

$$x_1(x_1^0 = \ell_{in}^0, x_2^0) = 0, \quad (6.8)$$

imply the validity of the following relation

$$u_1(x_1^0 = \ell_{in}^0) = -\ell_{in}^0. \quad (6.9)$$

From the deformation field, eqns (6.1), the components of the displacement gradient  $\nabla \mathbf{u}$ , relevant for the application of the expression (5.13), provides the configurational force component  $F_1^c$  as

$$\begin{aligned} u_{1,1}(x_1^0, x_2^0) &= u'(x_1^0) - x_2^0 \theta'(x_1^0) \cos \theta(x_1^0), \\ u_{2,1}(x_1^0, x_2^0) &= v'(x_1^0) - x_2^0 \theta'(x_1^0) \sin \theta(x_1^0). \end{aligned} \quad (6.10)$$

By considering the boundaries  $\partial \mathcal{S}_0^r$  and  $\partial \mathcal{S}_0^l$  coincident with the cross sections respectively located at  $x_1^{[r]0}$  and  $x_1^{[l]0}$ , the expression (5.13) for the configurational force component  $F_1^c$  reduces to

$$\begin{aligned} F_1^c &= \Psi(x_1^{[r]0}) - \Psi(x_1^{[l]0}) + \\ &\quad - [N_1 u' + N_2 v' + M \theta']|_{x_1^{[r]0}} + \\ &\quad + [N_1 u' + N_2 v' + M \theta']|_{x_1^{[l]0}}, \end{aligned} \quad (6.11)$$

where  $\Psi$  is the rod's elastic energy density, evaluated as

$$\Psi(x_1^0) = \int_{-\frac{h_0}{2}}^{\frac{h_0}{2}} \Phi dx_2^0. \quad (6.12)$$

Assuming that the two cross sections  $\partial \mathcal{S}_0^r$  and  $\partial \mathcal{S}_0^l$  are the cross sections respectively ‘just after’ and ‘just before’ the coordinate  $\ell_{in}^0$ , where the sliding sleeve exit is back transformed in the reference configuration, the configurational force component  $F_1^c$  (6.11) simplifies to

$$F_1^c = [\Psi(\ell_{in}^0)] - [N(\ell_{in}^0) \eta(\ell_{in}^0)] - M(\ell_{in}^{0+}) \theta'(\ell_{in}^{0+}),$$

(6.13)

where the brackets  $\llbracket \cdot \rrbracket$  denote the jump of the relevant quantity at the sliding sleeve exit,

$$\llbracket f(\ell_{in}^0) \rrbracket = f(\ell_{in}^{0+}) - f(\ell_{in}^{0-}), \quad (6.14)$$

and, because of the constraint (6.7), the following identities at the left and right limit points of the sliding sleeve exit hold

$$\eta(\ell_{in}^{0\pm}) = u'(\ell_{in}^{0\pm}), \quad N(\ell_{in}^{0\pm}) = N_1(\ell_{in}^{0\pm}), \quad v'(\ell_{in}^{0\pm}) = 0. \quad (6.15)$$

It is highlighted that  $N$ ,  $M$ ,  $\eta$ ,  $\theta'$ , and  $\Psi$  may display a jump in their value at the coordinate  $\ell_{in}^0$ .

Equation (6.13) provides the expression for the configurational force  $F_1^c$  acting on the variable-length Euler elastica by including axial deformability and a generic (possibly non-quadratic) rod's energy density  $\Psi$ . This equation reduces to that obtained in [5] when axial inextensibility and quadratic energy in the curvature,  $\theta'$ , are assumed.

It is finally observed that equation (6.13) can be interpreted as a jump condition for the material momentum balance law, which was introduced in the forerunning contribution by O'Reilly [35], who established a novel frontier in the configurational mechanics of structures, by enhancing a previous formulation by Kienzler and Herrmann [27]. More specifically, by introducing the concept of material force  $C(x_1^0)$ ,

$$C(x_1^0) = \Psi(x_1^0) - N(x_1^0)\eta(x_1^0) - M(x_1^0)\theta'(x_1^0), \quad (6.16)$$

the jump condition at the singularity point  $x_1^0 = \ell_{in}^0$  is given by

$$\llbracket C(\ell_{in}^0) \rrbracket = F_1^c, \quad (6.17)$$

which is coincident with eqn (6.13), by recalling that  $\theta'(\ell_{in}^{0-}) = 0$ , due to the presence of the sliding sleeve. Interestingly, the material force  $C(x_1^0)$ , eqn (6.16), for the one-dimensional model can be obtained as the integral of the energy-momentum tensor component  $P_{11} = \mathbf{e}_1 \cdot \mathbf{P} \mathbf{e}_1$  [expressed in a linearized kinematics (6.1)], calculated on the cross section of the rod

$$C(x_1^0) = \int_{-\frac{h_0}{2}}^{\frac{h_0}{2}} P_{11}(x_1^0, x_2^0) dx_2^0 = \int_{-\frac{h_0}{2}}^{\frac{h_0}{2}} [\Phi - u_{1,1}S_{11} - u_{2,1}S_{21}] dx_2^0. \quad (6.18)$$

In conclusion, the presence of the configurational force  $F_1^c$  at the sliding sleeve exit so far obtained for rod models [1, 5, 23, 29, 35, 36] is confirmed from a solid mechanics point of view.

### 6.3 Configurational force via a variational approach

Expression (6.13) for the configurational force component  $F_1^c$  is now derived through a variational approach. Attention is restricted to a specific loading condition, corresponding to dead loads at the two rod's ends, in particular a load  $-H^l \mathbf{e}_1$  is assumed to be applied at  $x_1^0 = 0$ , while a load  $-H^r \mathbf{e}_1 - P \mathbf{e}_2$  at  $x_1^0 = \ell_0$  (Fig. 6.1, bottom). The total potential energy  $\mathcal{V}$  is given by the difference of strain energy stored within the rod and the work done by the dead loadings,

$$\begin{aligned} \mathcal{V} = & \int_0^{\ell_{in}^{0-}} \Psi(\eta, \theta') dx_1^0 + \int_{\ell_{in}^{0+}}^{\ell_0} \Psi(\eta, \theta') dx_1^0 + \\ & + H^l x_1(0, 0) + H^r x_1(\ell_0, 0) + P x_2(\ell_0, 0). \end{aligned} \quad (6.19)$$

Recalling eqns (6.4), (6.7), and (6.8), the following kinematic relations hold

$$\begin{aligned} x_1(0, 0) &= - \int_0^{\ell_{in}^{0-}} (1 + \eta) dx_1^0, \\ x_1(\ell_0, 0) &= \int_{\ell_{in}^{0+}}^{\ell_0} (1 + \eta) \cos \theta dx_1^0, \\ x_2(\ell_0, 0) &= \int_{\ell_{in}^{0+}}^{\ell_0} (1 + \eta) \sin \theta dx_1^0, \end{aligned} \quad (6.20)$$

and the total potential energy  $\mathcal{V}$ , eqn (6.19), can be rewritten as

$$\begin{aligned} \mathcal{V}(\eta, \theta, \ell_{in}^0) = & \int_0^{\ell_{in}^{0-}} \Psi(\eta, \theta') dx_1^0 + \int_{\ell_{in}^{0+}}^{\ell_0} \Psi(\eta, \theta') dx_1^0 \\ & - H^l \int_0^{\ell_{in}^{0-}} (1 + \eta) dx_1^0 + H^r \int_{\ell_{in}^{0+}}^{\ell_0} (1 + \eta) \cos \theta dx_1^0 \\ & + P \int_{\ell_{in}^{0+}}^{\ell_0} (1 + \eta) \sin \theta dx_1^0. \end{aligned} \quad (6.21)$$

A variation in the configuration defined by the fields  $\eta(x_1^0)$  and  $\theta(x_1^0)$  and the configurational parameter  $\ell_{in}^0$  is considered, through the small positive parameter  $\epsilon$ , as

$$\begin{aligned} \eta(x_1^0) &\rightarrow \eta(x_1^0) + \epsilon \delta \eta(x_1^0), \\ \theta(x_1^0) &\rightarrow \theta(x_1^0) + \epsilon \delta \theta(x_1^0), \\ \ell_{in}^0 &\rightarrow \ell_{in}^0 + \epsilon \delta \ell_{in}^0, \end{aligned} \quad (6.22)$$

where, from the sliding sleeve constraint (6.7), the perturbations  $\delta\ell_{in}^0$  and  $\delta\theta(x_1^0)$  satisfy the following compatibility equation

$$\delta\theta(\ell_{in}^0) = -\theta'(\ell_{in}^0)\delta\ell_{in}^0. \quad (6.23)$$

Keeping into account that the axial force  $N$  and the bending moment  $M$  are work-conjugate to the axial deformation  $\eta$  and the generalized curvature  $\theta'$ , the following constitutive equations can be assumed

$$N = \frac{\partial\Psi}{\partial\eta}, \quad M = \frac{\partial\Psi}{\partial\theta'}, \quad (6.24)$$

so that, integration by parts, the sliding sleeve constraint conditions (6.7), and the compatibility condition (6.23), allow to evaluate the first variation  $\delta\mathcal{V}$  of the total potential energy as

$$\begin{aligned} \delta\mathcal{V}(\eta, \theta, \ell_{in}^0, \delta\eta, \delta\theta, \delta\ell_{in}^0) = & \int_0^{\ell_{in}^0} N\delta\eta dx_1^0 + \int_{\ell_{in}^0}^{\ell_0} N\delta\eta dx_1^0 - \int_{\ell_{in}^0}^{\ell_0} M'\delta\theta dx_1^0 + \\ & - H^l \int_0^{\ell_{in}^0} \delta\eta dx_1^0 + H^r \int_{\ell_{in}^0}^{\ell_0} \delta\eta \cos\theta dx_1^0 - H^r \int_{\ell_{in}^0}^{\ell_0} (1+\eta) \sin\theta \delta\theta dx_1^0 + \\ & - P \int_{\ell_{in}^0}^{\ell_0} \delta\eta \sin\theta dx_1^0 - P \int_{\ell_{in}^0}^{\ell_0} (1+\eta) \cos\theta \delta\theta dx_1^0 + \\ & + \left\{ -H^r [1+\eta(\ell_{in}^{0+})] - H^l [1+\eta(\ell_{in}^{0-})] + M(\ell_{in}^{0+})\theta'(\ell_{in}^{0+}) - [\Psi(\ell_{in}^0)] \right\} \delta\ell_{in}^0. \end{aligned} \quad (6.25)$$

The annihilation of the first variation  $\delta\mathcal{V}$  for every compatible perturbations  $\delta\eta(x_1^0)$ ,  $\delta\theta(x_1^0)$ , and  $\delta\ell_{in}^0$  provides the following equilibrium equations for the portion of the rod respectively outside

$$\begin{cases} M'(x_1^0) + H^r [1+\eta(x_1^0)] \sin\theta(x_1^0) + P[1+\eta(x_1^0)] \cos\theta(x_1^0) = 0, \\ N(x_1^0) = P \sin\theta(x_1^0) - H^r \cos\theta(x_1^0), \end{cases} \quad x_1^0 \in (\ell_{in}^0, \ell_0], \quad (6.26)$$

and inside

$$N(x_1^0) = H^l, \quad x_1^0 \in [0, \ell_{in}^0], \quad (6.27)$$

the sliding sleeve, together with the interface condition at the sliding sleeve end

$$H^r [1+\eta(\ell_{in}^{0+})] + H^l [1+\eta(\ell_{in}^{0-})] - M(\ell_{in}^{0+})\theta'(\ell_{in}^{0+}) + [\Psi(\ell_{in}^0)] = 0. \quad (6.28)$$

From eqns (6.26)<sub>2</sub> and (6.27) it follows that the axial force  $N(x_1^0)$  at the left and right limit points of the sliding sleeve exit are given by

$$N(\ell_{in}^{0-}) = H^l, \quad N(\ell_{in}^{0+}) = -H^r, \quad (6.29)$$

so that the jump in the normal force at the sliding sleeve end is provided by the reaction force component  $R_1$ , which remains determined from equilibrium as

$$R_1 = H^l + H^r. \quad (6.30)$$

On account of equations (6.29) and (6.30), a comparison between the axial equilibrium at the sliding sleeve exit, eqn (6.28), and expression (6.13), derived for the configurational force component  $F_1^c$ , implies the validity of equation (5.12), obtained with reference to the frictionless contact conditions.

## 6.4 Application to rods characterized by a quadratic energy density

Assuming the usual quadratic expression for the elastic energy density of the rod,

$$\Psi(x_1^0) = \frac{B[\theta'(x_1^0)]^2}{2} + \frac{K[\eta(x_1^0)]^2}{2}, \quad (6.31)$$

with  $B$  and  $K$  representing the (constant in space and positive) bending and axial stiffnesses, respectively, the application of equation (6.24) provides the constitutive relation

$$N(x_1^0) = K\eta(x_1^0), \quad M(x_1^0) = B\theta'(x_1^0), \quad (6.32)$$

so that the configurational force component  $F_1^c$ , eqn (6.13), reduces to

$$F_1^c = -\frac{B[\theta'(\ell_{in}^{0+})]^2}{2} - \frac{K[\eta(\ell_{in}^0)^2]}{2}. \quad (6.33)$$

Consequently the concentrated reaction force  $R_1$  becomes

$$R_1 = \frac{B[\theta'(\ell_{in}^{0+})]^2}{2} + \frac{K[\eta(\ell_{in}^0)^2]}{2}. \quad (6.34)$$

As a consequence of the assumed linear elastic axial behaviour, eqn (6.32), the equilibrium along the direction defined by  $\mathbf{e}_1$  is given by

$$K[\eta(\ell_{in}^{0+}) - \eta(\ell_{in}^{0-})] = -R_1, \quad (6.35)$$

providing an expression for the jump in the axial deformation at the sliding sleeve exit,  $[\eta(\ell_{in}^0)]$ . Introducing the average axial deformation  $\langle\eta(\ell_{in}^0)\rangle$  at the sliding sleeve exit

$$\langle\eta(\ell_{in}^0)\rangle = \frac{\eta(\ell_{in}^{0+}) + \eta(\ell_{in}^{0-})}{2}, \quad (6.36)$$

the concentrated reaction  $R_1$ , eqn (6.34), can finally be obtained as

$$R_1 = \frac{B [\theta' (\ell_{in}^{0+})]^2}{2 [1 + \langle \eta (\ell_{in}^0) \rangle]}, \quad (6.37)$$

which approaches, in the limit of vanishing axial deformation  $\eta (\ell_{in}^0)$  at the end of the sliding sleeve, the value for inextensible rods

$$\lim_{\eta(\ell_{in}^0) \rightarrow 0} R_1 = \frac{B [\theta' (\ell_{in}^{0+})]^2}{2}, \quad (6.38)$$

obtained in [5].



# 7

## Reaction force $R_1$ and applications in instability and dynamics

The plane strain problem of symmetric (frictionless, flat, and rigid) punches indenting an elastic solid of rectangular shape is further addressed. The purpose is to provide insight into the significance of the framework introduced in the previous Chapters in terms of both reliability of the obtained expressions and applicability of the results to the design of novel soft mechanisms.

In particular, the high reliability of the expression (4.42) for the contact reaction component  $R_1$  (obtained under the approximate assumption of uniform state at both the lateral edges of the rectangular domain) is assessed, through a comparison with results from Finite Element (FE) analyses at variable geometric parameters. Moreover, actuation mechanisms from Eulerian buckling and longitudinal dynamic ejection of the elastic solid due to transverse compression are presented, highlighting effects related to the presence of the reaction force  $R_1$ .

**Constitutive hyperelastic material models.** A specific hyperelastic material response is defined through the introduction of a specific strain energy density  $\Phi$  as a function of the principal stretches  $\lambda_i$  ( $i=I, II, III$ , so that  $\mathcal{J} = \lambda_I\lambda_{II}\lambda_{III}$ ). It is assumed that plane strain prevails, so that the out-of-plane principal stretch assumes a unit value,  $\lambda_{III} = \lambda_3 = 1$ . The following two material models are analyzed.

- Considering a compressible and initially isotropic material,

the strain energy density of the Storåkers model [43],

Storåkers model:

$$\Phi(\lambda_I, \lambda_{II}) = \sum_{k=1}^N \frac{2\mu_k}{\alpha_k^2} \left[ \lambda_I^{\alpha_k} + \lambda_{II}^{\alpha_k} - 2 + \frac{1}{\beta_k} (\mathcal{J}^{-\alpha_k \beta_k} - 1) \right], \quad (7.1)$$

only the first term is adopted, by setting  $N = 1$  in the summation characterizing the strain energy density,

‘First-term’ Storåkers model:

$$\Phi(\lambda_I, \lambda_{II}) = \frac{2\mu}{\alpha^2} \left[ \lambda_I^\alpha + \lambda_{II}^\alpha - 2 + \frac{1}{\beta} (\mathcal{J}^{-\alpha\beta} - 1) \right], \quad (7.2)$$

where  $\mu > 0$  is the ground-state shear modulus,  $\alpha \neq 0$  is a parameter affecting the nonlinear response, and  $\beta > -1/3$  is another parameter, related to the value of the ground-state Poisson’s ratio  $\nu \in (-1, 1/2)$  as

$$\beta = \frac{\nu}{1 - 2\nu}. \quad (7.3)$$

The principal components of the first Piola-Kirchhoff stress tensor  $\mathbf{S}$  can be obtained from eqn (2.62) as

$$S_i = 2\mu \frac{\lambda_i^\alpha - (\lambda_i \lambda_j)^{-\alpha\beta}}{\alpha \lambda_i}, \quad i \neq j, \quad i, j = I, II. \quad (7.4)$$

By assuming  $\alpha = 2$ , the strain energy density  $\Phi$  (7.2) reduces to that recently proposed by Pence and Gou [39] as a compressible version of the neo-Hookean material model,

Pence and Gou model:

$$\Phi(\lambda_I, \lambda_{II}) = \frac{\mu}{2} \left[ \lambda_I^2 + \lambda_{II}^2 - 2 + \frac{1}{\beta} (\mathcal{J}^{-2\beta} - 1) \right]. \quad (7.5)$$

- The incompressible and isotropic neo-Hookean material model [4]:

neo-Hookean model:

$$\Phi(\lambda_I, \lambda_{II}) = \frac{\mu}{2} (\lambda_I^2 + \lambda_{II}^2 - 2), \quad \lambda_I \lambda_{II} = 1, \quad (7.6)$$

---

where  $\mu > 0$  is the ground-state shear modulus. In the case of incompressible materials, the constitutive relation, eqn (2.62), becomes

$$S_i = -\frac{\Pi}{\lambda_i} + \frac{\partial\Phi}{\partial\lambda_i}, \quad (7.7)$$

where  $\Pi$  is the Lagrangian multiplier associated to the incompressibility constraint. Equation (7.7) leads to the principal components

$$S_i = -\frac{\Pi}{\lambda_i} + \mu\lambda_i, \quad i = \text{I, II}. \quad (7.8)$$

It is noted that, assuming  $\alpha = 2$ , the compressible model (7.5) approaches the incompressible one (7.6) in the limit  $\beta \rightarrow \infty$  (corresponding to  $\nu \rightarrow 1/2$ ). The above constitutive models are considered because also available as material models in the adopted Finite Element code.

**Common details of FE simulations.** FE simulations are performed through the commercial code Abaqus 2023. The rectangular elastic domain is modelled in both of the two compressible and incompressible versions, eqs (7.5) and (7.6). The elastic domain is meshed with bi-quadratic plane strain elements (CPE8) when the material is compressible, otherwise, a hybrid formulation is used (CPE8H). The boundary conditions prescribed on the sides of the rectangle are: (i.) free from tractions and constrained frictionless (ii.) bilateral (visualized with rollers) or (iii.) unilateral contact with a flat undeformable surface. In the numerical simulations the corner of the rigid constraint is smoothed with a quarter-of-circle arc of radius  $r$ .

Where the rigid surface is present, it is meshed with a linear rigid link (R2D2). To prevent interpenetration, the mesh size of the elastic body (the slave, defined on nodes) is chosen to be finer than the mesh size of the rigid constraint (the master, defined on segments). The adopted solver implements nonlinear geometry as well as unsymmetric matrix storage, enhanced through the introduction of a moderate energy dissipation when dynamic conditions prevail, to overcome ill-posedness at contact.

## 7.1 The horizontal reaction force $R_1$ at the corner of a frictionless flat punch

Two boundary value problems are considered for an elastic material occupying a rectangular domain in its undeformed configuration,  $\mathcal{B}_0$ , eqn (4.28). The sides of the domain have lengths  $h_0$  and  $\ell_0$ , Fig. 4.3 (left). In both problems the lower boundary  $\partial\mathcal{B}_0^b$  is entirely constrained by a horizontal bilateral frictionless constraint (a condition indicated with applied rollers) along a flat surface with unit normal  $\mathbf{e}_2$ . The upper boundary of the elastic solid,  $\partial\mathcal{B}_0^a$ , is partially constrained on its left part by a (frictionless, flat, and rigid) punch, defined by the outward unit normal  $-\mathbf{e}_2$ . The punch pushes the elastic solid remaining aligned parallel to  $\mathbf{e}_2$ , until a thickness  $h = \bar{\lambda}_2 h_0$  is reached, corresponding to a nominal transverse stretch  $\bar{\lambda}_2 < 1$ .

The two analyzed boundary value problems, called **BVP1** (Fig. 7.1 (top)) and **BVP2** (Fig. 7.1 (bottom)), differ in the boundary conditions provided on the lateral sides  $\partial\mathcal{B}^l$  (with normal  $\mathbf{n}_0^l = -\mathbf{e}_1$ ) and  $\partial\mathcal{B}^r$  (with normal  $\mathbf{n}_0^r = \mathbf{e}_1$ ) as follows.

- For **BVP1**: the boundary  $\partial\mathcal{B}_0^l$  is loaded through the application of a normal dead traction,  $\mathbf{S}^l \mathbf{n}_0^l = -S_{11}^l \mathbf{e}_1$ , while the boundary  $\partial\mathcal{B}_0^r$  is left traction-free,  $\mathbf{S}^r \mathbf{n}_0^r = \mathbf{0}$ . Equilibrium imposes the reaction force  $R_1$  to be the negative of the resultant of the applied tractions

$$R_1 = S_{11}^l h_0. \quad (7.9)$$

- For **BVP2**: the boundary  $\partial\mathcal{B}_0^l$  is left traction-free,  $\mathbf{S}^l \mathbf{n}_0^l = \mathbf{0}$ , while the boundary  $\partial\mathcal{B}_0^r$  is loaded through a normal dead traction,  $\mathbf{S}^r \mathbf{n}_0^r = S_{11}^r \mathbf{e}_1$ . Equilibrium imposes the reaction force  $R_1$  to be the negative of the resultant of the applied tractions

$$R_1 = -S_{11}^r h_0. \quad (7.10)$$

The end point of the flat punch (corresponding to either a sharp corner or the initial point of a rounded corner) is located at the back-transformed point  $\mathbf{y}_0 = (\ell_{in}^0, h_0/2)$ , belonging to  $\mathcal{B}_0^a$ , at a distance  $\ell_{in}^0 \in [0, \ell_0]$ .

The assumptions

$$\ell_0/h_0 > 2 \quad \text{and} \quad h_0 < \ell_{in}^0 < \ell_0 - h_0, \quad (7.11)$$

allow to neglect the perturbation introduced by the end (sharp or smooth) of the punch on the two lateral boundaries  $\partial\mathcal{B}_0^l$  and  $\partial\mathcal{B}_0^r$ ,

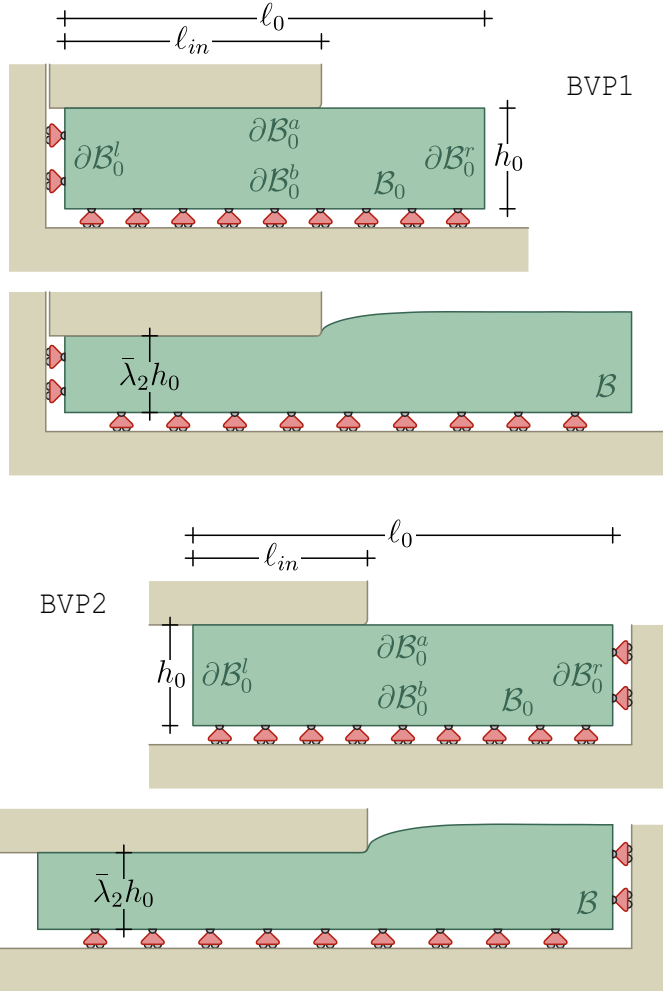


**Figure 7.1:** Boundary value problems analyzed called BVP1 (top) and BVP2 (bottom). Top: A rectangular block constrained by rollers on  $\partial\mathcal{B}_0^b$  and  $\partial\mathcal{B}_0^l$  and free  $\partial\mathcal{B}_0^r$  and constrained by a rigid wall on  $\partial\mathcal{B}_0^a$ . Bottom: A rectangular block constrained by rollers on  $\partial\mathcal{B}_0^b$  and  $\partial\mathcal{B}_0^r$  and free  $\partial\mathcal{B}_0^l$  and constrained by a rigid wall on  $\partial\mathcal{B}_0^a$ .

where the deformed state is approximated as uniform and therefore independent of  $x_2^0$ . Under this approximation, eqn (4.38) can be used to obtain the horizontal force  $R_1$  in the two following cases.

- For BVP1: the part of the boundary  $\partial\mathcal{B}_0^a$  outside the constraint and  $\partial\mathcal{B}_0^r$  are traction-free; moreover,  $\partial\mathcal{B}_0^r$  is unloaded,  $\lambda_1^r = \lambda_2^r = 1$  and  $\Phi^r = 0$ . Thus, the reaction force  $R_1$ , eqn (4.42),

becomes

$$R_1 = \frac{\Phi^l(\lambda_1^l, \lambda_2^l = \bar{\lambda}_2)}{\lambda_1^l} h_0, \quad (7.12)$$

an equation showing that the force is always positive. The two unknowns  $R_1$  and  $\lambda_1^l$  (the latter enforced to be coincident to  $1/\bar{\lambda}_2$  in the incompressible case) can be evaluated by solving eqns (7.9) and (7.12), together with the constitutive equation (7.4) [or eqn (7.7) in the incompressible case]. The result comes in a closed form for the incompressible case as

$$R_1 = \frac{(\bar{\lambda}_2^2 - 1)^2}{\bar{\lambda}_2} \frac{\mu h_0}{2}. \quad (7.13)$$

Although not expressible in a closed form, in the compressible case, for a small strain  $\bar{\varepsilon}_2 < 0$  defining  $\bar{\lambda}_2 = 1 + \bar{\varepsilon}_2$ , the following series expansions, truncated at the fourth-order can be obtained

$$\begin{aligned} R_1 &= \left[ 1 - \frac{(3-\alpha)(1-2\nu)}{3(1-\nu)} \bar{\varepsilon}_2 + \right. \\ &\quad \left. + \frac{(\alpha(3\alpha-20)+35)\nu^2 + \alpha(22-3\alpha)\nu + (\alpha-6)\alpha - 34\nu + 8}{12(1-\nu)^2} \bar{\varepsilon}_2^2 \right] \\ &\quad \times \frac{\mu h_0}{1-\nu} \bar{\varepsilon}_2^2 + o(\bar{\varepsilon}_2^4), \\ \lambda_1^l &= 1 + \left[ -1 + \frac{\bar{\varepsilon}_2}{2\nu} - \frac{3+\alpha(2\nu^2+\nu-1)-\nu(4+\nu)}{6(1-\nu)^2\nu} \bar{\varepsilon}_2^2 + \right. \\ &\quad \left. + \frac{17\alpha^2(2\nu^3+\nu^2+\nu-1)-\alpha(\nu(4\nu(\nu+2)-23)+9)}{24\nu(1-\nu)^3} \bar{\varepsilon}_2^3 \right. \\ &\quad \left. + \frac{\nu(\nu(\nu+6)-11)}{6\nu(1-\nu)^3} \bar{\varepsilon}_2^3 \right] \frac{\nu \bar{\varepsilon}_2}{1-\nu} + o(\bar{\varepsilon}_2^4); \end{aligned} \quad (7.14)$$

- For BVP2: the reaction force  $R_1$  is given by eqn (4.42) as

$$R_1 = \frac{\Phi^l(\lambda_1^l, \lambda_2^l = \bar{\lambda}_2) - \Phi^r(\lambda_1^r, \lambda_2^r)}{\lambda_1^r} h_0. \quad (7.15)$$

The four unknowns  $R_1$ ,  $\lambda_2^r$ ,  $\lambda_1^l$  and  $\lambda_1^r$  (the last two enforced to be coincident to  $1/\bar{\lambda}_2$  and to  $1/\lambda_2^r$  in the incompressible case) can be evaluated by solving eqns (7.10) and (7.15), together with the constitutive equation (7.4) [or eqn (7.7) in the incompressible case]. Similarly to BVP1, the result is

provided in a closed form for the incompressible case as

$$R_1 = \frac{1 - 10\bar{\lambda}_2^4 + \bar{\lambda}_2^8 + (1 + \bar{\lambda}_2^4) \sqrt{1 + 14\bar{\lambda}_2^4 + \bar{\lambda}_2^8} \mu h_0}{\bar{\lambda}_2^3 \sqrt{1 + \bar{\lambda}_2^4 + \sqrt{1 + 14\bar{\lambda}_2^4 + \bar{\lambda}_2^8}}} \frac{3\sqrt{6}}{3\sqrt{6}},$$

$$\lambda_2^r = \frac{\sqrt{1 + \bar{\lambda}_2^4 + \sqrt{1 + 14\bar{\lambda}_2^4 + \bar{\lambda}_2^8}}}{\sqrt{6}\bar{\lambda}_2}, \quad (7.16)$$

and as the following expansions in  $\bar{\varepsilon}_2$  truncated at the fourth-order for the compressible case

$$R_1 = \left[ 1 + \frac{\alpha(1 - 2\nu) - 3(1 - \nu)}{3(1 - \nu)} \bar{\varepsilon}_2 + \right.$$

$$+ \frac{\alpha^2(3(\nu - 1)\nu + 1) - 6\alpha(\nu - 1)(2\nu - 1) + 14(\nu - 1)^2}{12(1 - \nu)^2} \bar{\varepsilon}_2^2 \Big] \\ \times \frac{\mu h_0}{1 - \nu} \bar{\varepsilon}_2^2 + o(\bar{\varepsilon}_2^4),$$

$$\lambda_2^r = 1 + \left[ 1 + \frac{\alpha(1 - 2\nu) - 3(1 - \nu)}{3(1 - \nu)} \bar{\varepsilon}_2 + \right.$$

$$+ \frac{(3(\alpha - 2)\alpha + 5)\nu^2 - 3(\alpha - 3)\alpha\nu + (\alpha - 3)\alpha - 13\nu + 8}{12(1 - \nu)^2} \bar{\varepsilon}_2^2 \Big] \\ \times \frac{\nu}{2(1 - \nu)} \bar{\varepsilon}_2^2 + o(\bar{\varepsilon}_2^4),$$

$$\lambda_1^l = 1 - \left[ 1 - \frac{1}{2(1 - \nu)} \bar{\varepsilon}_2 + \frac{(2 - \nu)}{6(1 - \nu)^2} \bar{\varepsilon}_2^2 + \right.$$

$$- \frac{(2 - \nu)(3 - 2\nu)}{24(1 - \nu)^3} \bar{\varepsilon}_2^3 \Big] \frac{\nu}{1 - \nu} \bar{\varepsilon}_2 + o(\bar{\varepsilon}_2^4),$$

$$\lambda_1^r = 1 - \left[ 1 + \frac{\alpha(1 - 2\nu) - 3(1 - \nu)}{3(1 - \nu)} \bar{\varepsilon}_2 + \right.$$

$$+ \frac{(3(\alpha - 2)\alpha + 5)\nu^2 - 3(\alpha - 3)\alpha\nu + (\alpha - 3)\alpha - 10\nu + 5}{12(1 - \nu)^2} \bar{\varepsilon}_2^2 \Big] \\ \times \frac{\bar{\varepsilon}_2^2}{2} + o(\bar{\varepsilon}_2^4). \quad (7.17)$$

It is noted that the reaction force  $R_1$  and the stretches solving BVP1 and BVP2 are both characterized by the same structure of their expansions,

$$\begin{Bmatrix} R_1 \\ \lambda_1^r - 1 \\ \lambda_2^r - 1 \\ \lambda_1^l - 1 \end{Bmatrix} = \dots \bar{\varepsilon}_2^2 + \dots \bar{\varepsilon}_2^3 + \dots \bar{\varepsilon}_2^4, \quad (7.18)$$

$$\lambda_1^l - 1 = \dots \bar{\varepsilon}_2 + \dots \bar{\varepsilon}_2^2 + \dots \bar{\varepsilon}_2^3 + \dots \bar{\varepsilon}_2^4.$$

The value of the reaction force component  $R_1$ , obtained as the numerical solution of the system of nonlinear equations eqns (7.9), (7.12), and (7.4) [or eqn (7.7) in the incompressible case] for BVP1 (continuous lines) and eqns (7.10) (7.15), and (7.4) [or eqn (7.7) in the incompressible case] for BVP2 (dashed lines), is reported as a function of the imposed stretch  $\bar{\lambda}_2$  in Fig. 7.2 on the left (for different values of the ground-state Poisson's ratio  $\nu$ ) and as a function of the ground-state Poisson's ratio  $\nu$  (for different values of the imposed nominal stretch  $\bar{\lambda}_2$ ) on the right. Note that both neo-Hookean and Pence and Gou models are reported in the figure on the left, while the former model corresponds to the limit of  $\nu = 0.5$  on the right.

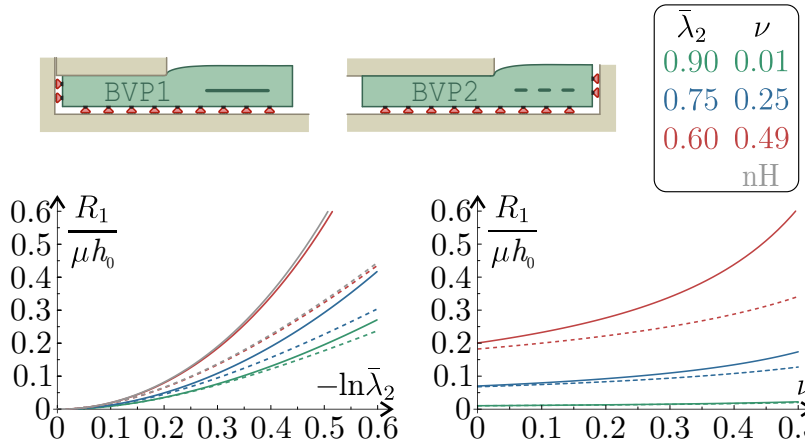


**Figure 7.2:** Normalized reaction force  $R_1/(\mu h_0)$  as a function of the imposed nominal stretch  $\bar{\lambda}_2$  (left, for the neo-Hookean material 'nH' and for the Pence-Gou material) and of the ground-state Poisson's ratio  $\nu$  (right) (for the Pence-Gou material). The continuous and dashed lines respectively correspond to the solution of BVP1 and BVP2, eqns (7.13) and (7.16) for the neo-Hookean material and the numerical solution of eqns (7.9), (7.12), and (7.4), and eqns (7.10) (7.15), and (7.4) for the Pence-Gou material.

**Reliability of the uniform state assumption at the boundaries  $\partial\mathcal{B}_0^l$  and  $\partial\mathcal{B}_0^r$ .** The curves describing the reaction force  $R_1$  in Fig. 7.2 are obtained by considering the uniformity of the stretches, and therefore of the strain energy, along each of the two lateral boundaries  $\partial\mathcal{B}_0^l$  and  $\partial\mathcal{B}_0^r$ . The reliability of this assumption is assessed by comparing  $R_1$  with the corresponding value  $R_1^{\text{FE}}$  numerically evaluated through finite element simulations, where both the neo-Hookean and the 'first-term' Storåkers models are available. The domain is discretized in 190 nodes (denser in the proximity of

$\ell_{in}/\ell_0 \rightarrow 0^+$  and  $\ell_{in}/\ell_0 \rightarrow 1^-$ ) in which a general static simulation is performed.

The map of relative difference  $(R_1^{\text{FE}} - R_1)/R_1^{\text{FE}}$  is reported for a neo-Hookean material with  $\ell_0/h_0 = 20$ , under an imposed nominal stretch  $\bar{\lambda}_2 = 0.7$  in Fig. 7.3 (lower part, on the left) for BVP1, for different ratios  $\ell_{in}/\ell_0 \in [0, 1]$  and  $r/h_0 \in [0.1, 0.5]$ , being  $r$  the radius of the rounded corner of the constraint (Fig. 7.3, upper part, right). The map shows that the relative difference  $(R_1^{\text{FE}} - R_1)/R_1^{\text{FE}}$  is confined to positive and very low values (less than  $3 \cdot 10^{-2}$ ) for  $\ell_{in}/\ell_0 \in [0.005, 0.98]$  (Fig. 7.3, bottom left), a minimum negative value (approximately  $-0.12$ ) is attained for  $\{\ell_{in}/\ell_0, r/h_0\} = \{0, 0.1\}$  (Fig. 7.3, above left), while a steep gradient arises and large (infinite in the limit case) values occur for  $\ell_{in}/\ell_0 \approx 1$  since  $R_1^{\text{FE}}$  vanishes when  $\ell_{in}/\ell_0 = 1$  (Fig. 7.3, bottom right). Therefore, the map confirms the reliability of evaluating the reaction force  $R_1$  through eqn (4.42), based on the approximation of homogeneity for the strain at each lateral sides of the elastic solid, except when one of the two sides  $\partial\mathcal{B}^l$  or  $\partial\mathcal{B}^r$  is located very close to the punch corner. Note that the results from FE are not included in Fig. 7.2, because they are simply superimposed to the curves.

## 7.2 Eulerian buckling induced by transverse compression

The rectangular elastic body  $\mathcal{B}_0$ , eqn (4.28), is partially subject to a symmetric transverse compression at its edges, corresponding to a nominal transverse stretch  $\bar{\lambda}_2 < 1$ , imposed by two parallel pairs of mirrored punches, spaced at a fixed distance  $d$  from each other, Fig. 7.4 (right). Horizontal reaction forces are acting at the corners of each of the punches,  $\{R_1^{al}, -R_1^{ar}, R_1^{bl}, -R_1^{br}\}\mathbf{e}_1$ . The force compresses the central part of the elastic body. Assuming a symmetric response with respect to the vertical direction at  $x_1^0 = \ell_0/2$ , a symmetry in the forces follows

$$R_1^{al} = R_1^{ar}, \quad R_1^{bl} = R_1^{br}. \quad (7.19)$$

The nominal transverse stretch  $\bar{\lambda}_2$  can be decreased starting from the undeformed state ( $\bar{\lambda}_2 = 1$ ), until a critical value  $\bar{\lambda}_2^{cr}$  is reached, for which the buckling of the elastic body occurs. This occurrence is always possible before a surface instability when the elastic body is sufficiently slender.

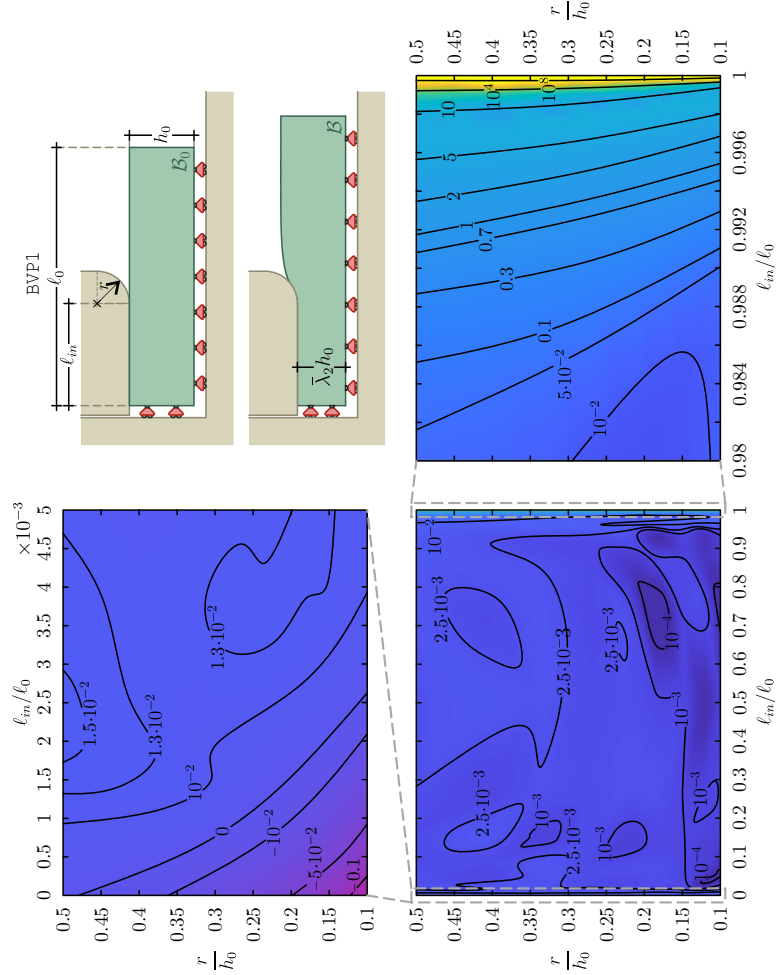


**Figure 7.3:** (Lower part, on the left) Map of relative difference  $(R_1 - R_1^{\text{FE}}) / R_1^{\text{FE}}$ , for different ratios  $\ell_{in}/\ell_0$  and  $r/h_0$  for a neo-Hookean elastic material with  $\ell_0/h_0 = 20$  at an imposed nominal stretch  $\bar{\lambda}_2 = 0.7$  for BVP1 (Upper part, on the right). Magnified map for small (upper part, on the left) and large (lower part, on the right) values of  $\ell_{in}/\ell_0$ , respectively showing the possibility of negative values and very large positive values for the relative difference.

The buckling condition is investigated through the reduced model of the extensible elastica with varying domain, as sketched in the inset of Fig. 7.4 (left) and described in Ch. 6. Under the mentioned symmetry condition, the internal force component along  $\mathbf{e}_2$  vanishes ( $N_2(x_1^0) = 0$ ) and, by further restricting the treatment to a quadratic strain energy density, eqn (6.31), for the rod, the

equilibrium equations (6.26) reduce to

$$\begin{cases} B\theta''(x_1^0) + R_1 [1 + \eta(x_1^0)] \sin \theta(x_1^0) = 0, \\ K\eta(x_1^0) = -R_1 \cos \theta(x_1^0), \end{cases} \quad x_1^0 \in (\ell_{in}^0, \ell_0 - \ell_{in}^0), \quad (7.20)$$

where  $\ell_{in}^0$  defines the undeformed coordinate  $x_1^0$  corresponding to the sliding sleeve exit, in the deformed configuration. The equilibrium equations (7.20) are complemented by the following boundary conditions and isoperimetric constraints

$$\begin{aligned} \theta(\ell_{in}^0) &= \theta(\ell_0 - \ell_{in}^0) = 0, \\ \int_{\ell_{in}^0}^{\ell_0 - \ell_{in}^0} [1 + \eta(x_1^0)] \cos \theta(x_1^0) dx_1^0 &= d, \\ \int_{\ell_{in}^0}^{\ell_0 - \ell_{in}^0} [1 + \eta(x_1^0)] \sin \theta(x_1^0) dx_1^0 &= 0. \end{aligned} \quad (7.21)$$

In the equilibrium equations (7.20),  $R_1$  is the resultant reaction force aligned parallel to  $\mathbf{e}_1$  and exerted by each pair of sliding sleeves on the elastic solid,  $R_1 = R_1^{al} + R_1^{bl}$ . The buckling condition can be

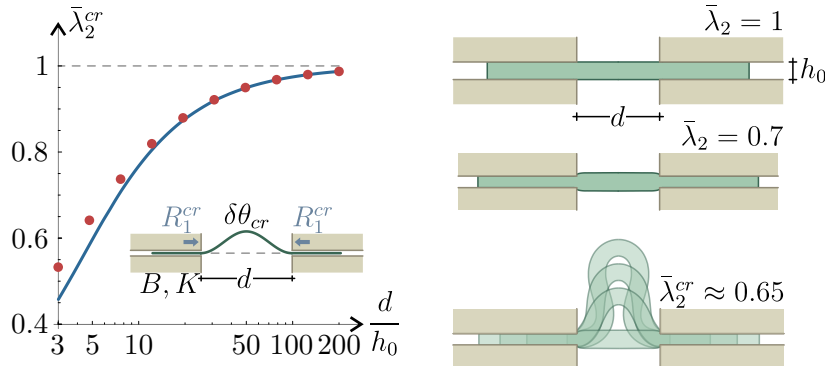


**Figure 7.4:** Eulerian buckling from transverse compression exerted by two pairs of symmetric (frictionless, flat, and rigid) punches. Left: Critical value of the nominal transverse stretch  $\bar{\lambda}_2^{cr}$  for a Pence and Gou elastic material with  $\nu = 0.25$  as a function of the slenderness parameter  $d/h_0$ . Semi-analytical prediction (blue curve) from the extensible elastica of varying-length (sketched in the inset) vs FE results (red dots). Right: Deformed shape evolution at decreasing transverse stretch  $\bar{\lambda}_2$  for an elastic rectangular solid with  $d/h_0 = 5$ . Unstable ejection occurs at the critical stretch  $\bar{\lambda}_2^{cr} \approx 0.65$ . Symmetry with respect to the central vertical axis has been enforced.

investigated by analyzing small perturbations  $\delta\theta(x_1^0)$  and  $\delta\eta(x_1^0)$  in

the rotation and axial deformation fields around the trivial straight configuration defined by

$$\theta_{eq}(x_1^0) = 0, \quad \eta_{eq}(x_1^0) = -\frac{R_1}{K}, \quad x_1^0 \in (\ell_{in}^0, \ell_0 - \ell_{in}^0), \quad (7.22)$$

for which a linearization of the equilibrium equations (7.20) leads to

$$\begin{cases} B\delta\theta''(x_1^0) + R_1 \left[ 1 - \frac{R_1}{K} \right] \delta\theta(x_1^0) = 0, \\ \delta\eta(x_1^0) = 0, \end{cases} \quad x_1^0 \in (\ell_{in}^0, \ell_0 - \ell_{in}^0), \quad (7.23)$$

while a linearization of the isoperimetric constraints to

$$\left[ 1 - \frac{R_1}{K} \right] (\ell_0 - 2\ell_{in}^0) = d, \quad \int_{\ell_{in}^0}^{\ell_0 - \ell_{in}^0} \delta\theta(x_1^0) dx_1^0 = 0. \quad (7.24)$$

A non-trivial equilibrium configuration can be found for the critical reaction force  $R_1^{cr}$  and the corresponding critical rotation field  $\delta\theta_{cr}(x_1^0)$ , which can be evaluated as

$$\begin{aligned} R_1^{cr} &= \frac{4\pi^2 B}{d^2 + \frac{4\pi^2 B}{K}}, \\ \delta\theta_{cr}(x_1^0) &= \bar{\theta} \cos \left[ \frac{2\pi (x_1^0 - \ell_{in}^0)}{\ell_0 - 2\ell_{in}^0} \right], \\ x_1^0 &\in (\ell_{in}^0, \ell_0 - \ell_{in}^0), \end{aligned} \quad (7.25)$$

where  $\bar{\theta}$  represents a small amplitude, which remains arbitrary within the limits of a linear perturbation analysis.

By assuming  $B = Eh_0^3/12$  and  $K = Eh_0$ , with  $E = 2\mu/(1-\nu)$  being the ground-state Young modulus under plane strain for the Pence and Gou model (7.5), the critical reaction force  $R_1^{cr}$  (7.25) reduces to

$$R_1^{cr} = \frac{\pi^2 h_0^2}{3d^2 + \pi^2 h_0^2} \frac{2\mu h_0}{1-\nu}. \quad (7.26)$$

The critical force  $R_1^{cr}$  is reached for the straight configuration of the extensible elastica,  $\theta(s) = 0$ , equivalent to a ‘trivial’ configuration of the elastic body of rectangular shape, satisfying vertical symmetry at  $x_2^0$ . The four tangential reactions at the punch corners have all the same values,

$$R_1^{al} = R_1^{ar} = R_1^{bl} = R_1^{br}, \quad (7.27)$$

so that the elastic rectangular domain can be reduced to its quarter, loaded as for BVP2.

The critical force  $R_1^{cr}$  can be evaluated using eqn. (7.26), but has to be expressed in terms of a critical transverse stretch  $\bar{\lambda}_2^{cr}$ , through the  $J$ -integral, which can in turn be approximated as the solution of nonlinear equation (7.15). The corresponding ‘semi-analytical’ critical stretch  $\bar{\lambda}_2^{cr}$  is reported as a continuous curve in Fig. 7.4 (left) for a Pence and Gou material with  $\nu = 0.25$ , as a function of the slenderness parameter  $d/h_0$ .

As a complement to the above, the second-order expansion of the reaction force  $R_1$  for BVP2, eqn (7.17)<sub>1</sub>, leads to an approximation for the critical stretch  $\bar{\lambda}_2^{cr}$  referred to a ‘first-term’ Storåkers material, obtained for large values of  $d/h_0$  as

$$\begin{aligned} \bar{\lambda}_2^{cr} = 1 - \pi \sqrt{\frac{2}{3}} \frac{h_0}{d} + \pi^2 \frac{3(1-\nu) - \alpha(1-2\nu)}{9(1-\nu)} \frac{h_0^2}{d^2} + \\ + \pi^3 \frac{\alpha^2 [11(1-\nu)\nu - 2] + 12\alpha(1-\nu)(1-2\nu) + 15(1-\nu)^2}{54\sqrt{6}(1-\nu)^2} \frac{h_0^3}{d^3} + \\ - \pi^4 \frac{[3(1-\nu) - \alpha(1-2\nu)] \{ \alpha^2 [1 + 5\nu(1-\nu)] - 6\alpha(1-\nu)(1-2\nu) + 72(1-\nu)^2 \}}{486(1-\nu)^3} \frac{h_0^4}{d^4} \\ + o(h_0^4/d^4), \quad (7.28) \end{aligned}$$

which reduces to a mere geometric relation when the approximation is truncated at first-order.

**Critical stretch  $\bar{\lambda}_2^{cr}$  for buckling from FE simulations.** The FE model described in the previous Section is here adopted by considering that the punches end with a rounded corner, rounded with  $r = d/50$ . Symmetry is imposed with respect to the vertical direction at  $x_1^0 = \ell_0/2$ . A symmetric imperfection is introduced in the initial undeformed geometry to trigger the bifurcation in the numerical analysis. In particular, instead of rectangular shape, the central portion of the elastic domain,  $x_1^0 \in [(\ell_0 - d)/2, (\ell_0 + d)/2]$ , has been implemented as a parallelogram with internal angles very close to  $\pi/2$ , namely, equal to  $\pi/2 \pm \pi/10^4$ . Results are reported in Fig. 7.4 (left) for the Pence and Gou model, characterized by  $\nu = 0.25$  (for which surface instability is estimated to occur for  $\bar{\lambda}_2^{si} \approx 0.473$ ), for a constant ratio  $\ell_0/d = 3$  and for different slenderness  $d/h_0$ . The critical transverse stretches  $\bar{\lambda}_2^{cr}$ , numerically evaluated through a Riks analysis, are reported as dots. The numerical results are in excellent agreement with the ‘semi-analytical’ predictions obtained from the extensible elastica model. The evolution of the deformed shape is reported in Fig. 7.4 (right) for a rectangular

elastic domain of initial slenderness  $d/h_0 = 5$ , at three decreasing levels of transverse stretch,  $\bar{\lambda}_2 = \{1, 0.7, 0.65\}$ . The smallest of the reported stretch corresponds to the critical value  $\bar{\lambda}_2^{cr}$ , for which the system buckles following an unstable branch and therefore suffers a spontaneous and uncontrolled ejection from the compressing constraints. This is similar to the response of other structural systems constrained by sliding sleeves investigated in [8] and [9].

### 7.3 Dynamic longitudinal ejection of incompressible solids through transverse compression

Equilibrium has been so far enforced, as a consequence of the constraint applied on  $\partial\mathcal{B}^l$  in BVP1 or on  $\partial\mathcal{B}^r$  in BVP2. When such a constraint is removed after imposing  $\bar{\lambda}_2 < 1$ , the punch reaction  $R_1$  is unbalanced. As a consequence, the elastic solid is pushed by the reaction component  $R_1(t)$  away from the constraint, thus producing its complete ejection. The Newton's second law can be expressed by [44]

$$R_1(t) = \rho_0 \ell_0 h_0 \ddot{x}_1^c(t), \quad (7.29)$$

where  $\rho_0$  is the mass density of the elastic solid in the undeformed state,  $x_1^c(t)$  is the horizontal coordinate of the center of mass, and a superimposed dot represents the derivative with respect to time  $t$ .

While the extension of the  $J$ -integral measure to dynamics and the analysis of the influence of inertia are left to future investigation, the ejection process of the elastic body is simply analyzed, assuming that the constraint on  $\partial\mathcal{B}^l$  in BVP1 is instantaneously removed, after transverse loading,  $\bar{\lambda}_2 < 1$ . A neo-Hookean material is assumed and a simplified approach is developed, based on the following two assumptions.

1. The reaction force  $R_1(t)$  maintains the constant value  $R_1$  evaluated during a quasi-static transverse compression, eqn (7.12), in which  $\lambda_1^l = 1/\bar{\lambda}_2$ .
2. The coordinate of the center of mass  $x_1^c(t)$  of the deformed elastic body is approximated with the center of mass of an equivalent domain realized as the discontinuous union of two rectangular solids, one with the thickness of the space between the constraints (so that  $\lambda_1 = 1/\lambda_2 = 1/\bar{\lambda}_2$ ) and the other with the height of the unloaded elastic solid (so that  $\lambda_1 = \lambda_2 = 1$ ).

Under the above assumptions, the position of the center of mass is approximated as

$$x_1^c(t) = \frac{\ell_0}{2} - \frac{\bar{\lambda}_2 \ell_{in}(t) [2\ell_0 - (1 + \bar{\lambda}_2) \ell_{in}(t)]}{2\ell_0}, \quad (7.30)$$

and the Newton's second law (7.29) can be rewritten as a nonlinear second-order differential equation,

$$\rho_0 [(1 - \bar{\lambda}_2) \ell_{in}(t) + \ell_0] \ddot{\ell}_{in}(t) + \rho_0 (1 - \bar{\lambda}_2) \dot{\ell}_{in}^2(t) + \Phi^l(\bar{\lambda}_2) = 0, \quad (7.31)$$

where  $\ell_{in}(t)$  is the portion of elastic solid inside the constraint at time  $t$ .

Under the initial conditions

$$\ell_{in}(0) = \bar{\ell}_{in}, \quad \dot{\ell}_{in}(0) = 0, \quad (7.32)$$

the evolution in time of  $\ell_{in}(t)$  is obtained as the solution of the nonlinear ordinary differential equation (7.31) as

$$\ell_{in}(t) = \sqrt{\left( \frac{\ell_0}{1 - \bar{\lambda}_2} + \bar{\ell}_{in} \right)^2 - \frac{\Phi^l(\bar{\lambda}_2) t^2}{\rho_0(1 - \bar{\lambda}_2)}} - \frac{\ell_0}{1 - \bar{\lambda}_2}. \quad (7.33)$$

The time  $t_{eje}$  for which the complete ejection is predicted,  $\ell_{in}(t_{eje}) = 0$ , follows as

$$t_{eje} = \sqrt{\frac{\rho_0 \bar{\ell}_{in} [2\ell_0 + (1 - \bar{\lambda}_2) \bar{\ell}_{in}]}{\Phi^l(\bar{\lambda}_2)}}. \quad (7.34)$$

For a neo-Hookean material (7.6), the evolution in time of  $\ell_{in}(t)$ , eqn (7.33), and the corresponding ejection time  $t_{eje}$ , eqn (7.34), simplify as

$$\begin{aligned} \ell_{in}(t) &= \sqrt{\left( \frac{\ell_0}{1 - \bar{\lambda}_2} + \bar{\ell}_{in} \right)^2 - \frac{\mu t^2 (1 + \bar{\lambda}_2)^2 (1 - \bar{\lambda}_2)}{2\rho_0 \bar{\lambda}_2^2}} - \frac{\ell_0}{1 - \bar{\lambda}_2}, \\ t_{eje} &= \frac{\bar{\lambda}_2 \bar{\ell}_{in}}{1 - \bar{\lambda}_2} \sqrt{\frac{2\rho_0}{\mu} \left( \frac{2\ell_0}{\bar{\ell}_{in}} + 1 - \bar{\lambda}_2 \right)}. \end{aligned} \quad (7.35)$$

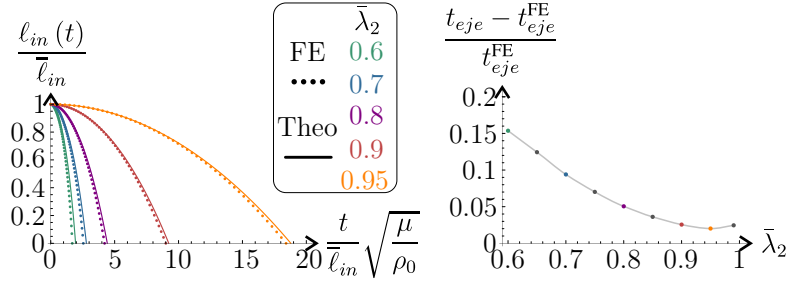


**Figure 7.5:** Left: Dimensionless representation of the instantaneous length  $\ell_{in}(t)$  of material inside the constraint as a function of time, for different nominal transverse stretch  $\bar{\lambda}_2$ , applied to a neo-Hookean material with  $\bar{\ell}_{in} = 0.9\ell_0$ . Results from the estimation (7.35)<sub>1</sub> (continuous lines) are compared with FE simulations (dots). Right: Relative error in the time for complete ejection, where  $t_{eje}$  is given by the estimate (7.35)<sub>2</sub>, while  $t_{eje}^{\text{FE}}$  by the FE simulations.

**Dynamic ejection from FE simulations.** The previously described FE model is exploited below to analyze the dynamic ejection problem for a neo-Hookean material, subject to a transverse stretch larger than that corresponding to surface instability,  $\bar{\lambda}_2 < \lambda_2^{si} \approx 0.544$ . The simulations are carried out in two steps, the first is the static analysis already presented for BVP1, while in the second step the elastic solid is instantaneously released and the motion analyzed via implicit dynamic with moderate dissipation solver. The first step is performed to start from  $\bar{\ell}_{in} = 0.9\ell_0$ , for an undeformed geometry of the material defined by  $\ell_0/h_0 = 20$ . The corner of the punch is modeled as rounded with  $r = h_0/10$ .

The evolution in time of  $\ell_{in}(t)$  is reported in Fig. 7.5 (left), with a continuous line for the approximate solution (7.35)<sub>1</sub> and with dots for the FE simulations. Different initial stretches  $\bar{\lambda}_2$  are investigated. The agreement is excellent, as can also be observed from the curve on the right, reporting the relative difference in the ejection time  $(t_{eje}^{\text{FE}} - t_{eje})/t_{eje}^{\text{FE}}$  as a function of  $\bar{\lambda}_2$ .

Four snapshots of representative configurations at different instants of time (including the configuration at the release time  $t = 0$ ) are reported in Fig. 7.6. The contour plots reported inside the deformed elastic solid depict the kinetic energy density  $\tau$  (in the upper half-part of the solid) and elastic strain energy density  $\Phi$  (in the lower half-part). At the release time ( $t = 0$ ), the kinetic energy density  $\tau$  is null over the whole solid (blue region), while the strain energy density  $\Phi$  is almost piecewise uniform, because the elastic body is slender and the corners of the rigid constraints introduce

only a small perturbation. As shown by the three snapshots taken after the release time, the spatial piecewise uniformity is essentially maintained for both kinetic and strain energy densities throughout the ejection process, during which a continuous transfer of elastic to kinetic energy occurs.

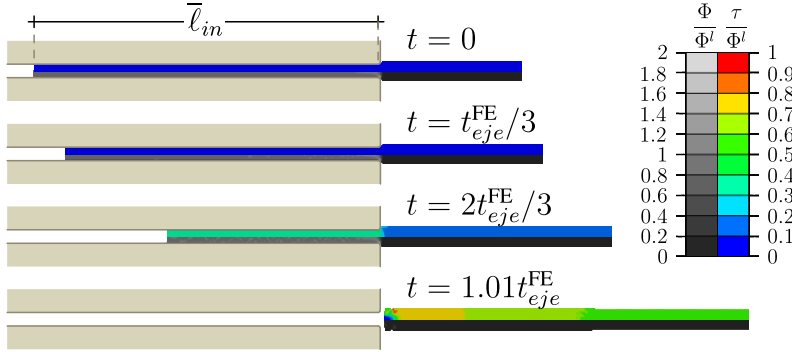


**Figure 7.6:** Four snapshots (obtained with a FE analysis) of representative configurations of a neo-Hookean solid (of unloaded aspect ratio  $\ell_0/h_0 = 20$ ), during its ejection from a rigid frictionless constraint as the effect of a nominal transverse stretch  $\bar{\lambda}_2 = 0.7$ . Different instants of time  $t$  are considered, including the release time  $t = 0$ , where the kinetic energy is null. Inside the solid, contour plots are reported of the kinetic energy density  $\tau$  (on the upper half-part of the solid) and of the elastic strain energy density  $\Phi$  (on the lower half-part), both divided by the value of the latter at the left edge of the elastic domain,  $\Phi^l$ .



## Conclusions

Concepts developed within the framework of defect mechanics, involving use of energy-momentum tensor and leading to path independent  $J$ -integral to be equal to the energy release rate for defect movement, have been extended to the mechanics of frictionless contact between an elastic solid and a rigid, flat punch. Within a quasi-static setting, it has been shown that a sharp or smooth corner, present at the end of a frictionless punch indenting a planar surface of an elastic solid, produces a (concentrated, for sharp corner) Newtonian force aligned parallel to the surface and coincident with the configurational force in that direction. This force component, so far passed unnoticed, may influence failure of material at contact or may induce Eulerian buckling or movement in a transversely compressed elastic slab. The investigated deformational mechanisms can be used for soft actuation or to explain migration of soft matter from stiffer to more compliant constrain environment.

Along this research line, a future development may be the extension of the  $J$ -integral definition to a dynamic framework, in order to investigate the inertia effect during the ejection process, as well as the post-critical behaviour. Furthermore, the present framework could be extended to the presence of a frictionless compliant contactor, removing the infinite rigidity assumption.



## Appendices

### A Another example of use of the energy-momentum tensor C for rectangular domains under dead loading conditions

A dead loading is symmetrically applied to a portion of a rectangular (two-dimensional) body defined as

$$\mathbf{S}\mathbf{n}_0 = \pm S_{22}\mathbf{e}_2, \quad \text{on } \partial\mathcal{B}_0^a \cup \partial\mathcal{B}_0^b. \quad (\text{A.1})$$

The scalar product of equation (4.21) with  $\mathbf{e}_1$  and an account of symmetry imply

$$\begin{aligned} \mathbf{e}_1^0 \cdot \mathbf{F}^T \mathbf{S}\mathbf{n}_0 \Big|_{\partial\mathcal{B}_0^a} &= S_{22}\mathbf{e}_2 \cdot \mathbf{F}(x_2^0 = h_0/2)\mathbf{e}_1 = \\ &= -S_{22}\mathbf{e}_2^0 \cdot \mathbf{F}(x_2^0 = -h_0/2)\mathbf{e}_1 = \mathbf{e}_1^0 \cdot \mathbf{F}^T \mathbf{S}\mathbf{n}_0 \Big|_{\partial\mathcal{B}_0^b}, \end{aligned} \quad (\text{A.2})$$

which in turn, by considering a uniform distribution  $S_{22}$ , leads to

$$\begin{aligned} \int_{\partial\mathcal{B}_0^l} \Phi(x_1^0 = 0) - \int_{\partial\mathcal{B}_0^r} \Phi(x_1^0 = l_0) \\ - 2S_{22} \int_{\partial\mathcal{B}_0^{a,\sigma}} \mathbf{e}_2 \cdot \mathbf{F}(x_2^0 = h_0/2) \mathbf{e}_1 = 0. \end{aligned} \quad (\text{A.3})$$

Equation (A.3) is exact. In an approximate way, it is now assumed that the loaded and unloaded portions of the boundaries  $\partial\mathcal{B}_0^a$  and  $\partial\mathcal{B}_0^b$  are both large enough that the edge  $\partial\mathcal{B}_0^r$  is unloaded,  $\Phi(x_1^0 = l_0) = 0$ , while the edge  $\partial\mathcal{B}_0^l$  is uniformly deformed, so that  $\Phi(x_1^0 =$

$0) = \Phi^l$  is independent of  $x_2^0$ . Under these approximations, equation (A.3) becomes

$$\Phi^l = -\frac{2S_{22}}{h_0} \int_{\partial\mathcal{B}_0^a} F_{21}(x_2^0 = h_0/2) \, dx_1^0. \quad (\text{A.4})$$

Equation (A.4) allows to calculate the elastic energy  $\Phi^l$  corresponding to a uniaxial compression,  $\mp S_{22}$ , or tension,  $\pm S_{22}$ , generated by a given nominal traction (A.1) as a function of a geometric quantity,  $F_{21}$ , related to the mean inclination of the curved portion of portion of the boundary  $\partial\mathcal{B}_0^{a,\sigma}$ , where the dead loading is applied.

## B Reaction force at a frictionless contact from the principle of virtual works

With reference to Fig. 4.2, a body subject to (referential) dead volume force  $\mathbf{b}_0$ , under prescribed displacement on  $\partial\mathcal{B}_0^u$ , dead loading  $\boldsymbol{\sigma}_0$  on  $\partial\mathcal{B}_0^\sigma$ , and in frictionless contact with the smooth and rigid constraint on  $\partial\mathcal{B}_0^{\text{tou}}$ , is assumed to be in equilibrium with the displacement field  $\mathbf{u}^*$ , deformation gradient  $\mathbf{F}^*$ , first Piola-Kirchhoff stress  $\mathbf{S}^*$ . The total potential energy  $\mathcal{V}$  of the system at equilibrium is given by

$$\mathcal{V}(\mathbf{F}^*, \mathbf{u}^*, \boldsymbol{\sigma}_0, \mathbf{b}_0) = \int_{\mathcal{B}_0} \Phi(\mathbf{F}^*) - \int_{\partial\mathcal{B}_0^\sigma} \boldsymbol{\sigma}_0 \cdot \mathbf{u}^* - \int_{\mathcal{B}_0} \mathbf{b}_0 \cdot \mathbf{u}^*. \quad (\text{B.1})$$

A rigid-body displacement vector  $\delta\xi$  is applied to the rigid constraint, so that as a consequence, all the fields in the elastic solid are perturbed and, in particular, the displacement and its gradient as follows

$$\mathbf{u}(\delta\xi) = \mathbf{u}^* + \delta\mathbf{u}(\delta\xi), \quad \mathbf{F}(\delta\xi) = \mathbf{F}^* + \delta\mathbf{F}(\delta\xi). \quad (\text{B.2})$$

Accordingly, the total potential energy of the system at equilibrium after the rigid-body perturbation of the frictionless constraint becomes

$$\begin{aligned} \mathcal{V}(\mathbf{F}(\delta\xi), \mathbf{u}(\delta\xi), \boldsymbol{\sigma}_0, \mathbf{b}_0) &= \int_{\mathcal{B}_0} \Phi(\mathbf{F}^* + \delta\mathbf{F}(\delta\xi)) + \\ &- \int_{\partial\mathcal{B}_0^\sigma} \boldsymbol{\sigma}_0 \cdot (\mathbf{u}^* + \delta\mathbf{u}(\delta\xi)) - \int_{\mathcal{B}_0} \mathbf{b}_0 \cdot (\mathbf{u}^* + \delta\mathbf{u}(\delta\xi)). \end{aligned} \quad (\text{B.3})$$

The change in the total potential energy  $\delta\mathcal{V}$  between the configurations is given by

$$\delta\mathcal{V}(\mathbf{F}^*, \mathbf{u}^*, \boldsymbol{\sigma}_0, \mathbf{b}_0, \delta\xi) = \mathcal{V}(\mathbf{F}(\delta\xi), \mathbf{u}(\delta\xi), \boldsymbol{\sigma}_0, \mathbf{b}_0) - \mathcal{V}(\mathbf{F}^*, \mathbf{u}^*, \boldsymbol{\sigma}_0, \mathbf{b}_0). \quad (\text{B.4})$$

Under the assumption that the perturbation  $\delta\xi$  is small, implying that  $\delta\mathbf{u}$  and  $\delta\mathbf{F}$  are of the same order, the change in the total potential energy  $\delta\mathcal{V}$  can be approximated at first-order as

$$\begin{aligned} \delta\mathcal{V}(\mathbf{F}^*, \mathbf{u}^*, \boldsymbol{\sigma}_0, \mathbf{b}_0, \delta\xi) &= \int_{\mathcal{B}_0} \mathbf{S}^* \cdot \delta\mathbf{F}(\delta\xi) - \int_{\partial\mathcal{B}_0^\sigma} \boldsymbol{\sigma}_0 \cdot \delta\mathbf{u}(\delta\xi) \\ &\quad - \int_{\mathcal{B}_0} \mathbf{b}_0 \cdot \delta\mathbf{u}(\delta\xi), \end{aligned} \quad (\text{B.5})$$

where, from eqn (2.62),

$$\mathbf{S}^* = \left. \frac{\partial \Phi(\mathbf{F})}{\partial \mathbf{F}} \right|_{\mathbf{F}^*}. \quad (\text{B.6})$$

The virtual work principle, expressed with reference to the unperturbed static fields and to the perturbed kinematic fields, yields

$$\begin{aligned} \int_{\partial\mathcal{B}_0^{\text{tou}}} \delta\mathbf{u}(\delta\xi) \cdot \mathbf{S}^* \mathbf{n}_0 &= \int_{\mathcal{B}_0} \mathbf{S}^* \cdot \delta\mathbf{F}(\delta\xi) - \int_{\partial\mathcal{B}_0^\sigma} \boldsymbol{\sigma}_0 \cdot \delta\mathbf{u}(\delta\xi) \\ &\quad - \int_{\mathcal{B}_0} \mathbf{b}_0 \cdot \delta\mathbf{u}(\delta\xi). \end{aligned} \quad (\text{B.7})$$

Note that the detaching from the contact can only occur from the grazing zone, where  $\mathbf{S}^* \mathbf{n}_0 = \mathbf{0}$ , eq. (4.7), so that

$$\int_{\partial\mathcal{B}_0^{\text{tou}}} \delta\mathbf{u}(\delta\xi) \cdot \mathbf{S}^* \mathbf{n}_0 = \int_{\partial\mathcal{B}_0^C} \delta\mathbf{u}(\delta\xi) \cdot \mathbf{S}^* \mathbf{n}_0, \quad (\text{B.8})$$

proving that detaching does not affect the integral.

A comparison with equation (B.5) leads to

$$\delta\mathcal{V}(\mathbf{F}^*, \mathbf{u}^*, \boldsymbol{\sigma}_0, \mathbf{b}_0, \delta\xi) = \int_{\partial\mathcal{B}_0^C} \delta\mathbf{u}(\delta\xi) \cdot \mathbf{S}^* \mathbf{n}_0. \quad (\text{B.9})$$

It is noted that in general the perturbed displacement  $\delta\mathbf{u}(\delta\xi)$  does not coincide with  $\delta\xi$  along  $\partial\mathcal{B}_0^C$ , because the elastic body may slip along the boundary in contact. However, the contact condition

$$\Sigma(\mathbf{x}^* - \delta\xi) = 0, \quad (\text{B.10})$$

for small perturbations provides

$$\mathbf{q}(\mathbf{x}^*) \cdot (\delta \mathbf{u}(\delta \boldsymbol{\xi}) - \delta \boldsymbol{\xi}) = 0, \quad (\text{B.11})$$

where  $\mathbf{q}(\mathbf{x}^*)$  is the normal vector to  $\Sigma$  at  $\mathbf{x}^*$

$$\mathbf{q}(\mathbf{x}^*) = \frac{\partial \Sigma(\mathbf{x})}{\partial \mathbf{x}} \Big|_{\mathbf{x}^*}, \quad (\text{B.12})$$

which is parallel to  $\mathbf{S}^* \mathbf{n}_0$  because of the frictionless contact condition, eq. (4.9). Therefore, equation (B.9) can be rewritten as

$$\delta \mathcal{V}(\mathbf{F}^*, \mathbf{u}^*, \boldsymbol{\sigma}_0, \mathbf{b}_0, \delta \boldsymbol{\xi}) = \delta \boldsymbol{\xi} \cdot \int_{\partial \mathcal{B}_0^C} \mathbf{S}^* \mathbf{n}_0, \quad (\text{B.13})$$

because vector  $\delta \boldsymbol{\xi}$  is constant.

Equation (B.13) shows that the total potential energy variation due to a small perturbation  $\delta \boldsymbol{\xi}$  in the position of the frictionless constraint is the negative of the scalar product between  $\delta \boldsymbol{\xi}$  and the resultant of the force  $\mathbf{R}^c$  that the constraint applies to the body,

$$\mathbf{R}^c = \int_{\partial \mathcal{B}_0^C} \mathbf{S}^* \mathbf{n}_0, \quad (\text{B.14})$$

namely,

$$\delta \mathcal{V} = \mathbf{R}^c \cdot \delta \boldsymbol{\xi}. \quad (\text{B.15})$$

Finally, noticing that

$$\delta \mathcal{V} = \frac{\partial \mathcal{V}}{\partial \boldsymbol{\xi}} \cdot \delta \boldsymbol{\xi}, \quad (\text{B.16})$$

due to the arbitrariness of  $\delta \boldsymbol{\xi}$ , the reaction force transmitted by frictionless constraint to the solid is obtained

$$\mathbf{R}^c = \frac{\partial \mathcal{V}}{\partial \boldsymbol{\xi}}. \quad (\text{B.17})$$

## Bibliography

- [1] C Armanini et al. “Configurational forces and nonlinear structural dynamics”. In: *Journal of the Mechanics and Physics of Solids* 130 (2019), pp. 82–100. ISSN: 0022-5096.
- [2] R Ballarini and G Royer-Carfagni. “A Newtonian interpretation of configurational forces on dislocations and cracks”. In: *Journal of the Mechanics and Physics of Solids* 95 (2016), pp. 602–620.
- [3] J Barber. *Contact Mechanics*. Springer, 2018.
- [4] D Bigoni. *Nonlinear solid mechanics: bifurcation theory and material instability*. Cambridge University Press, 2012.
- [5] D Bigoni et al. “Eshelby-like forces acting on elastic structures: theoretical and experimental proof”. In: *Mechanics of Materials* 80 (2015), pp. 368–374.
- [6] D Bigoni et al. “Torsional locomotion”. In: *Proceedings of the Royal Society A* 470 (2014), p. 20140599.
- [7] D. Bigoni, F Dal Corso, and M Gei. “The stress concentration near a rigid line inclusion in a prestressed, elastic material. Part II. Implications on shear band nucleation, growth and energy release rate”. In: *Journal of the Mechanics and Physics of Solids* 56 (2008), pp. 839–857.
- [8] F Bosi et al. “Development of configurational forces during the injection of an elastic rod”. In: *Extreme Mechanics Letters* 471 (2015), pp. 83–88.

- [9] A Cazzolli and F Dal Corso. “The elastica sling”. In: *European Journal of Mechanics, A/Solids* 105.3 (2024), p. 105273.
- [10] P Chadwick. “Applications of an energy-momentum tensor in non-linear elastostatics”. In: *Journal of Elasticity* 5 (1975), pp. 249–258.
- [11] GP Cherepanov. “The propagation of cracks in a continuous medium”. In: *Journal of Applied Mathematics and Mechanics* 31.3 (1967), pp. 503–512.
- [12] M Ciavarella, DA Hills, and G Monno. “The influence of rounded edges on indentation by a flat punch”. In: *Proceedings of the Institution of Mechanical Engineers, Part C: Journal of Mechanical Engineering Science* 212.4 (1998), pp. 319–328.
- [13] M Ciavarella, G Macina, and GP Demelio. “On stress concentration on nearly flat contacts”. In: *The Journal of Strain Analysis for Engineering Design* 37.6 (2002), pp. 493–501.
- [14] F Dal Corso et al. “Serpentine locomotion through elastic energy release”. In: *Journal of the Royal Society Interface* 14 (2017), p. 20170055.
- [15] JD Eshelby. “The Continuum Theory of Lattice Defects”. In: ed. by F Seitz and D Turnbull. Vol. 3. Solid State Physics. Academic Press, 1956, pp. 79–144.
- [16] JD Eshelby. “The elastic energy-momentum tensor”. In: *Journal of Elasticity* 5.3-4 (1975), pp. 321–335.
- [17] JD Eshelby. “The force on an elastic singularity”. In: *Philosophical Transactions of the Royal Society of London. Series A, Mathematical and Physical Sciences* 244.877 (1951), pp. 87–112.
- [18] H Flanders. “Differentiation under the integral sign”. In: *The American Mathematical Monthly* 80 (1973), pp. 615–627.
- [19] AE Giannakopoulos, TC Lindley, and S Suresh. “Aspects of equivalence between contact mechanics and fracture mechanics: theoretical connections and a life-prediction methodology for fretting-fatigue”. In: *Acta Materialia* 46.9 (1998), pp. 2955–2968.
- [20] M Goudarzi et al. “Dispersion of rigid line inclusions as stiffeners and shear band instability triggers”. In: *International Journal of Solids and Structures* 210–211 (2021), pp. 255–272.

- [21] ME Gurtin. *An introduction to continuum mechanics*. Academic press, 1982.
- [22] ME Gurtin. “The nature of configurational forces”. In: *Fundamental Contributions to the Continuum Theory of Evolving Phase Interfaces in Solids: A Collection of Reprints of 14 Seminal Papers*. Springer, 1999, pp. 281–314.
- [23] JA Hanna, H Singh, and EG Virga. “Partial constraint singularities in elastic rods”. In: *Journal of Elasticity* 133.1 (2018), pp. 105–118.
- [24] GA Holzapfel. *Nonlinear solid mechanics: a continuum approach for engineering science*. 2002.
- [25] A Isomursu et al. “Directed cell migration towards softer environments”. In: *Nature Materials* 21.877 (2022), pp. 1081–1090.
- [26] KL Johnson. *Contact mechanics*. Cambridge University Press, 1985.
- [27] R Kienzler and G Herrmann. *Mechanics in Material Space*. Springer, 2000.
- [28] HK Kim. “Study on the edge rounding with consulting contact mechanics”. In: *Tribology International* 183 (2023), p. 108426.
- [29] P Koutsogiannakis et al. “Stabilization against gravity and self-tuning of an elastic variable-length rod through an oscillating sliding sleeve.” In: *Journal of the Mechanics and Physics of Solids* 181 (2023), p. 105452.
- [30] A Liakou and E Detournay. “Constrained buckling of variable length elastica: Solution by geometrical segmentation”. In: *International Journal of Non-Linear Mechanics* 99 (2018), pp. 204–217.
- [31] L Ma and AM Korsunsky. “Surface dislocation nucleation from frictional sliding contacts”. In: *International Journal of Solids and Structures* 45.22–23 (2008), pp. 5936–5945.
- [32] L Ma and AM Korsunsky. “Vector J-integral analysis of crack initiation at the edge of complete sliding contact”. In: *Proceedings of the Royal Society A: Mathematical, Physical and Engineering Sciences* 462 (2006), pp. 1805–1820.
- [33] A Magnusson, M Ristinmaa, and C Ljung. “Behaviour of the extensible elastica solution”. In: *International Journal of Solids and Structures* 38.46 (2001), pp. 8441–8457.

- [34] GA Maugin. “Material forces: concepts and applications”. In: *ASME Applied Mechanics Re-views* 48.5 (1995), pp. 213–245.
  - [35] OM O'Reilly. “A material momentum balance law for rods”. In: *Journal of Elasticity* 86 (2007), pp. 155–172.
  - [36] OM O'Reilly. *Modeling nonlinear problems in the mechanics of strings and rods*. Springer, 2017.
  - [37] OM O'Reilly. “Some perspectives on Eshelby-like forces in the elastica arm scale”. In: *Proceedings of the Royal Society A: Mathematical, Physical and Engineering Sciences* 471.2174 (2015), p. 20140785.
  - [38] RW Ogden. *Non-linear elastic deformations*. Courier Corporation, 1997.
  - [39] TJ Pence and K Gou. “On compressible versions of the incompressible neo-Hookean material”. In: *Mathematics and Mechanics of Solids* 20.2 (2015), pp. 157–182.
  - [40] JR Rice. “A path independent integral and the approximate analysis of strain concentration by notches and cracks”. In: *Journal of Applied Mechanics* 35.2 (1968), pp. 379–386.
  - [41] JR Rice. “Mathematical Analysis in the Mechanics of Fracture”. In: ed. by H Liebowitz. Vol. 2. *Fracture: An Advanced Treatise*. Academic Press, 1968, pp. 191–311.
  - [42] MH Sadd. *Elasticity: Theory, Applications, and Numerics*. Academic Press, 2020.
  - [43] B Storåkers. “On material representation and constitutive branching in finite compressible elasticity”. In: *Journal of the Mechanics and Physics of Solids* 34.2 (1986), pp. 125–145.
  - [44] C Truesdell and RA Toupin. “The classical Field theories”. In: ed. by Flügge S. Vol. III/1. *Encyclopedia of Physics*. Springer-Verlag, 1960.
  - [45] ZQ Wang and E Detournay. “Eshelbian force on a steadily moving liquid blister”. In: *International Journal of Engineering Science* 170 (2022), p. 103591.
  - [46] YJ Xie and DA Hills. “Crack initiation at contact surface”. In: *Theoretical and Applied Fracture Mechanics* 40.3 (2003), pp. 279–283.
  - [47] YJ Xie et al. “Applications of conservation integral to indentation with a rigid punch”. In: *Engineering Fracture Mechanics* 76.7 (2009), pp. 949–957.
-



A homogeneous elastic solid, bounded by a flat surface in its unstressed configuration, undergoes a finite strain when in frictionless contact against a rigid and rectilinear constraint, ending with a rounded or sharp corner, in a two-dimensional formulation. With a strong analogy to fracture mechanics, it is shown that (i.) a path-independent  $J$ -integral can be defined for frictionless contact problems, (ii.) which is equal to the energy release rate  $G$  associated with an infinitesimal growth in the size of the frictionless constraint, and thus gives the value of the configurational force component along the sliding direction. Furthermore, it is found that (iii.) such a configurational sliding force is the Newtonian force component exerted by the elastic solid on the constraint at the frictionless contact. Assuming the kinematics of an Euler-Bernoulli rod for an elastic body of rectangular shape, the results (i.)-(iii.) lead to a new interpretation from a nonlinear solid mechanics perspective of the configurational forces recently disclosed for one-dimensional structures of variable length. Finally, approximate but closed-form solutions (validated with finite element simulations) are exploited to provide further insight into the effect of configurational forces. In particular, two applications are presented which show that a transverse compression can lead to Eulerian buckling or to longitudinal dynamic motion, both realizing novel examples of soft actuation mechanisms. As an application to biology, our results may provide a mechanical explanation for the observed phenomenon of negative durotaxis, where cells migrate from stiffer to softer environments.